MACROSCOPIC AND SPECTROSCOPIC INVESTIGATION OF INTERACTIONS OF ARSENIC WITH SYNTHESIZED PYRITE

A Dissertation

by

EUN JUNG KIM

Submitted to the Office of Graduate Studies of
Texas A&M University
in partial fulfillment of the requirements for the degree of

DOCTOR OF PHILOSOPHY

December 2008

Major Subject: Civil Engineering

MACROSCOPIC AND SPECTROSCOPIC INVESTIGATION OF INTERACTIONS OF ARSENIC WITH SYNTHESIZED PYRITE

A Dissertation

by

EUN JUNG KIM

Submitted to the Office of Graduate Studies of
Texas A&M University
in partial fulfillment of the requirements for the degree of

DOCTOR OF PHILOSOPHY

Approved by:

Chair of Committee,	Bill Batchelor
Committee Members,	Robin Autenrieth
	Richard H. Loeppert
	Kung-Hui Chu
Head of Department,	David V. Rosowsky

December 2008

Major Subject: Civil Engineering

ABSTRACT

Macroscopic and Spectroscopic Investigation of Interactions of Arsenic with Synthesized Pyrite. (December 2008)

Eun Jung Kim, B.S. University of Seoul;

M.S., Pohang University of Science and Technology

Chair of Advisory Committee: Dr. Bill Batchelor

Sulfide minerals have been suggested to play an important role in regulating dissolved metal concentrations in anoxic environments. Pyrite is the most common sulfide mineral and it has shown an affinity for arsenic, but little is known about the arsenic retention mechanisms of pyrite. In this study, interactions of arsenic with pyrite were investigated in an anoxic environment to understand geochemical cycling of arsenic better and to predict arsenic fate and transport in the environment better. A procedure using microwaves was studied to develop a fast and reliable method for synthesizing pyrite. Arsenic-pyrite interactions were investigated using macroscopic (solution phase experiments) and microscopic (X-ray photoelectron spectroscopic investigation) approaches.

Pyrite was successfully synthesized within a few minutes via reaction of ferric iron and hydrogen sulfide under the influence of irradiation by a conventional microwave oven. The SEM-EDX study revealed that the nucleation and growth of pyrite occurred on the surface of elemental sulfur, where polysulfides are available. Compared

to conventional heating, microwave energy results in rapid (< 1 minute) formation of smaller particulates of pyrite. Higher levels of microwave power can form pyrite even faster, but faster reaction can lead to the formation of pyrite with defects.

Arsenic removal by pyrite was strongly dependent on pH and arsenic species. Both arsenite (As(III)) and arsenate (As(V)) had a strong affinity for the pyrite surface under acidic conditions, but As(III) was removed more effectively than As(V). Under acidic conditions, arsenic removal continued to occur almost linearly with time until complete removal was achieved. However, under neutral to alkaline conditions, fast removal was followed by slow removal and complete removal was not achieved in our experimental conditions. A BET isotherm equation provided the best fit to arsenic removal data, suggesting that surface precipitation occurred at high arsenic/pyrite ratio. The addition of competing ions did not substantially affect the ultimate distribution of arsenic between the pyrite surface and the solution, but changing pH affected arsenic stability on pyrite.

X-ray photoelectron spectroscopy revealed that under acidic conditions, arsenic was removed and formed solid phases similar to As_2S_3 and As_4S_4 by reaction with pyrite. However, under neutral to alkaline conditions, arsenic was removed and formed As(III)-O and As(V)-O surface complexes, as well as As_2S_3/As_4S_4-like precipitates. As pH increases, the amount of arsenic that formed As_2S_3/As_4S_4-like precipitates decreased, while the amount that formed As(III)-O and As(V)-O surface complexes increased. Under alkaline conditions, a FeAsS-like phase was also detected.

ACKNOWLEDGEMENTS

I am grateful to all those who have assisted me to finish this dissertation. Especially, I would like to thank my advisor, Dr. Bill Batchelor, for his guidance, support, and encouragement throughout the course of this research. I would also like to thank my committee members, Dr. Robin Autenrieth, Dr. Richard H. Loeppert, and Dr. Kung-Hui Chu, for their helpful discussion and advices.

I would like to acknowledge the support and friendship of all my friends and colleagues. Their assistance and advice were invaluable resources to my research, and they made my time at Texas A&M University a great experience.

Finally, special thanks to my family for their encouragement and support through my entire life and to my husband and best friend, Yoon E, for his support and love.

TABLE OF CONTENTS

CHAPTER Page

LIST OF FIGURES

Page

Page

Page

LIST OF TABLES

Page

CHAPTER I

INTRODUCTION

Arsenic contaminated drinking water has been a big problem in many parts of the world including Bangladesh, China, India, Taiwan, Mexico, and the USA (1). Bangladesh is reported as having the worst case of arsenic contamination. Thousands of people there have been suffering from arsenic driven diseases, and millions of them are estimated to be exposed to arsenic contaminated drinking water or at risk of being exposed (2). Exposure of humans to elevated concentrations of arsenic in drinking water posses significant health risks, such as Blackfoot disease, skin, lung and bladder cancers, and disorders of the immune, nervous and reproductive systems (3). In 2001 following a reassessment of health effects, the US EPA reduced the maximum contaminant level (MCL) for arsenic in drinking water from 50 μg/L to 10 μg/L (4).

Arsenic is a trace element that occurs naturally in the atmosphere, water, soils, and rocks. Arsenic is present as a major constituent of many minerals including sulfides and oxides such as realgar (As_4S_4), orpiment (As_2S_3), arsenopyrite (FeAsS), arsenolite (As_2O_3), and scorodite ($FeAsO_4 \cdot 2H_2O$). Arsenic can be released to the surface and subsurface water by natural processes such as weathering and sedimentation and by human activities such as mining, smelting, burning of fossil fuels, and applying agricultural chemicals. In water, arsenic occurs as different protonated oxyanionic forms

---

This dissertation follows the style of *Environmental Science and Technology*.

depending on redox condition and pH. Trivalent arsenite ($H_nAsO_3^{n-3}$) generally exists in reduced conditions such as groundwater and pentavalent arsenate ($H_nAsO_4^{n-3}$) is dominant in oxidized conditions such as natural surface water (1).

Mineral-water interactions play important roles in controlling the fate and transport of arsenic in natural water (1,5,6). Oxides of iron, aluminum, and manganese are known to be the major minerals controlling arsenic concentration in aquifers because of their chemistry and abundance (1,5,6). Among oxides, iron oxides are considered to be the most important sinks for arsenic, therefore, the interactions of arsenic with iron oxide minerals, such as hydrous ferric oxide (HFO), goethite, and hematite, have been extensively investigated (7-9). Under reduced conditions, however, reductive dissolution of iron oxides containing arsenic is also considered as an important source of arsenic in natural water (1,6,10).

Sulfide minerals have been suggested to play an important role in regulating dissolved metal concentrations in anoxic environments (11-13). Commonly known as "Fool's Gold", pyrite is an iron disulfide (FeS_2) that is the most common sulfide mineral and it is widely found in sediments, sedimentary rocks, and hydrothermal ores. Sedimentary pyrite has controlled the oxygen level of the atmosphere and the sulfate concentration in seawater over a long period of time. Pyrite plays an important role as an electron source in geochemical processes in the environment (14,15). Natural pyrite contains various amounts of trace elements such as arsenic (As), lead (Pb), cobalt (Co), nickel (Ni), and selenium (Se) at concentrations that range from a few ppm to tens of

thousands ppm. For example, arsenic contents in pyrite can vary between 2 and 96,000 ppm (16). Thus, interactions of trace elements with pyrite have received great attention.

A strong correlation between arsenic concentration and pyrite contents in marine sediments suggested capture of arsenic by pyrite (11). The examination of sediments in Milltown Reservoir showed that vertical transition of redox states resulted in the shift in partitioning of arsenic from oxides into sulfides (13). Investigation of the Clio mine samples showed that pyrite contains arsenic up to 3.9 wt.% and suggested that most arsenic is present as a solid solution in pyrite (17). X-ray absorption spectroscopy studies and electronic structure calculations suggest that arsenic substitutes for sulfur in pyrite by forming As-S dianion groups (17,18).

Laboratory studies on interactions of arsenic with pyrite have been published (19-23). Farquhar et al. (19) investigated the effect of pH (pH 5.5 – 6.5) on As(III) and As(V) adsorption on makinawite and pyrite using X-ray absorption spectroscopy. Arsenic species retained their original oxidation states on the pyrite surface. Their study suggested formation of outer-sphere complexes by the interactions of arsenic with pyrite. On the other hand, Bostick et al. (20,21) suggested formation of strong inner-sphere complexes or surface precipitates by reactions between As(III) and pyrite. They suggested that initial formation of an FeAsS-like precipitate might be followed by conversion to As_2S_3 by the reaction between As(III) and pyrite. These studies have shown the affinity of pyrite for arsenic, but have not fully described arsenic retention mechanisms.

The goal of this research is to investigate interactions of arsenic with pyrite in an anoxic environment in order to better understand removal of arsenic in treatment systems and its behavior in natural environments. A clear understanding of the interactions between pyrite and arsenic under anoxic conditions is important in understanding geochemical cycling of arsenic and predicting arsenic fate and transport. This goal will be accomplished through the following objectives: 1) Develop fast and reliable pyrite synthesis method; 2) Evaluate arsenic removal characteristics of synthesized pyrite; 3) Evaluate surface characteristics of pyrite after reaction with arsenic. Microwaves have been successfully applied to synthesis of inorganic compounds such as metal (Cu, Hg, Bi, Zn, Pb, Cd) sulfide nanoparticles as well as synthesis of organic compounds and these reactions typically occur within a few minutes (24,25). Microwave synthesis of pyrite was studied with solutions of $FeCl_3$ and NaHS and results are presented in Chapter II. Arsenic removal by synthesized pyrite was evaluated as a function of pH, arsenic concentrations, reaction time, and competing ions and the results will be presented in Chapter III. Finally, the surface of pyrite reacted with arsenic was characterized using X-ray photoelectron spectroscopy (XPS), in order to investigate the possible formation of arsenic compounds and the results are presented in Chapter IV.

CHAPTER II

MICROWAVE SYNTHESIS OF PYRITE AND CHARACTERIZATION

2.1 Introduction

Commonly known as "Fool's Gold", iron disulfide pyrite (FeS_2) is the most common sulfide mineral and is widely found in sediments, sedimentary rocks, and hydrothermal ores. Sedimentary pyrite has controlled the oxygen level of the atmosphere and the sulfate concentration in seawater over a long period of time. Pyrite plays an important role as an electron source in geochemical processes in the environment (14,15).

Due to its abundance and its important role in nature, sedimentary pyrite formation has been studied extensively (15,26-31). Pyrite has been suggested to form either by direct nucleation and crystal growth (26,27) or by replacement of iron monosulfide (FeS) precursors (15,28-31). Generally, pyrite formation via FeS precursor was considered as a key mechanism. However, direct formation of pyrite by the reaction of Fe^{2+} with disulfide S_2^{2-} was suggested by Roberts et al. (26). Rickard (27) proposed the mechanism of pyrite formation through the direct solution reaction between polysulfide and Fe^{2+}.

$$Fe^{2+} + S_5S^{2-} + HS^- \rightarrow FeS_2 + S_4S^{2-} + H^+ \quad (2.1)$$

The polysulfide and Fe^{2+} are the products of dissolution of elemental sulfur and FeS in sulfide solution, respectively. According to Luther (28), the reaction of Fe^{2+} and Fe^{3+} solutions with polysulfide solutions synthesizes pyrite via "FeS", which consists of solid

FeS and the soluble complexes $Fe(SH)^+$ and $[Fe(SH)(S_x)]^-$. Shoonen and Barnes (29) reported extremely slow kinetics of pyrite nucleation at low temperature, which supported the insignificance of direct pyrite formation via nucleation.

The FeS precursor is formed by the reaction between ferrous iron (Fe^{2+}) and aqueous sulfide (S^{2-}). Sulfide in nature is derived by bacterial reduction of dissolved sulfate and the decomposition of organic sulfur compounds (15).

$$Fe^{2+} + S^{2-}(aq) \rightarrow FeS\ (s) \quad (2.2)$$

FeS can be converted to pyrite either by addition of sulfur (reaction 2.3) (15) or by loss of Fe^{2+} from FeS (reaction 2.4) (30).

$$FeS + S^0 \rightarrow FeS_2 \quad (2.3)$$

$$2FeS\ (s) + 2H^+ \rightarrow FeS_2 + Fe^{2+} + H_2 \quad (2.4)$$

The source of sulfur in reaction 3 was proposed to be elemental sulfur, hydrogen sulfide, polysulfides, thiosulfate, sulfites, thiols, sulfonates, and other inorganic or organic sulfur species (15,30,32).

Synthesis of pyrite in the marine environment is believed to take a long time; however, rapid formation of pyrite has been reported when iron monosulfide is undersaturated but pyrite is oversaturated (33). In laboratory experiments, pyrite was synthesized over time periods lasting from several hours to 1 year, depending on reaction conditions such as pH, temperature, and source of Fe and S (34). At temperatures below 100°C, the rate of pyrite formation is relatively slow. Pyrite was formed in a few days or in a few weeks or as long as one year. However, increasing temperature has been shown to enhance the rate of pyrite formation (31,34).

Recently, microwave energy has been widely applied in organic and inorganic synthesis. In microwave synthesis, heat is generated by the interaction between microwaves and the absorbing medium, which leads to rapid and selective heating (35). Also, microwave heating reduces temperature and concentration gradients in the reaction medium, compared to other methods of heating. Compared to conventional heating methods, microwave synthesis is reported to have the advantage of producing small particles, a narrow particle size distribution and high purity as well as a short reaction time (24,25). Microwaves have been successfully applied to synthesis of inorganic compounds such as metal (Cu, Hg, Bi, Zn, Pb, Cd) sulfide nanoparticles as well as synthesis of organic compounds within several minutes (24,25).

The goal of this research is to develop a rapid and simple method to synthesize pyrite particles using microwave irradiation. Previous methods have successfully synthesized pyrite by the reaction of ferric iron (Fe^{3+}) in sulfide solutions (26,36). Here, microwave synthesis of pyrite was studied with $FeCl_3$ and NaHS solutions. The effects of reaction time, microwave power, and solution concentrations on pyrite formation were investigated.

2.2 Experimental Section

2.2.1 Pyrite Synthesis

Pyrite was synthesized by the reaction of Fe^{3+} in sulfide solutions. The iron and sulfide solutions were prepared by dissolving ferric chloride ($FeCl_3 \cdot 6H_2O$) and sodium hydrosulfide ($NaHS \cdot xH_2O$) in deaerated deionized water. The deaerated deionized water was prepared by bubbling purified nitrogen gas through deionized water for at least 2 hours. Deionized water was obtained from a Millipore Milli-Q system. Then the water was stored in an anaerobic chamber containing gas of 5% hydrogen and 95% nitrogen overnight.

Pyrite synthesis experiments were conducted in a glove box containing nitrogen gas. The iron and sulfide solutions with total volume of 200 mL were mixed in polypropylene bottles and the pH of the solution was adjusted to pH 4.0 by adding 5 M NaOH or 5 M HCl. Various iron and sulfide concentrations were tested, but the molar ratio of iron to sulfide was fixed at 0.5. The mixed solutions were placed in a conventional domestic microwave oven (1150 W, 2.45 GHz) and received microwave energy for times from a few seconds to several minutes. In some experiments, the percentage of time irradiated was also varied as well as the total time. The reacted samples were rapidly cooled in cold water to room temperature and 10 mL of 5 N HCl was added to remove HCl soluble compounds such as FeS. Since pyrite does not react with HCl, the only solids remaining would be pyrite. The remaining solids were filtered and dried in the anaerobic chamber. The effects of reagent concentration, reaction time, and percent time of microwave irradiation on pyrite synthesis were tested.

2.2.2 Quantification of Synthesized Pyrite

In some experiments, synthesized pyrite was quantitatively measured by dissolving the solids remaining after HCl wash with nitric acid by boiling for 5 minutes. Pyrite does not react with HCl, but it reacts with hot nitric acid (37). The amount of pyrite was evaluated by measuring liberated iron concentration. The liberated iron concentration was measured using a UV-Vis spectrophotometer (Hewlett Packard G1103A) at 562 nm after developing purple color by the reaction with ferrozine.

2.2.3 Solid Characterization

The solid products were identified with X-ray diffraction (XRD). The morphology and particle size were characterized by JEOL JSM-6400 scanning electron microscope (SEM) and its chemical composition was evaluated with energy dispersive X-ray (EDX) spectroscopy under the SEM. The specific surface area of selected particles was determined using multi-point BET isotherm using N_2 as the adsorbate. The oxidation state of iron and sulfur on the surface of synthesized pyrite was characterized by Kratos Axis Ultra Imaging X-ray photoelectron spectroscopy (XPS) with monochromatic Al K-α X-rays. Broad scan was obtained using 80 eV pass energy, while narrow high resolution scans of Fe 2p and S 2p were obtained using 40 eV pass energy. The charge effect was corrected using C 1s from contamination at 284.6 ± 0.1 eV. The obtained spectra were fitted using a curve-fitting program (XPSPEAK41). The spectra were fitted using a least-squares procedure with peaks of 80% of Lorentzian-Gaussian

peak shape after subtraction of a Shirley baseline. The component peaks were identified by comparison of their binding energies with literature values (Table 2.1).

Table 2.1 XPS binding energies of Fe2p and S2p for chemical species reported in the literature

	Species	Binding energy (eV)	References
Fe ($2p_{3/2}$)	Fe(II)-S	707.2	Bostick and Fendorf (21)
		707.0 (FeS_2 bulk), 706.05, 707.95	Nesbitt and Muir (38)
		707.5 ± 0.2	Bonnissel-Gissinger et al. (39)
		706.5, 707.45, 708.4	Pratt et al. (40)
	Fe(III)-S	709.3	Bostick and Fendorf (21)
		708.75, 709.85, 710.85, 711.75	Nesbitt and Muir (38)
	Fe(III)-OH	711.3	Bostick and Fendorf (21)
		710.3, 711.3, 712.4, 713.45	Nesbitt and Muir (38)
S ($2p_{3/2}$)	FeS_2 (bulk)	162.6	Bostick and Fendorf (21)
	FeS	160.8	NIST XPS database
	S_2^{2-}	162.4	Nesbitt and Muir (38)
		162.4 - 162.5, 162.7	Bonnissel-Gissinger et al. (39)
	S^{2-}	161.2	Bostick and Fendorf (21)
		161.65	Nesbitt and Muir (38)
		161.1, 161.3	Bonnissel-Gissinger et al. (39)
	polysulfide	163.8, 163.2	Bostick and Fendorf (21)
		163.6	Nesbitt and Muir (38)
		165.3, 164.2, 163.8	Bonnissel-Gissinger et al. (39)
	$S_2O_3^{2-}$	166.8, 166.9	Bostick and Fendorf (21)
		166.45	Nesbitt and Muir (38)
	SO_4^{2-}	169.1, 169.0	Bostick and Fendorf (21)
		168.25	Nesbitt and Muir (38)
		169.1, 168.5	Bonnissel-Gissinger et al. (39)

2.3 Results and Discussion

2.3.1 Pyrite Formation by Microwave Irradiation and Characterization

The experiments were conducted with the solutions of 0.1 M of $FeCl_3$ and 0.2 M of NaHS at 20% microwave power (cycle of 6 sec on and 24 sec off). A black precipitate was immediately formed after mixing the $FeCl_3$ and NaHS solutions, which indicated the possible formation of unstable amorphous FeS. After adjusting pH of mixed solutions, the solutions were reacted in microwave ovens for 4, 6, 8, and 10 minutes. The SEM images of solid products at each reaction time are shown in Figure 2.1. After 4 min, big particles were detected, which were identified as elemental sulfur by the EDX spectra (Figure 2.2a). Small particles occurred as aggregates of crystals on the surface of elemental sulfur after 6 minutes, and with time, more particles having size of around 0.2 μm were produced. The particles formed at 10 minutes were identified as pyrite based on the EDX spectra (Figure 2.2b).

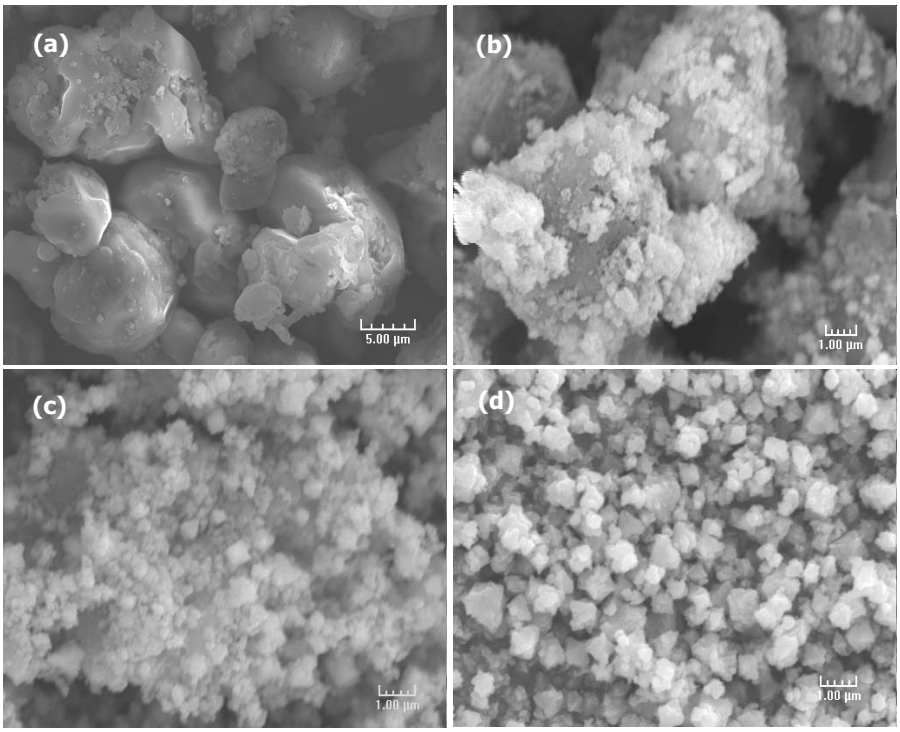

Figure 2.1 SEM images of particles formed after (a) 4 min, (b) 6 min, (c) 8 min, and (d) 10 min by microwave irradiation.

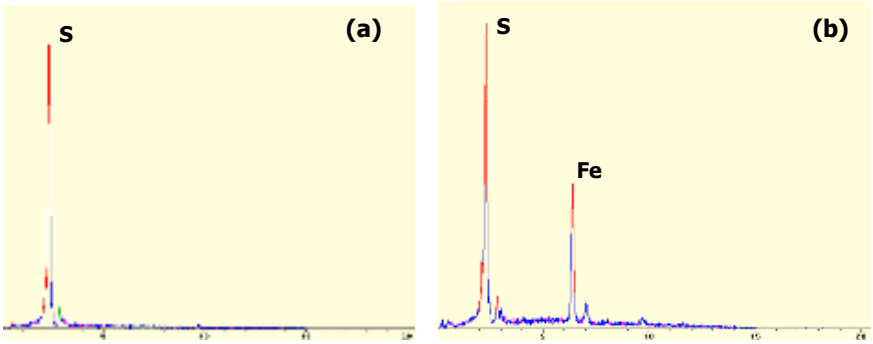

Figure 2.2 EDX spectra of particles formed after (a) 4 min and (b) 10 min by microwave irradiation.

The particles formed by microwave irradiation for 10 min were further identified by X-ray diffraction. The XRD pattern indicated the presence of pyrite and elemental sulfur (Figure 2.3a). After washing with acetone and carbon disulfide, sulfur was removed and only pyrite was identified by XRD (Figure 2.3b).

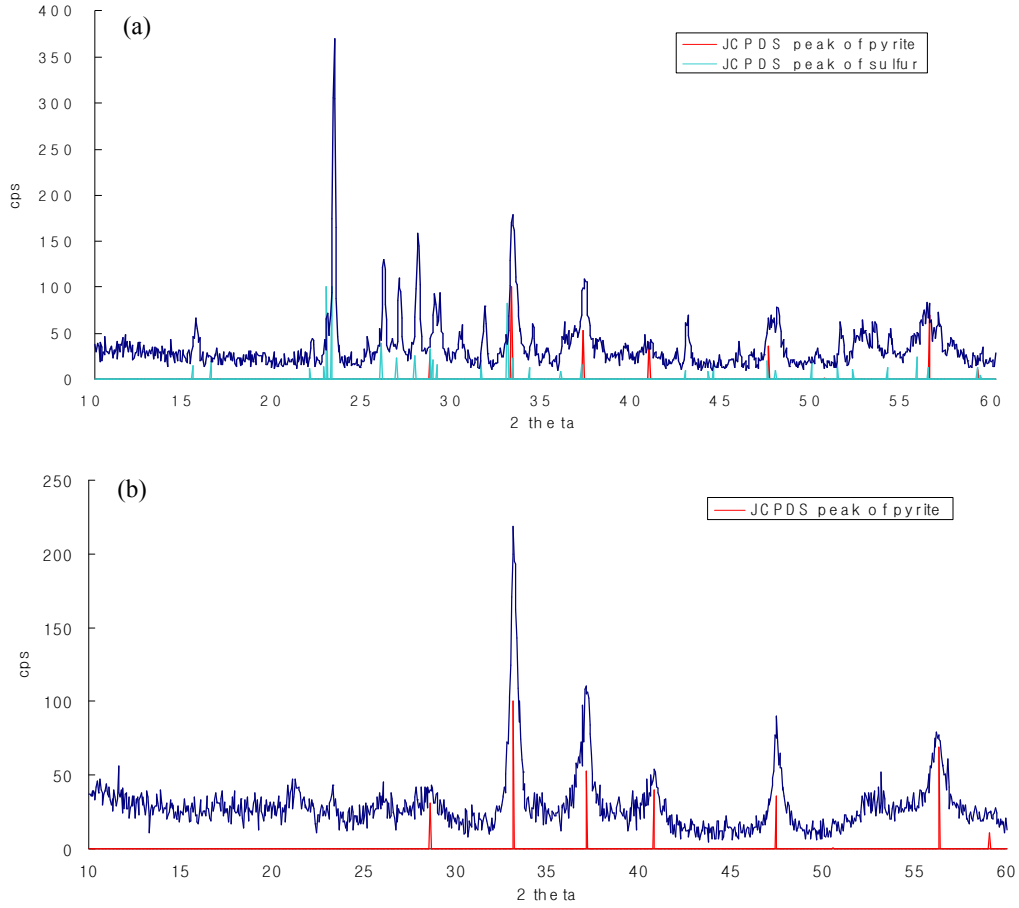

Figure 2.3 X-ray diffraction patterns of particles formed by microwave irradiation for 10 minutes. (a) before wash, (b) after wash with acetone, and CS_2.

The surface of the particles formed by microwave irradiation for 10 min was further investigated by XPS. The broad scan of particle surface is shown in Figure 2.4. The surface consisted of iron, sulfur, oxygen, and carbon. The sulfur to iron atomic concentration ratio was around 2, which is consistent with pyrite (Table 2.2).

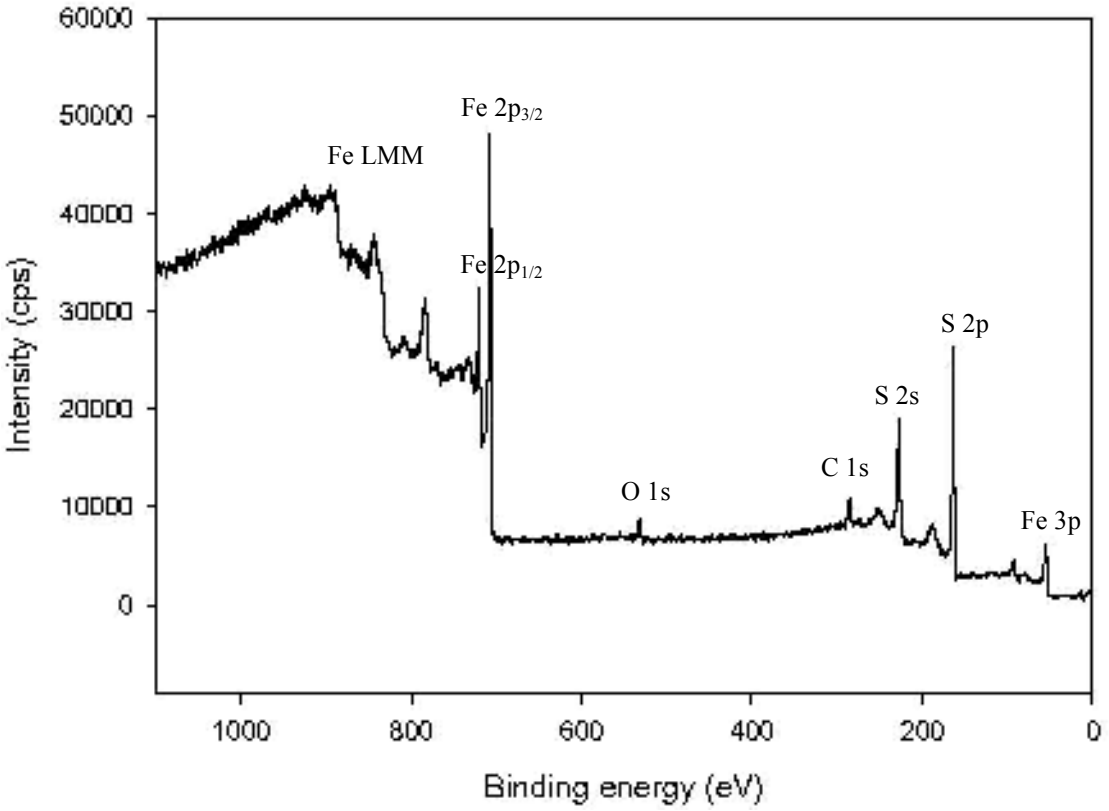

Figure 2.4 XPS broad scan of particles formed by microwave irradiation for 10 minutes.

Table 2.2 XPS analysis of particles formed by microwave irradiation for 10 minutes

	Fe 2p	S 2p	O 1s
Atomic Concentration (%)	30.92	64.23	4.84

Figure 2.5 presents the Fe 2p and S 2p spectra of pyrite. The XPS data were fitted using a curve-fitting program, XPSPEAK41. In Figure 2.5, circles represent XPS data and thick solid curves represent the fit to the data. For S 2p, S $2p_{1/2}$ is separated from $2p_{3/2}$ by 1.18 eV and the area was 1/2 of $2p_{3/2}$. Thin solid curves represent Fe $2p_{3/2}$ and S $2p_{3/2}$ composite peaks and dotted curves are S $2p_{1/2}$ composite peaks. The parameters are shown in Table 2.3. The major peaks of Fe $2p_{3/2}$ and S $2p_{3/2}$ spectra were at 706.9 eV and 162.4 eV, respectively, which are the characteristic peaks of pyrite in agreement with the reported values in literature (Table 2.1). The S 2p spectra also contain smaller peaks at 161.4 eV and 163.6 eV, which are interpreted to be monosulfide (S^{2-}) and polysulfide (S_n^{2-}), respectively (38,39,41). The presence of monosulfide at the pyrite surface was suggested to be formed by sulfur released from broken S-S bonds that remains bonded to Fe (41,42). The pyrite used here was synthesized with Fe^{3+} and HS^- using microwave energy. The fast synthesis by high energy may result in the rupture of S-S bonds and could produce monosulfide on the pyrite surface. The S 2p spectrum indicates the absence of highly oxidized sulfur, i.e. sulfate, on the surface. The Fe $2p_{3/2}$ spectrum contains high binding energy tail fitted with peaks of Fe(III)-S, Fe(III)-OH, and Fe(III)-SO_4^{2-}, which indicates that the surface of pyrite is slightly oxidized.

The BET specific surface area for the pyrite particles was measured to be 15.9 m^2/g, which is about four times higher than the reported surface area (4.1 m^2/g) of pyrite synthesized without heating (36). Microwave irradiation formed pyrite with high surface area.

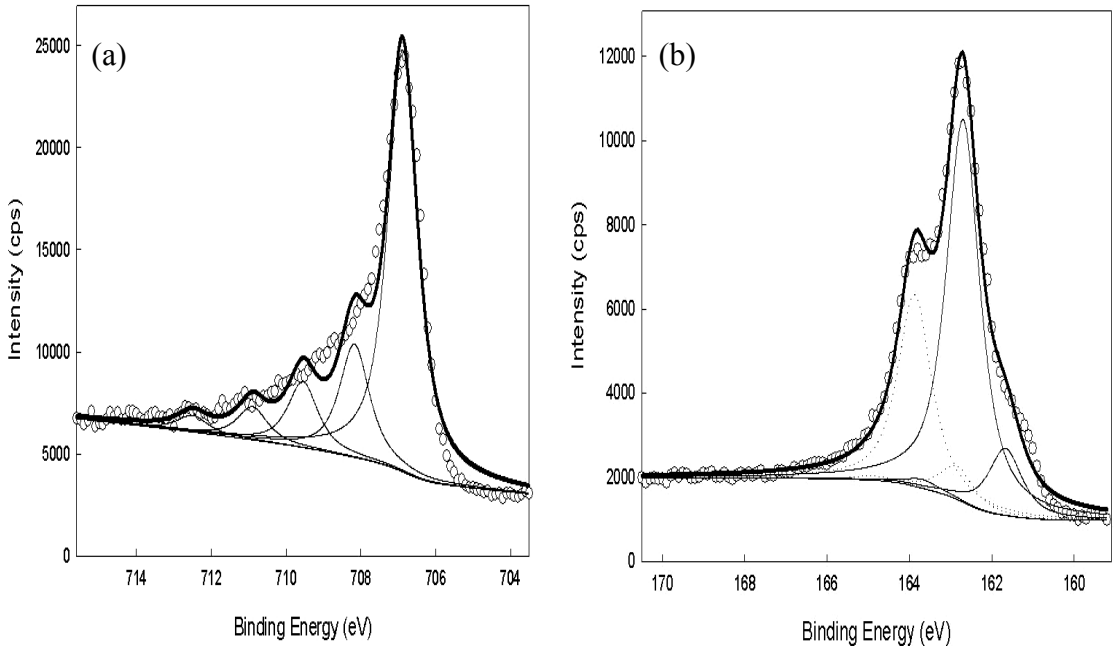

Figure 2.5 XPS spectra of particles formed by microwave irradiation for 10 minutes (a) Fe 2p, (b) S 2p.

Table 2.3 XPS peak parameters of particle formed by microwave irradiation for 10 minutes

Binding energy (eV)		FWHM (eV)	Area (%)	Surface species
Fe ($2p_{3/2}$)	706.9	0.958	64.8	Fe(II)-S
	708.2	0.958	17.4	Fe(II)-S
	709.6	0.958	10.1	Fe(III)-S
	710.9	0.958	5.1	Fe(III)-OH
	712.5	0.958	2.58	Fe(III)-SO4
S ($2p_{3/2}$)	161.4	0.969	14.7	S^{2-}
	162.4	0.969	83.4	S_2^{2-} (FeS_2)
	163.6	0.969	1.96	Polysulfide
	167.9	0.969	-	SO_4^{2-}

2.3.2 Mechanism of Pyrite Formation by the Reaction between Ferric Iron and Sulfide

Elemental sulfur was observed during the early stage of the reaction (Figure 2.1a). It is expected that a certain amount of elemental sulfur would be formed by the redox reaction between ferric iron and sulfide ions (26,36). Ferric iron oxidizes hydrogen sulfide to form elemental sulfur and ferric iron is reduced to form ferrous iron (26).

$$HS^- + 2Fe^{3+} \rightarrow S^0 + 2Fe^{2+} + H^+ \qquad (2.5)$$

As soon as solutions of ferric iron and hydrogen sulfide were mixed, black particles were formed. After 4 min reaction, HCl was observed to dissolve almost all of these black particles leaving only elemental sulfur, as shown in Figure 2.1a. Those black particles are believed to be amorphous FeS formed by reaction between ferrous iron and hydrogen sulfide.

$$Fe^{2+} + HS^- \rightarrow FeS + H^+ \qquad (2.6)$$

The SEM study revealed that pyrite particles were formed on the surface of elemental sulfur (Figure 2.1b, c). According to Berner (15), the presence of elemental sulfur is essential to form pyrite, since pyrite was formed only with an excess of elemental sulfur. The surface of elemental sulfur was suggested to promote pyrite crystallization. Pyrite formation on the elemental sulfur was also observed by Graham and Ohmoto (43). Pyrite was suggested to form by two pathways, based on their hydrothermal experiments: (1) nucleation and growth on FeS precursor surface and (2) nucleation and growth on S^0 surface. The pyrite that was formed on the surface of

elemental sulfur was suggested to be synthesized by the reaction between polysulfides and Fe^{2+} ion (43).

Pyrite formation by the reaction between polysulfides and Fe^{2+} ion was proposed by Rickard (27) and Luther (28). Polysulfides are formed by the reaction of elemental sulfur and hydrogen sulfide, which leads to the accumulation of polysulfides on or near the surface of elemental sulfur. Also, polysulfides in solution are not stable at high temperature (43). Thus, the nucleation and growth of pyrite seems to occur on the surface of elemental sulfur, where polysulfides are available.

Pyrite formation by ferric iron and hydrogen sulfide reaction using microwave energy can be summarized by following reactions (26,36,43).

$$2Fe^{3+} + HS^- = 2Fe^{2+} + S^0 + H^+ \qquad (2.7)$$

$$(n\text{-}1)S^0 + HS^- = S_n^{2-} + H^+ \qquad (2.8)$$

$$Fe^{2+} + S_n^{2-} + HS^- = FeS_2 + S_{n-1}^{2-} + H^+ \qquad (2.9)$$

2.3.3 Effect of Percent Time of Microwave Irradiation

Effect of the percent time of microwave irradiation on pyrite formation was studied using solutions containing 0.1 M $FeCl_3$ and 0.2 M NaHS. These solutions were reacted at microwave power levels applied for 20, 50, and 100% of the time over periods of 10, 4, and 2 min, respectively. Each reaction time was determined as the time when the solution started to boil based on preliminary experiments and resulted in approximately equal amounts of microwave energy supplied to the solutions.

Figure 2.6 shows SEM images of pyrite formed by microwave reaction with different percent time of irradiation. Noticeable differences of particle size and shape were not found at different percent times of irradiation, but more aggregate particles were observed when higher percentages were used. Similar clustering of single pyrite crystals was also observed in the high temperature experiments by Luther (28). High percentages of irradiation times can increase temperature more rapidly, and also can reach higher temperature according to the "superheating effect" (44). This means that temperatures above the boiling point can be observed when a solvent is irradiated by microwave energy. The higher temperatures seem to result in more clustering of particles.

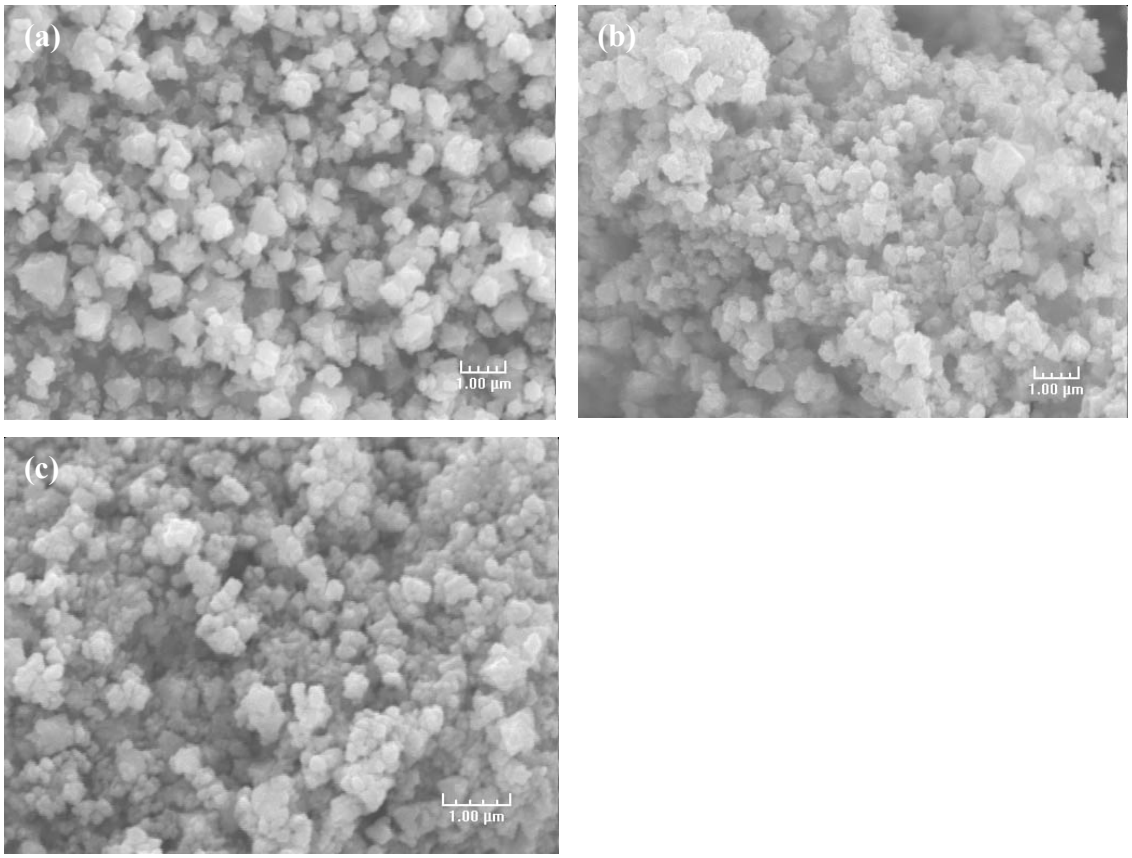

Figure 2.6 SEM images of particles formed by microwave irradiation at power of (a) 20% for 10 min, (b) 50% for 4 min, and (c) 100% for 2 min.

The amount of pyrite formed by microwave irradiation with different percent time of irradiation is shown in Figure 2.7. As percent time of irradiation increases, the amount of pyrite formed decreases. Figure 2.8 shows the amount of pyrite synthesized with reaction time using percent time of irradiation of 20% and 100%. With 20%, the amount of pyrite synthesized started to increase in 6 minutes and rapidly increase between 6 and 10 minutes. After 10 minutes, about 40% of initial iron added was transformed to pyrite (Figure 2.8a). At 100% irradiation, about 15% of initial iron was

transformed to pyrite within 1 min reaction. But, the amount of pyrite synthesized was reduced as reaction time increased (Figure 2.8b).

Lower yield of pyrite was observed at higher microwave power. Low yields of metal sulfides were also reported when the percentage of time irradiated was larger than 40% (total power: 650 W) (25). Pyrite was formed within 1 min at 100% irradiation. High power of microwave irradiation accelerates the rate of pyrite formation. However, the longer microwave reaction at high power results in the loss of pyrite. Fast reaction can lead the formation of crystals with defects (45), which can be transformed by microwave irradiation to other forms such as FeS. Pyrite was reported to be decomposed to pyrrhotite-like Fe-S phase and elemental sulfur when exposed to microwave energy (46).

$$(1\text{-}x)\ FeS_2 \rightarrow Fe_{1-x}S + (1 - 2x)\ S^0 \qquad (2.10)$$

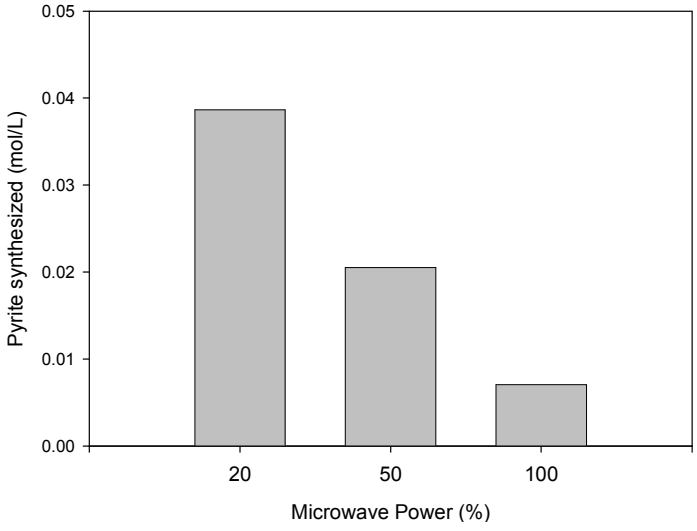

Figure 2.7 The amount of pyrite formed using microwave power applied at 20, 50, and 100 % of the time. Solutions contained 0.1 M $FeCl_3$ and 0.2 M NaHS.

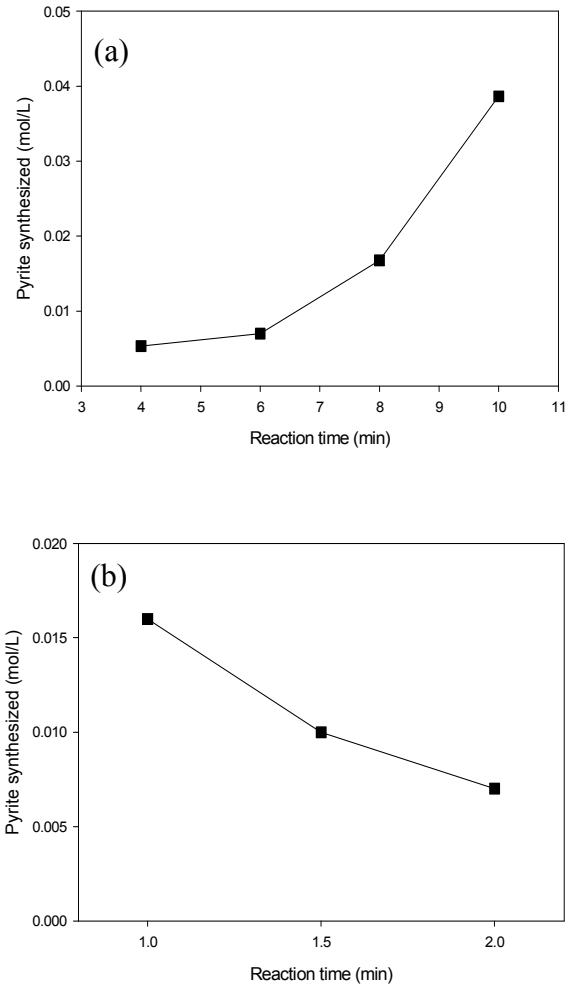

Figure 2.8 The amount of pyrite synthesized with reaction time by microwave irradiation at (a) 20%, (b) 100 % of the time. Solutions contained 0.1 M $FeCl_3$ and 0.2 M NaHS.

2.3.4 Effect of Reagent Concentration

Effect of reagent concentrations was examined using three solutions: 0.01 M $FeCl_3$/0.02 M NaHS, 0.05 M $FeCl_3$/0.1 M NaHS, and 0.1 M $FeCl_3$/0.2 M NaHS. Each solution was reacted with microwave energy at power of 20% over a period of 10 min. Figure 2.9 shows that particle size becomes smaller when reagent concentration is increased. The particle size of pyrite was around 0.1 μm when 0.1 M $FeCl_3$/0.2 M NaHS solutions were used (Figure 2.9c). This is opposite to previously reported results that showed small particle formation with low reagent concentration in the early aging stage at room temperature (36). Formation of crystals occurs with nucleation followed by particle growth. Increasing temperature has been shown to enhance the rate of pyrite formation (31,34). The rate of nucleation increases with increasing solute concentration (saturation ratio, actual concentration/solubility). With high concentration, more nuclei might form at high reagent concentrations. If the relative increase in the number of particles is greater than the relative increase in the concentration of reagents, then smaller particles would result even if all of the reagents formed particles.

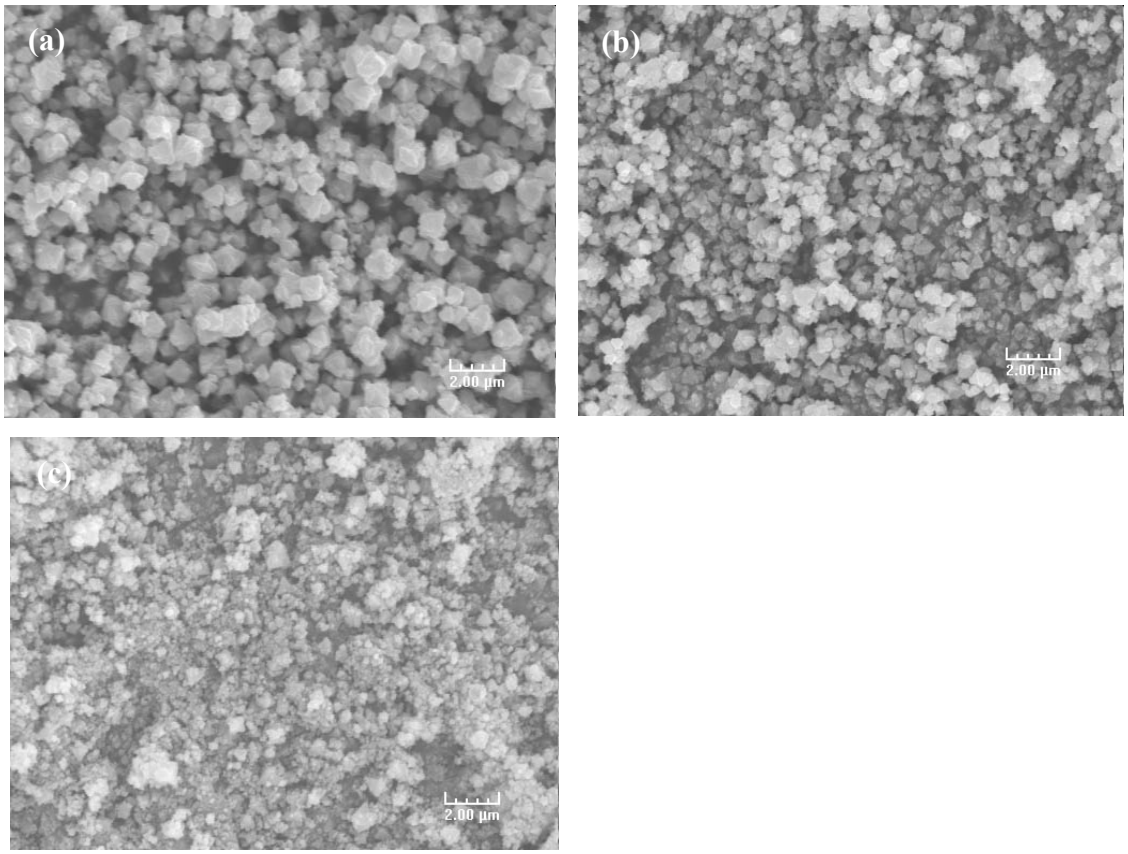

Figure 2.9 SEM images of particles formed by reactions between (a) 0.01 M $FeCl_3$/0.02 M NaHS, (b) 0.05 M $FeCl_3$/0.1 M NaHS, and (c) 0.1 M $FeCl_3$/0.2 M NaHS.

CHAPTER III

ARSENIC REMOVAL BY SYNTHESIZED PYRITE

3.1 Introduction

Arsenic is a naturally occurring toxic element having adverse effects on human health. Exposure of humans to elevated concentrations of arsenic in drinking water posses significant health risks, such as Blackfoot disease, skin, lung and bladder cancers, and disorders of the immune, nervous and reproductive systems (3). Arsenic is present as a major constituent of many minerals including sulfides and oxides such as realgar (As_4S_4), orpiment (As_2S_3), arsenopyrite (FeAsS), arsenolite (As_2O_3), and scorodite ($FeAsO_4 \cdot 2H_2O$). Arsenic can be released to the surface and subsurface water by natural processes such as weathering and sedimentation and by human activities such as mining, smelting, burning of fossil fuels, and applying agricultural chemicals. In water, arsenic occurs as different protonated oxyanionic forms depending on redox condition and pH. Trivalent arsenite ($H_nAsO_3^{n-3}$, n=0-3) generally exists in reduced conditions such as groundwater and pentavalent arsenate ($H_nAsO_4^{n-3}$, n=0-3) is dominant in oxidized conditions such as natural surface water (1).

Mineral-water interactions play important roles in controlling the fate and transport of arsenic in natural water (1,5,6). Oxides of iron, aluminum, and manganese are known to be the major minerals controlling arsenic concentration in aquifers, because of their chemistry and abundance (1,5,6). Among oxides, iron oxides are considered as the most important sinks for arsenic; therefore, the interactions of arsenic

with iron oxide minerals, such as hydrous ferric oxide (HFO), goethite, and hematite, have been extensively investigated (7-9). Under reduced conditions, however, reductive dissolution of iron oxides containing arsenic is also considered as an important source of arsenic in natural water (1,6,10).

Sulfide minerals have been suggested to play an important role in regulating dissolved metal concentrations in anoxic environments (11-13,47,48). The examination of sediments in Milltown Reservoir (13) showed that vertical transition of redox states resulted in the shift in partitioning of arsenic from oxides into sulfides. Pyrite (FeS_2) is the most common sulfide mineral, which plays an important role as an electron source in geochemical processes in the environment (15). Natural pyrite contains various amounts of trace elements such as arsenic (As), lead (Pb), cobalt (Co), nickel (Ni), and selenium (Se) at concentrations that range from a few ppm to tens of thousands ppm. For example, arsenic contents in pyrite can vary between 2 and 96,000 ppm (16). Thus, interactions of trace elements with pyrite have received great attention.

A strong correlation between arsenic concentration and pyrite contents in marine sediments suggested capture of arsenic by pyrite (11). Investigation of the Clio mine samples showed that pyrite contains arsenic up to 3.9 wt.% and suggested that most arsenic is present as a solid solution in pyrite (17). Arsenic is suggested to substitute for sulfur in pyrite forming As-S dianion groups according to the X-ray absorption spectroscopy studies and the electronic structure calculations (17,18).

Farquhar et al. (19) investigated As(III) and As(V) adsorption on makinawite and pyrite in aqueous solution (pH 5.5-6.5) using X-ray absorption spectroscopy. Arsenic

species retained original oxidation states on the pyrite surface. Their study suggested formation of outer-sphere complexes by the interactions of arsenic with pyrite. On the other hand, Bostick et al. (20,21) suggested formation of strong inner-sphere complexes or surface precipitates by reactions between As(III) and pyrite. They suggested that initial formation of FeAsS-like precipitate might be followed by conversion to As_2S_3 by the reaction between As(III) and pyrite. Several other studies on interactions of arsenic with pyrite have been published (22,23). These studies have shown the affinity of pyrite for arsenic, but arsenic retention mechanisms are not fully understood yet.

The objective of this study is to investigate interactions of arsenic with pyrite in an anoxic environment. During arsenic-mineral interactions, simultaneous reactions might occur at particle-water interfaces, such as adsorption/desorption, precipitation, and oxidation/ reduction (49). Sorption reactions of arsenic on mineral surfaces are generally considered as the most important process controlling arsenic concentration and transport in natural water (1,5,6). In this chapter, arsenic removal by synthesized pyrite will be characterized using solution phase experiments and the surface of pyrite that has reacted with arsenic will be characterized using X-ray photoelectron spectroscopy (XPS), in order to investigate the possible formation of arsenic compounds.

3.2 Experimental Section

3.2.1 Materials

All solutions were prepared using deaerated and deionized water. This water was prepared by bubbling purified nitrogen gas through deionized water for at least 2 hours. Deionized water was obtained from a Millipore Milli-Q system (18 MΩ). Then the water was purged overnight in an anaerobic chamber containing a mixture of 5% hydrogen and 95% nitrogen gases. Arsenite (As(III)) and arsenate (As(V)) solutions were prepared by dissolving $NaAsO_2$ and $Na_2HAsO_4 \cdot 7H_2O$, respectively (Sigma-Aldrich).

Pyrite was synthesized in a glove box containing nitrogen gas. Iron and sulfide solutions were prepared by dissolving ferric chloride ($FeCl_3 \cdot 6H_2O$) and sodium hydrosulfide ($NaHS \cdot xH_2O$) in deaerated deionized water. The 0.1 M iron solution and the 0.2 M sulfide solution were mixed in a polypropylene bottle and the pH of the mixture was adjusted to pH 4.0 by adding 5 M NaOH or 5 M HCl. Then, the mixed solutions were placed in a conventional microwave oven (1150 W, 2.45 GHz) and allowed to react for 10 minutes at a setting of 20% (microwave power applied for 20% of the time). The reacted samples were rapidly cooled to room temperature by placing them in cold water. The solids were washed with HCl, acetone, and carbon disulfide. The solid products were identified as pyrite by XRD. The surface area for the particles was determined to be 15.9 m^2/g with a multipoint BET isotherm using N_2 as the adsorbate. Pyrite was dried and stored in the anaerobic chamber before use.

3.2.2 Removal Experiments

A completely mixed batch reactor system was applied in all experiments. All steps in the preparation of samples and their reaction were carried out at room temperature in an anaerobic atmosphere containing 5% hydrogen and 95% nitrogen.

The pyrite suspension was allowed to react with arsenic under various conditions. The effect of pH on removal was investigated by adjusting the pH from pH 2 to pH 11 using 0.1 M HCl or 0.1 M NaOH. The suspensions were continuously mixed on a shaker at 8 rpm for 24 hours during these experiments. After reaction, the suspensions were filtered through 0.2-μm membrane filters and pH of the solutions was measured immediately. The final pH was reported.

Removal experiments were conducted by varying initial concentrations of As(III) and As(V) between 0 and 1000 μM. Variation in pH was minimized by using 0.01 M acetate (pH 4), MOPS (4-morpholinepropanesulfunic acid, pH 7), or CAPS (3-cyclohexylamion-1-propanesulfonic acid, pH 10) buffers. Experiments to evaluate the effect of competing anions were conducted by adding $Na_2HPO_4 \cdot 7H_2O$, Na_2SO_4, $NaNO_3$, and $Na_2SiO_3 \cdot 9H_2O$ as a source of phosphate, sulfate, nitrate, and silicate, respectively. Pyrite suspensions (1 g/L) were allowed to react with 100 μM of As(III) and As(V) in the presence of 0, 1, and 10 mM of anions. Sorption experiments were carried out in 20-mL polyethylene vials. The suspensions were continuously mixed on a shaker at 8 rpm for 24 hours. After reaction, the suspensions were filtered through 0.2-μm membrane filters.

Removal kinetics were investigated with pyrite suspensions prepared in 0.02 M buffer solutions (acetate, MOPS, CAPS) in 250-ml reaction vessels. Reactions were initiated by adding arsenic standard solution to a pyrite suspension. The suspension was agitated using a magnetic stirrer. A 10-mL aliquot was sampled from the suspension at each reaction time for up to 26 days. The samples were immediately filtered using 0.2-μm membrane filters, and the filtrates were stored at 2 °C until analysis. The effects of arsenic species, pH, pyrite dose, arsenic initial concentrations, and sulfide were investigated.

The concentrations of arsenic in filtrates were measured to determine extents of arsenic sorption and reaction. Arsenic was analyzed using an atomic absorption spectrometer coupled with continuous hydride generation system (HGAAS). Arsenic was reduced to arsine (AsH_3) gas by continuous flow of sodium borohydride (1.5% $NaBH_4$ in 0.5% NaOH). The arsine gas was transferred to the flame AA by argon carrier gas and its concentration was measured. The method detection limit (MDL) for As(III) was 0.18 μg/L and for As(V) was 0.85 μg/L.

3.2.3 X-ray Photoelectron Spectroscopy

The surfaces of arsenic-reacted pyrite were characterized by X-ray photoelectron spectroscopy (XPS) in order to investigate the oxidation states of arsenic, iron, and sulfur on the surface and the possible formation of arsenic compounds. The XPS spectra were obtained using Kratos Axis Ultra Imaging XPS with monochromatic Al K-α X-rays. Broad scan was obtained using 80 eV pass energy, while narrow high resolution scans of As 3d, Fe 2p, and S 2p were obtained using 40 eV pass energy.

The charge effect was corrected using C 1s from contamination at 284.5 ± 0.1 eV. The obtained spectra were fitted using a curve-fitting program (XPSPEAK41). The spectra were fitted using a least-squares procedure with peaks of 80% of Lorentzian-Gaussian peak shape after subtraction of a Shirley baseline. The component peaks were identified by comparison their binding energies with literature values (Table 3.1).

Table 3.1 XPS binding energies of Fe2p, S2p and As 3d for chemical species reported in the literature

	Species	Binding energy (eV)	References
Fe ($2p_{3/2}$)	Fe(II)-S	707.2	Bostick and Fendorf (21)
		707.0 (FeS_2 bulk), 706.05, 707.95	Nesbitt and Muir (38)
		707.5 ± 0.2	Bonnissel-Gissinger et al. (39)
		706.5, 707.45, 708.4	Pratt et al. (40)
	Fe(III)-S	709.3	Bostick and Fendorf (21)
		708.75, 709.85, 710.85, 711.75	Nesbitt and Muir (38)
	Fe(III)-OH	711.3	Bostick and Fendorf (21)
		710.3, 711.3, 712.4, 713.45	Nesbitt and Muir (38)
S ($2p_{3/2}$)	FeS_2 (bulk)	162.6	Bostick and Fendorf (21)
	FeS	160.8	NIST XPS database
	S_2^{2-}	162.4	Nesbitt and Muir (38)
		162.4 - 162.5, 162.7	Bonnissel-Gissinger et al. (39)
	S^{2-}	161.2	Bostick and Fendorf (21)
		161.65	Nesbitt and Muir (38)
		161.1, 161.3	Bonnissel-Gissinger et al. (39)
	Polysulfide	163.8, 163.2	Bostick and Fendorf (21)
		163.6	Nesbitt and Muir (38)
		165.3, 164.2, 163.8	Bonnissel-Gissinger et al. (39)
	$S_2O_3^{2-}$	166.8, 166.9	Bostick and Fendorf (21)
		166.45	Nesbitt and Muir (38)
	SO_4^{2-}	169.1, 169.0	Bostick and Fendorf (21)
		168.25	Nesbitt and Muir (38)
		169.1, 168.5	Bonnissel-Gissinger et al. (39)
As ($3d_{5/2}$)	As(-I)-S	41.2	Nesbitt et al (50)
	As(0)	41.8	Nesbitt et al (50)
	As_4S_4	43.1	Bullen et al (51), NIST XPS database (52)
	As_2S_3	43.4, 43.5	Bullen et al (51), NIST XPS database (52)
	As_2S_5	44.4	NIST XPS database (52)
	As(I)-O	43.47	Nesbitt et al (50)
	As(III)- O	44.54, 44.4	Nesbitt et al (50,53)
	As(V)-O	45.28, 45.15	Nesbitt et al (50,53)

3.3 Results and Discussion

3.3.1 Removal Kinetics

3.3.1.1 Effect of pH

Pyrite was reacted with As(III) and As(V) for an extended period of time at various pH and the concentrations in solution determined (Figure 3.1). At pH 7 and 10, dissolved As(III) concentration rapidly decreased at the beginning of the experiment. Nearly 65% of the amount of As(III) removed after 120 hours was removed within the first 5 minutes at pH 7, and about 50% was removed within the first hour at pH 10. As(III) removal at pH 7 and 10 was nearly complete within 24 hours with only slight changes of concentrations observed after that time. On the other hand, As(III) removal at pH 4 was slower than at pH 7 and 10 at the early stage of removal, but it continued to occur until complete removal was achieved. Slight removal of As(V) at pH 7 and 10 occurred within the first 5 minutes and further removal was not observed for an extended period time. On the other hand, As(V) concentration at pH 4 decreased almost linearly with time over the extent of the experiment.

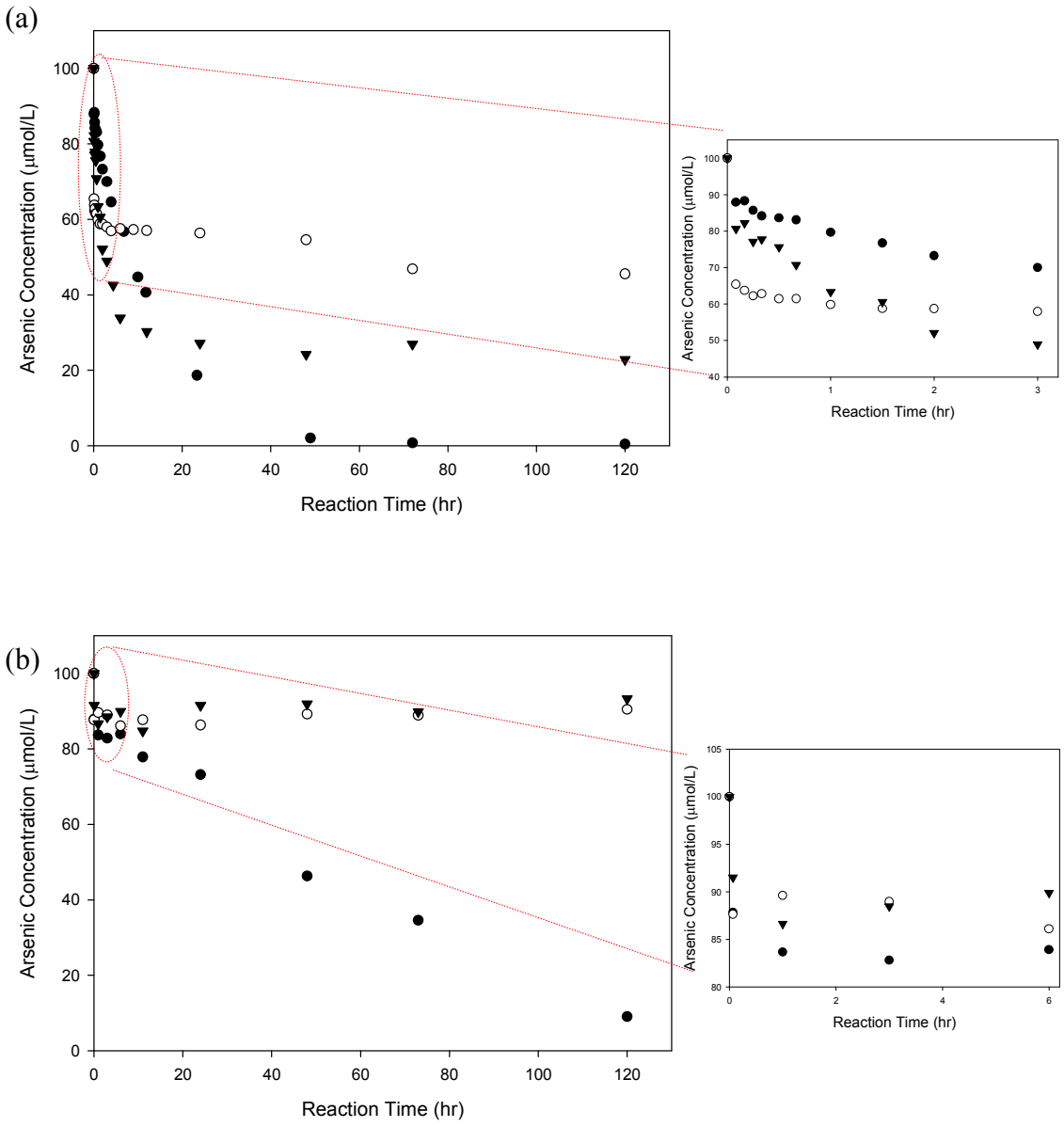

Figure 3.1 Arsenic concentrations over time in presence of pyrite. Initial concentration of arsenic =100 µM. dose of pyrite = 1 g/L, (a) As(III), (b) As(V) (● pH 4, ○ pH 7, ▼ pH 10).

The kinetics of removal can be interpreted using different kinetic models. Here, the kinetic data were analyzed using pseudo-first-order, pseudo-second-order, and Elovich rate equations. These rate equations were combined with a material balance equation for a batch reactor to produce differential equations that can be solved to predict how concentrations change with time. The material balance combined with a pseudo-first-order equation is generally expressed as:

$$\frac{dq_t}{dt} = k_1(q_e - q_t) \qquad (3.1)$$

where, q_e and q_t are solid-phase concentrations at equilibrium and at time t, respectively, and k_1 is the pseudo-first-order rate constant. The integrated form of the equation becomes:

$$q_t = q_e(1 - e^{-k_1 t}) \qquad (3.2)$$

The pseudo-second-order equation combined with a material balance equation for a batch system is:

$$\frac{dq_t}{dt} = k_2(q_e - q_t)^2 \qquad (3.3)$$

where k_2 is the pseudo-second-order rate constant. When the equation is integrated, it becomes:

$$q_t = \frac{k_2 q_e{}^2 t}{1 + k_2 q_e t} \qquad (3.4)$$

The Elovich equation has been extensively applied to describe the kinetics of adsorption on minerals (54,55). The rate of sorption is commonly observed to be very fast at first and then to become slower as equilibrium is reached. This equation has been known to

fit this behavior well and has been applied for chemisorption kinetics. The Elovich equation combined with a batch material balance is expressed as:

$$\frac{dq_t}{dt} = \alpha e^{-\beta q_t} \qquad (3.5)$$

where α and β are constants. The constant α is the initial rate. The integrated form of this equation is:

$$q_t = \frac{1}{\beta}\ln(\alpha\beta t + 1) \qquad (3.6)$$

These three kinetic models were applied to describe the kinetic data for removal of As(III) and As(V) . For As(V), only the data at pH 4 were analyzed, since no concentration changes were observed during reaction at pH 7 and pH 10. Plots of the data for As(III) at pH 4, pH 7, and pH 10 with predictions by the three kinetic models are shown in Figure 3.2. Data for As(V) at pH 4 with predictions of the three kinetic models are shown in Figure 3.3. The constants and correlation coefficients calculated by nonlinear regression analysis are summarized in Table 3.2.

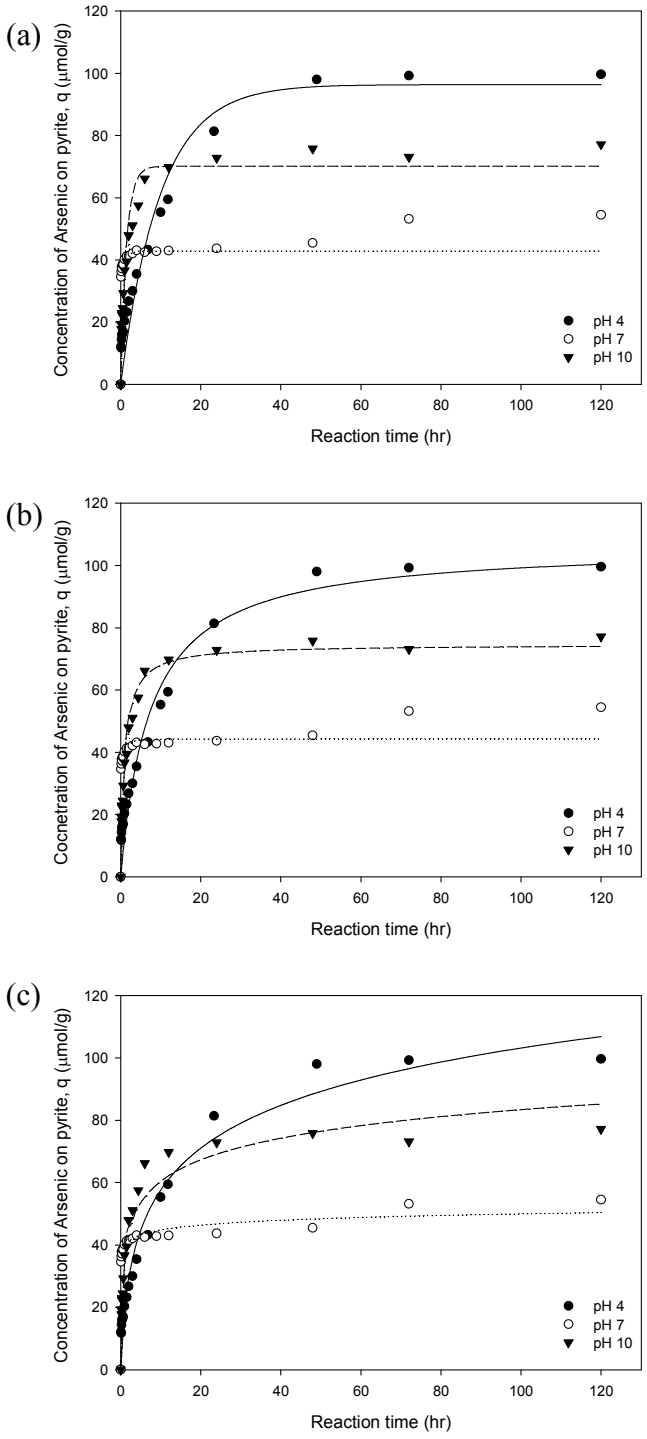

Figure 3.2 Kinetics of As(III) removal by pyrite at pH 4, 7, and 10 fitted by (a) pseudo-first order, (b) pseudo-second order, and (c) Elovich equations.

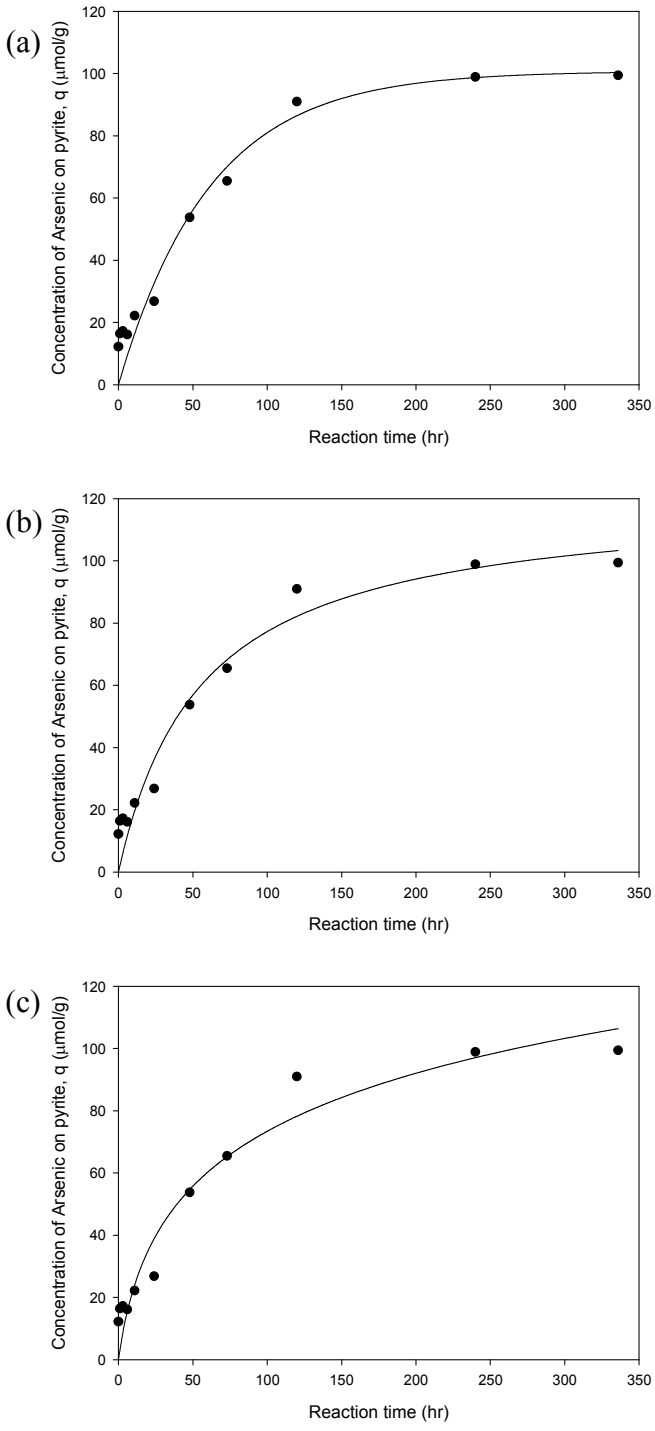

Figure 3.3 Kinetics of As(V) removal by pyrite at pH 4 fitted by (a) pseudo-first order, (b) pseudo-second order, and (c) Elovich equations.

Table 3.2 Results of fitting kinetic models to data of As(III) and As(V) removal at different pH[a]

Equation	parameter	As(III)			As(V)
		pH4	pH 7	pH 10	pH 4
Pseudo first order	k_1 (hr^{-1})	0.101 (±30.9%)	15.8 (±59.3%)	0.684 (±33.1%)	0.016 (±41.4%)
	q_e (μmol g^{-1})	96.4 (±10.7%)	42.8 (±5.82%)	70.1 (±9.05%)	101 (±14.6%)
	r^2	0.933	0.826	0.908	0.948
Pseudo second order	k_2 (g hr^{-1} μmol^{-1})	0.00126 (±43.6%)	0.592 (±71.1%)	0.0138 (±32.5%)	0.000148 (±80.2%)
	q_e (μmol g^{-1})	107 (±10.7%)	44.4 (±5.36%)	74.6 (±9.05%)	121 (±20.6%)
	r^2	0.954	0.882	0.960	0.946
Elovich	α (μmol g^{-1} hr^{-1})	32.7 (±38.8%)	1.18.E+08 (±367%)	416 (±65.7%)	3.5 (±75.1%)
	β (g μmol^{-1})	0.0493 (±15.4%)	0.448 (±20.5%)	0.100 (±14.8%)	0.0351 (±38.8%)
	r^2	0.969	0.970	0.953	0.941

[a] Uncertainties represent 95% confidence limits expressed in % relative to estimate for parameters

All three models describe the data well, as shown by their good correlation coefficients ($r^2 > 0.90$), except for the pseudo-first-order model with data for As(III) at pH 7. The correlation coefficients showed that the Elovich equation yielded the best fit to data for As(III) at pH 4 and pH 7. At pH 4 and pH 7, correlation coefficients increase in the order: pseudo-first order < pseudo-second order < Elovich. The pseudo-second-order equation yielded the best fit to data for As(III) at pH 10 and the Elovich equation yielded the second best fit. On the other hand, all three models fit the data for As(V) at

pH 4 relatively well and had similar correlation coefficients, but the correlation coefficients showed that the pseudo-first-order equation yielded the best fit.

Sorption of inorganics to minerals has been reported as two-step process (56-58). Rapid initial uptake is followed by slow uptake processes. The first step involves sorption to external sites, and slow second step can include the formation of the multinuclear surface complexes, the formation of solid solutions and surface precipitates, particle-particle interactions, adsorbate diffusion into the interior of porous particles, and other slow chemical reactions (56-58). Initially, arsenic would be removed by sorption to the external sites of pyrite rapidly. Then reaction on the pyrite surface such as formation of arsenic sulfide and surface precipitates would follow.

The rate constants obtained from each kinetic model showed distinct differences at different pH and between arsenic species. The coefficient in the Elovich equation (α) that should equal the initial rate of removal is extremely high in the fit to data using As(III) at pH 7. At this pH, nearly 65% of the amount of As(III) removed after 120 hours was removed within the first 5 minutes and only slight changes of concentrations were observed after that time. Within the first 5 minutes initial As(III) removal is much faster than removal at later times, so a slight change of reaction time could cause a big difference in the ability to accurately calculate coefficients during a regression. This might have led to an extremely high initial rate coefficient value and its large 95% confidence limit. The rates of arsenic removal by pyrite are in the order: As(III) at pH 7 >> As(III) at pH 10 > As(III) at pH 4 > As(V) at pH 4. Arsenic removal at pH 7 and pH 10 was nearly complete within several minutes and several hours, respectively, and

further removal was limited. This rapid removal at pH 7 and pH 10 indicates that arsenic was removed mainly by rapid sorption to external sites at these pH ranges. On the other hand, the kinetics of arsenic removal on pyrite at pH 4 was different from the kinetics at pH 7 and at pH 10. It was also different from common chemisorption kinetics, which typically shows faster removal at early times and slower removal at later times. The kinetics of As(III) removal by pyrite at pH 4 was slower than at pH 7 or pH 10 during the early stage of removal, but removal continued to occur until all As(III) was removed. This was also observed for As(V) removal by pyrite at pH 4. Arsenic removal by pyrite at low pH seems to be controlled mainly by the second slow uptake processes. As(V) removal was slower than As(III) removal. This might be due to additional reduction reactions that As(V) would undergo in the formation of arsenic sulfide precipitates.

3.3.1.2 Effect of As(III) Initial Concentrations

The kinetics of As(III) removal at pH 4 were further investigated with various As(III) initial concentrations. The kinetics of As(III) removal by pyrite at three initial As(III) concentrations of 20, 100, and 500 μM are illustrated in Figure 3.4. The constants and correlation coefficients calculated by nonlinear regression analysis are

summarized in Table 3.3. Nearly complete removal of As(III) was reached within 48 hours and 96 hours for 20 μM and 100 μM As(III) initial concentration, respectively. For 500 μM, arsenic removal continued to occur during the experiment and was expected to continue for an extended time period. The equilibrium solid-phase concentration was estimated to be about 500 μmol/g using the pseudo-first-order equation, which yielded the best fit (Table 3.3).

The pseudo-first- and second-order rate constants decreased as initial arsenic concentrations increased and the change was in proportion to the change in concentration. However, there was little change in α, which is the coefficient in the Elovich equation that should equal the initial rate, among different initial concentrations. This suggests that the rate of arsenic sorption to the external sites of pyrite, which governs initial rate, doesn't seem to be affected by initial arsenic concentration, but the rate of consequent surface reaction may be lowered at higher concentrations.

Table 3.3 Results of fitting kinetic models to data for removal of As(III) at different As(III) initial concentrations [a]

Equation	Parameter	Initial As(III) Concentration		
		20 μM	100 μM	500 μM
Pseudo first order	k_1 (hr^{-1})	0.094 (±17.4%)	0.033 (±13.5%)	0.0058 (±69.2%)
	q_e (μmol g^{-1})	19.9 (±5.51%)	101 (±5.96%)	503 (±49.8%)	
	r^2	0.985	0.995	0.984
Pseudo second order	k_2 (g hr^{-1} μmol^{-1})	0.00504 (±32.3%)	2.53.E-04 (±36.2%)	3.69.E-06 (±149%)
	q_e (μmol g^{-1})	22.4 (±7.74%)	125 (±10.9%)	891 (±63.6%)	
	r^2	0.980	0.991	0.983
Elovich	α (μmol g^{-1} hr^{-1})	4.60 (±54.4%)	4.96 (±34.3%)	2.94 (±26.3%)
	β (g μmol^{-1})	0.220 (±22.4%)	0.0292 (±24.7%)	0.00254 (79.4%)	
	r^2	0.951	0.982	0.982

[a] Uncertainties represent 95% confidence limits expressed in % relative to estimate for parameters

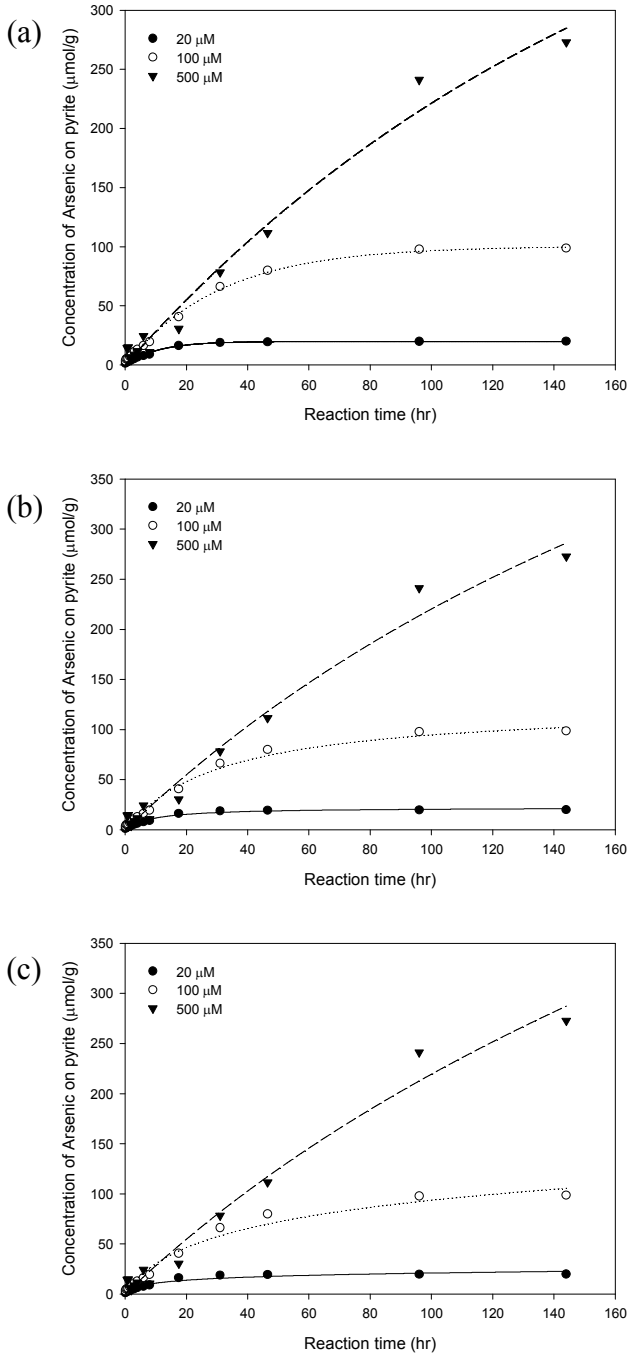

Figure 3.4 Kinetics of As(III) removal by pyrite (1 g/L) at As(III) initial concentrations of 20, 100, and 500 μM and at pH 4 with model fits using (a) pseudo-first order, (b) pseudo-second order, and (c) Elovich equations.

3.3.1.3 Effect of Pyrite Dose

The kinetics of As(III) removal at pH 4 were further investigated with different pyrite doses (Figure 3.5). As(III) (100 μM) was reacted with pyrite doses of 0.35 g/L and 1 g/L for 25 days (600 hours). With a pyrite dose of 1 g/L, As(III) removal was nearly completed within 5 days and remained on the solid for extended time periods. With a pyrite dose of 0.35 g/L, As(III) continued to be removed for up to 25 days, at which time almost complete removal was achieved. Fast removal was achieved with a high dose of pyrite. Arsenic removal with a low dose of pyrite was slower than with a high dose of pyrite, but continued to occur until complete removal was achieved. At the last sampling time, the solid-phase concentration of As(III) in experiments with pyrite dose of 0.35 g/L was about 2.5 times higher than that in experiments with a pyrite dose of 1 g/L.

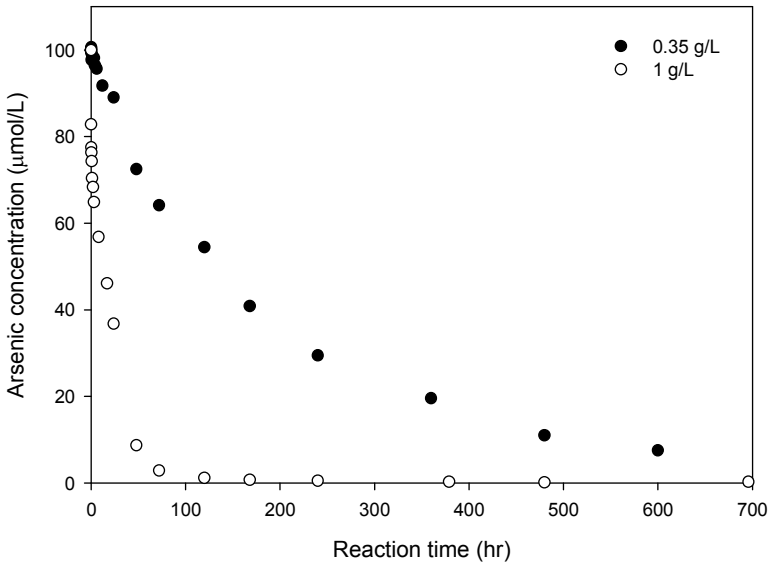

Figure 3.5 Kinetics of As(III) removal by different doses of pyrite (0.35 and 1 g/L) using an initial As(III) concentration of 100 μM.

3.3.1.4 Effect of Sulfide

Addition of sulfide may influence arsenic removal by pyrite by forming arsenic sulfides like orpiment. Sulfide at concentrations of 0, 1 and 10 mM was added with arsenic to suspensions containing 1 g/L pyrite at pH 4 and allowed to react for 24 hours (Figure 3.6). Arsenic concentrations decreased over time in the absence of sulfide, but the addition of sulfide caused an initial decrease in arsenic concentration of about 50%. However, addition of 10 mM of sulfide initially decreased arsenic concentration rapidly, but further removal was minimal over the 24-hr reaction time.

Arsenic could be removed by sorption to the external sites of pyrite and subsequently undergo surface reactions like surface precipitation of arsenic sulfide or other solid phases. Arsenic removal by surface precipitation of arsenic sulfide solid phases on pyrite can occur by initial arsenic surface complexation followed by partial dissolution of pyrite and subsequent reaction of the released sulfide ions and the sorbed arsenic (59). Without added sulfide, arsenic concentration continually decreased, possibly by formation of arsenic sulfide surface precipitates by the reaction with sulfide ions released by partial pyrite dissolution. Addition of sulfide may initially stimulate the precipitation of arsenic sulfide solid phases, which could cause the initial decrease in arsenic concentration. However, addition of higher concentrations of sulfide decreased further arsenic removal after an initial decrease (Figure 3.6). Equilibrium calculations using Visual Minteq showed that the presence of higher concentrations of sulfide in solution increased concentrations of soluble arsenic sulfide complexes. About 30% of the arsenic was present as soluble arsenic sulfide complexes with 10 mM sulfide

addition, while almost 100% of the arsenic precipitated as As_2S_3(am) with 1 mM sulfide addition. Addition of sulfide may improve arsenic removal by stimulating the precipitation of arsenic sulfide solid phases. However, the higher level of sulfide addition could form soluble arsenic sulfide complexes, which could lower arsenic removal rate from the solution.

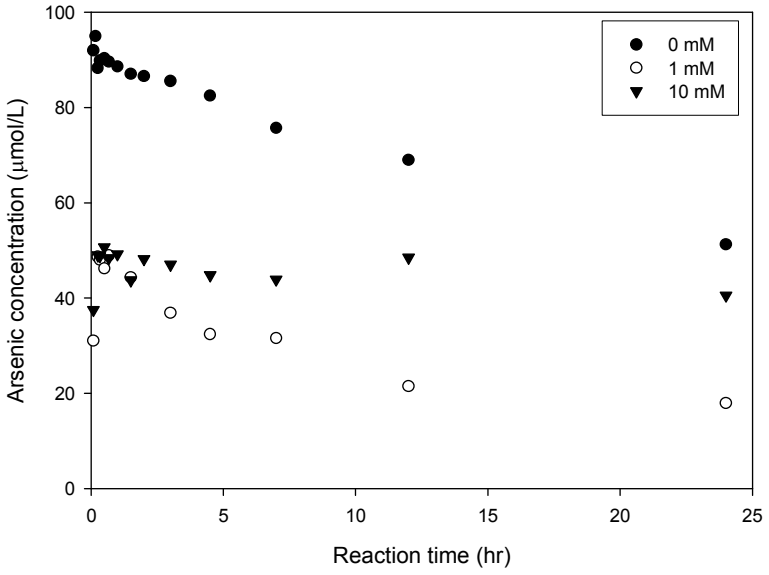

Figure 3.6. Effect of sulfide on removal of As(III). 100 µmol/L of As(III) was reacted with 1 g/L pyrite.

3.3.2 Arsenic Removal Characteristics

3.3.2.1 Effect of pH on Extent of Removal

Since pH is an important factor affecting cation and anion adsorption, the effect of the solution pH on arsenic removal by pyrite was studied over the pH range of pH 2 to pH 12. The results of these experiments are shown in Figure 3.7 and show that arsenic removal was strongly dependent on solution pH. Both As(III) and As(V) have a strong affinity for the pyrite surface at low pH. Arsenic removal was highest at the lowest pH and it decreased with increasing pH. As(III) removal sharply decreased between pH 3 and pH 7. As(III) removal dropped to 20% near pH 9 and removal increased above pH 9. As(V) removal dropped more sharply than As(III) between pH 2 and pH 6. As(V) removal was almost negligible (<10%) when pH increased above pH 5.5.

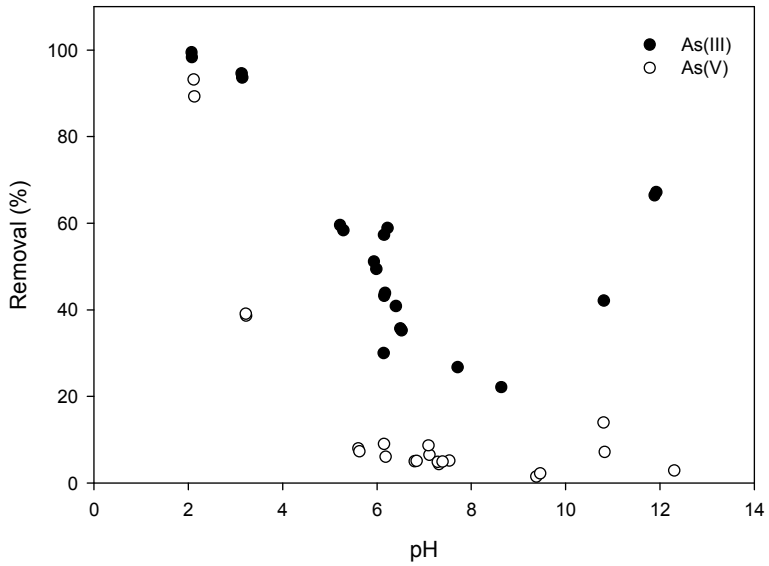

Figure 3.7 Effect of pH on removal of As(III) and As(V) by pyrite. 100 μmol/L of arsenic was reacted with 1 g/L pyrite.

The preliminary experiments showed that slight oxidation of pyrite surface could cause quite different results for arsenic removal. The preliminary removal experiments were conducted under aerobic conditions even though all solutions and pyrite were prepared under anaerobic conditions, so slight oxidation of pyrite was expected during reaction. In these experiments, As(III) removal by pyrite increased with increasing pH until pH 7 and maximum removal was achieved in the range pH 7 to pH 9. Removal of As(III) slightly decreased at pH above pH 9.

The results of the current study are quite different from those that have been previously reported for As(III) removal by pyrite and by iron oxides. As(III) removal on pyrite was reported to be lowest at low pH and highest at alkaline pH (20-22), while As(V) removal was reported to be higher at acidic pH and lower at alkaline pH ($3<pH<9$) (22). These previous results seem to resemble more the results of arsenic removal by iron oxides than the results of the current study. As(III) removal by iron oxides increases with increasing pH until a broad maximum was reached at neutral and alkaline pH, i.e. in the range pH 6 to pH 10. On the other hand, As(V) removal by iron oxides is strong at acidic pH and decreases with increasing pH (7,8). However, it should be mentioned that some experimental conditions used in previously reported studies by others are different from those used in this study, so direct comparisons do not seem to be possible. Zouboulis et al. (22) studied arsenic removal with pyrite collected from a mine under aerobic conditions and they mentioned that a superficial layer on the pyrite surface was oxidized. Therefore, the oxidized pyrite surface might cause different results as was indicated by the results of the preliminary experiments conducted in this research.

Bostick et al (20,21) conducted experiments under anaerobic conditions and they were cautious to prevent pyrite oxidation. They reacted As(III) with pyrite for only 30 minutes, while arsenic was reacted with pyrite for 24 hrs in the current study. The kinetic data in this study showed slow removal at acidic pH and fast initial removal at neutral and alkaline pH. Thus, different reaction times might cause different results for removals.

In the systems containing arsenic and pyrite, pH affects both the soluble arsenic species and the surface charge of pyrite. For As(III), $H_3AsO_3^0$ is dominant up to pH 9.2, and $H_2AsO_3^-$ is dominant between pH 9.2 and pH 12 (1). As(V) exists in solution as $H_2AsO_4^-$ between pH 2.2 and pH 6.9, and $HAsO_4^{2-}$ between pH 6.9 and pH 11.5. $H_3AsO_4^0$ and AsO_4^{3-} are present in extremely acidic and alkaline conditions, respectively (1). Thiol (≡S-H) and metal hydroxide (≡Fe-OH) groups have been known to be the primary functional groups on the pyrite surface (39,60). Under acidic conditions, thiol groups are believed to play an important role in the reactivity of pyrite both in initial removal and subsequent surface reactions (39). At low pH, the protonation of the pyrite surface makes it less negatively charged, while at high pH, the deprotonation of the surface makes it more negatively charged. The point of zero charge (pzc) of synthesized pyrite was reported at pH 2.3 (60). Meanwhile, the pzc for oxidized natural pyrite was reported to be between pH 6 and pH 7 (61). Therefore, above pH 2.3, the pyrite surface would be negatively charged if it were not oxidized, but a positively charged surfaces might be observed at higher pH if the surface were oxidized.

As discussed in the kinetic section (3.3.1.1), arsenic removal by pyrite can be interpreted as a two-step process, in which rapid adsorption on the external surface is the first step and subsequent slow surface reaction to form multinuclear surface complexes and surface precipitates is the second step. The dependence on pH of surface charge and speciation of functional groups on the pyrite surface seems to affect both arsenic adsorption and subsequent surface reaction. Removal of As(V) was more sensitive to pH change than was As(III). As(V) in solution is present in a negatively charged form above pH 2.2, where the pyrite surface is negatively charged. Therefore, as the pH is raised above pH 2.2, there would be greater repulsive electrostatic forces as the surface charge became more negative, resulting in reduced removal. Meanwhile, As(III) is present as a neutral species below pH 9.2. The major functional group on the surface of pyrite would be the thiol group (≡S-H) under acidic conditions (39,60). Therefore, under acidic conditions, arsenic in the solution might be removed by adsorption and subsequent reaction with thiol groups of pyrite surface forming arsenic sulfide such as orpiment (As_2S_3). The surface reaction in acidic condition will be discussed more in the X-ray spectroscopic investigation section. The decrease of sorption with increasing pH could be explained by the decrease of thiol group on the surface and increasing orpiment solubility with increasing pH (62). Equilibrium calculations using Visual Minteq showed increased soluble arsenic sulfide complexes at neutral to basic pH values. The increased removal of As(III) above pH 9 might be due to the sorption onto iron hydroxide (≡Fe-OH) groups, which are the primary functional groups on the pyrite surface at high pH.

3.3.2.2 Effect of Arsenic Concentration

The effect of the arsenic concentration on arsenic removal by pyrite (1 g/L) was studied by varying initial concentrations of As(III) and As(V) between 0 and 1000 μM. Sorption isotherms are used to describe equilibrium relationships between the sorption density and soluble sorbate concentration at given temperature (63). Langmuir, BET and Freundlich isotherms are commonly used to explain experimental equilibrium sorption data and characterize sorbent surfaces. The sorption isotherm equations and parameters are:

Langmuir isotherm:

$$q = \frac{q_{\max} b C_e}{1 + b C_e} \qquad (3.7)$$

BET isotherm:

$$q = \frac{q_{\max} k_1 \frac{C_e}{k_2}}{(1 - \frac{C_e}{k_2})(1 + (k_1 - 1)\frac{C_e}{k_2})} \qquad (3.8)$$

Freundlich isotherm:

$$q = K C_e^{1/n} \qquad (3.9)$$

where C_e is the equilibrium concentration (μmol/L), q is the sorption density (μmol/g), $q_{\max}$ is the maximum possible sorption density, and b is the affinity of the sorbent on the sorbate. k_1 measures the affinity of the sorbent for the surface and k_2 indicates the

solubility of sorbent. *K* describes the adsorption density under standard conditions and *n*, indicates how the binding strength changes as the sorption density changes.

The experiments on removal of arsenic used a reaction time of one day. Conditions of apparent steady state and equilibrium appeared to be reached within one day for experiments at pH 7 and pH 10, but were not reached in experiments at pH 4 during the experiment. This applies to both As(III) and As(V). Therefore, the data from the experiments at pH 4 with As(III) and As(V) cannot be used to develop equilibrium relationships between concentrations of arsenic on the solid and in solution. However, these three equations were applied to describe the data from experiments with As(III) and As(V).

Figure 3.8 shows how the Langmuir, BET, and Freundlich equations fit data for As(III) on pyrite at pH 4, 7, and 10. Figure 3.9 shows them for As(V) on pyrite at pH 4. The isotherm constants and correlation coefficients calculated by nonlinear regression analysis are summarized in Table 3.4. All three relationships describe the data well as measured by their good correlation coefficients ($r^2 > 0.89$). However, the correlation coefficients showed that the BET equation yielded the best fit to most of the experimental data and the Langmuir equations had the worst fit for all cases.

The Langmuir equation describes the interaction with the surface as occurring in a single monolayer and doesn't consider interactions between molecules on the surface. It exhibits saturation of removal capacity in a monolayer surface, which is expressed as maximum possible sorption density, q_{max} in equation (1). However, in these experiments, removal of arsenic continued to increase as dissolved arsenic concentration increased

rather than approaching maximum values. Especially at pH 7 and pH 10, arsenic removal was enhanced greatly at the highest solution arsenic concentrations. This indicates that surface reactions such as surface precipitation might be occurring at high arsenic/pyrite ratios and this behavior cannot be described by the Langmuir equation.

As(III) removal by pyrite was affected by pH. The amount of As(III) removed per mass of pyrite was highest at pH 4, which was about twice that observed at pH 7 and pH 10. Concentrations of As(III) on pyrite were similar at pH 7 and pH 10 when the concentration in solution was higher, but concentrations of As(III) on pyrite were higher at pH 7 than pH 10, when concentrations in solution were lower. According to the BET model, the maximum solid-phase concentrations of As(III) on pyrite were 75.2, 39.7, and 35.5 μmol/g at pH 4, pH7, and pH 10, respectively. Figure 3.10 shows the relationship of solid-phase and solution-phase concentrations of As(III) and As(V) on pyrite at pH 4. As(V) was removed to a lesser extent than As(III) at pH 4, with a maximum solid-phase concentration of 56.1 μmol/g.

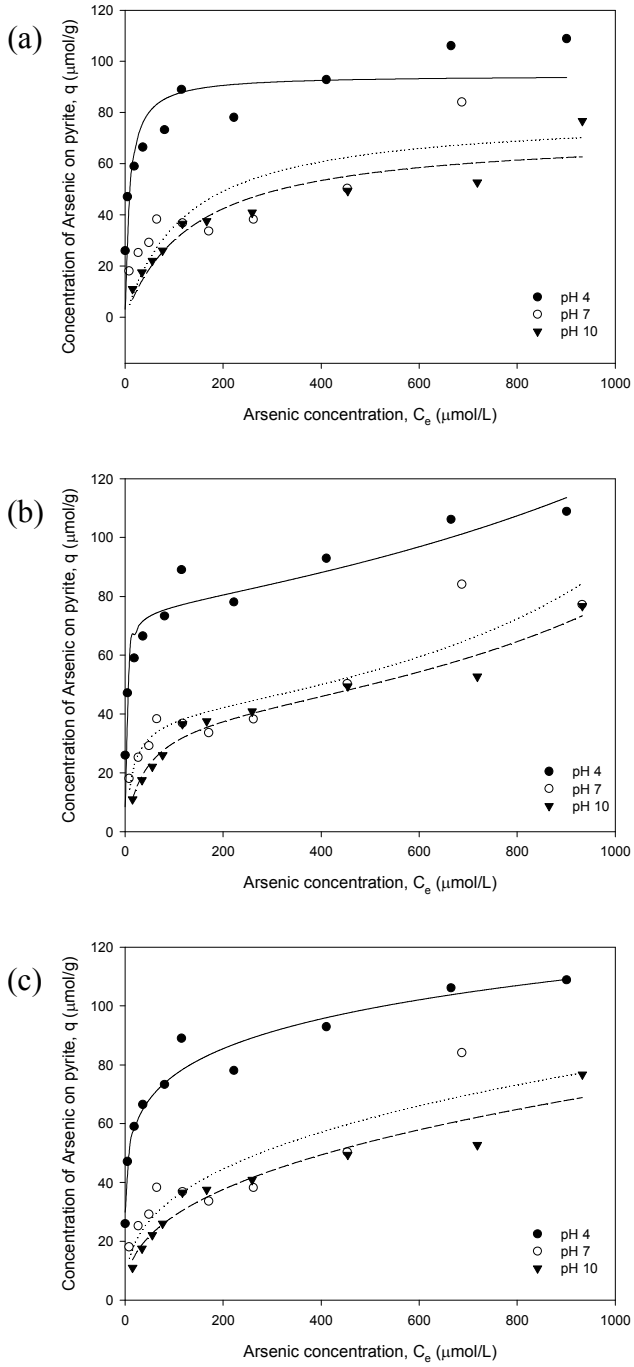

Figure 3.8 Relationship of concentration of As(III) on pyrite and in solution after 24 hr. Pyrite dose =1 g/L, initial concentration of As(III) = 25 to 1000 μmol/L, pH 4, 7, and 10. The lines are (a) Langmuir, (b) BET, and (c) Freundlich models.

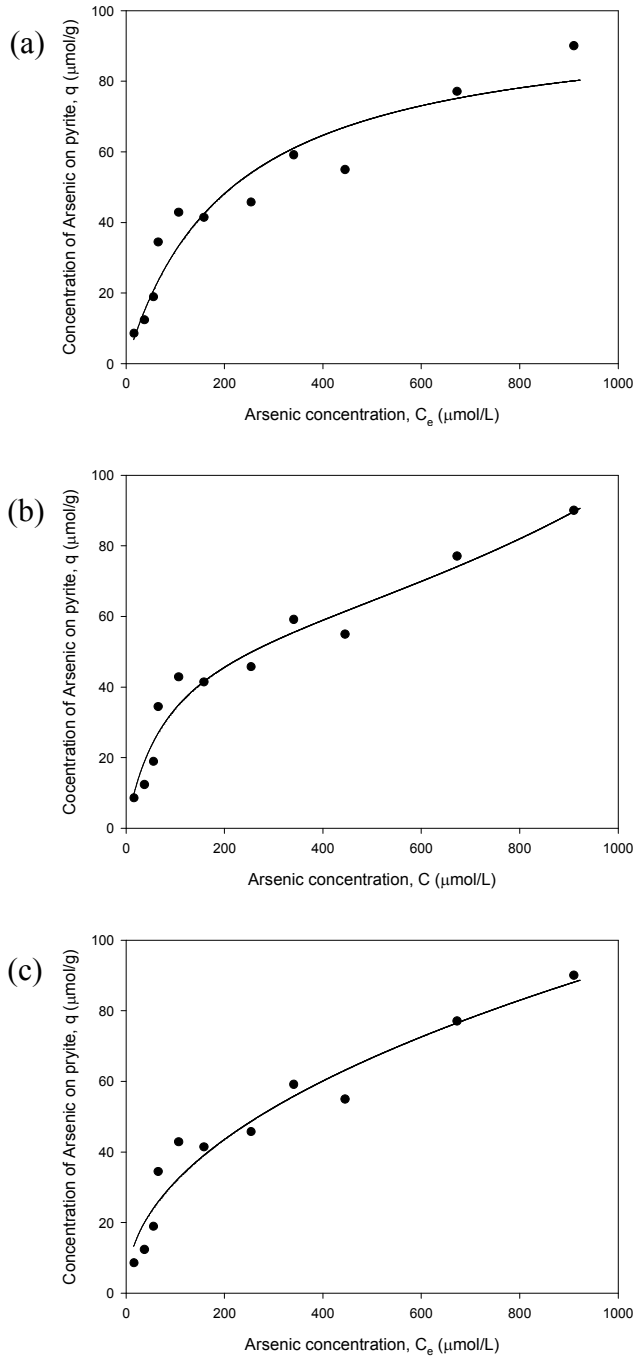

Figure 3.9 Relationship of concentration of As(V) on pyrite and in solution after 24 hr. Pyrite dose = 1 g/L, initial concentration of As(V) = 25 to 1000 μmol/L, pH 4. The lines are (a) Langmuir, (b) BET, and (c) Freundlich models.

Table 3.4 Results of fitting of Langmuir, BET, and Freundlich models to data at different pH

Model	Parameters	As(III)			As(V)
		pH 4	pH 7	pH 10	pH4
Langmuir	q_{max} (μmol/g)	94.6	79.4	72.2	98.5
	b (L/μmol)	0.113	0.00800	0.00714	0.00479
	r^2	0.976	0.942	0.891	0.970
BET	q_{max} (μmol/g)	75.2	39.7	39.5	56.1
	k_1	1110	122	49.9	29.3
	k_2 (μmol/L)	2660	1750	1970	2250
	r^2	0.990	0.975	0.970	0.978
Freundlich	K	36.3	6.74	4.69	3.72
	n	6.19	2.80	2.55	2.15
	r^2	0.996	0.974	0.938	0.975

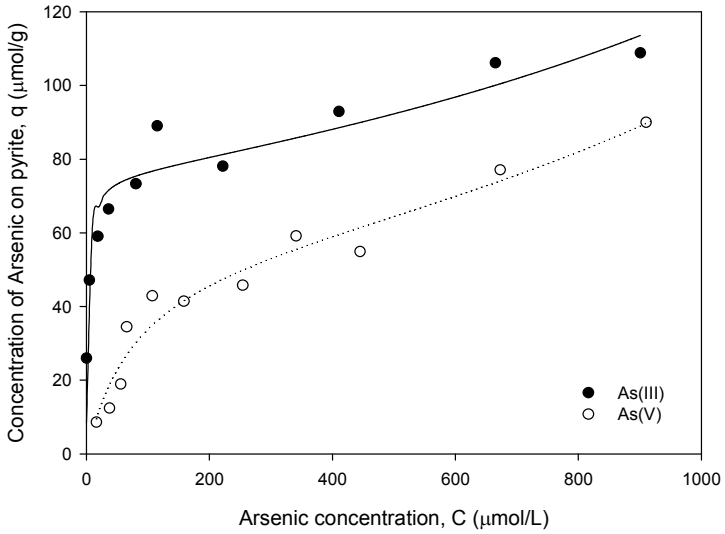

Figure 3.10 Relationship of concentrations of As(III) and As(V) on pyrite and in solution after 24 hr. Pyrite dose = 1 g/L, initial concentration of As(V) = 25 to 1000 μmol/L, initial concentration of As(III) = 25 to 1000 μmol/L, pH 4. The lines are the BET model fits.

3.3.2.3 Effect of Competing Anions

The competing effect of anions on arsenic removal by pyrite was evaluated with phosphate (PO_4^{2-}), sulfate (SO_4^{2-}), silicate (SiO_3^{2-}), and nitrate (NO_3^-) ions. Figure 3.11 presents the effect of individual anions at three concentration levels (0.1, 1, and 10 mM) on both As(III) and As(V) removal by pyrite at pH 4. Sulfate, nitrate, and silicate ions with concentrations up to 10 mM had no significant effect on As(III) removal. But, the presence of 1 mM of phosphate reduced the As(III) removal by pyrite from 74.9 % to 65.4% and 10 mM of phosphate reduced it to 24.5%. As(V) removal was more strongly affected by the presence of anions than As(III) removal. The presence of 10 mM of phosphate and silicate reduced the As(V) removal from 18.5% to 3.5% and 4.4%, respectively. Sulfate slightly decreased As(V) removal, while nitrate slightly increased As(V) removal.

Since phosphorous (P) and arsenic have similar atomic structure and chemical state, phosphate is reported to compete with arsenic in many natural and treatment system (1). Phosphate compete sorption sites with arsenic, which results reduced removal of both arsenite and arsenate by pyrite when phosphate was present. Silicate reduced only arsenate removal by pyrite. Sulfate and nitrate showed moderate or no effect on arsenic removal by pyrite, which indicates that pyrite has higher affinity for arsenic than sulfate and nitrate.

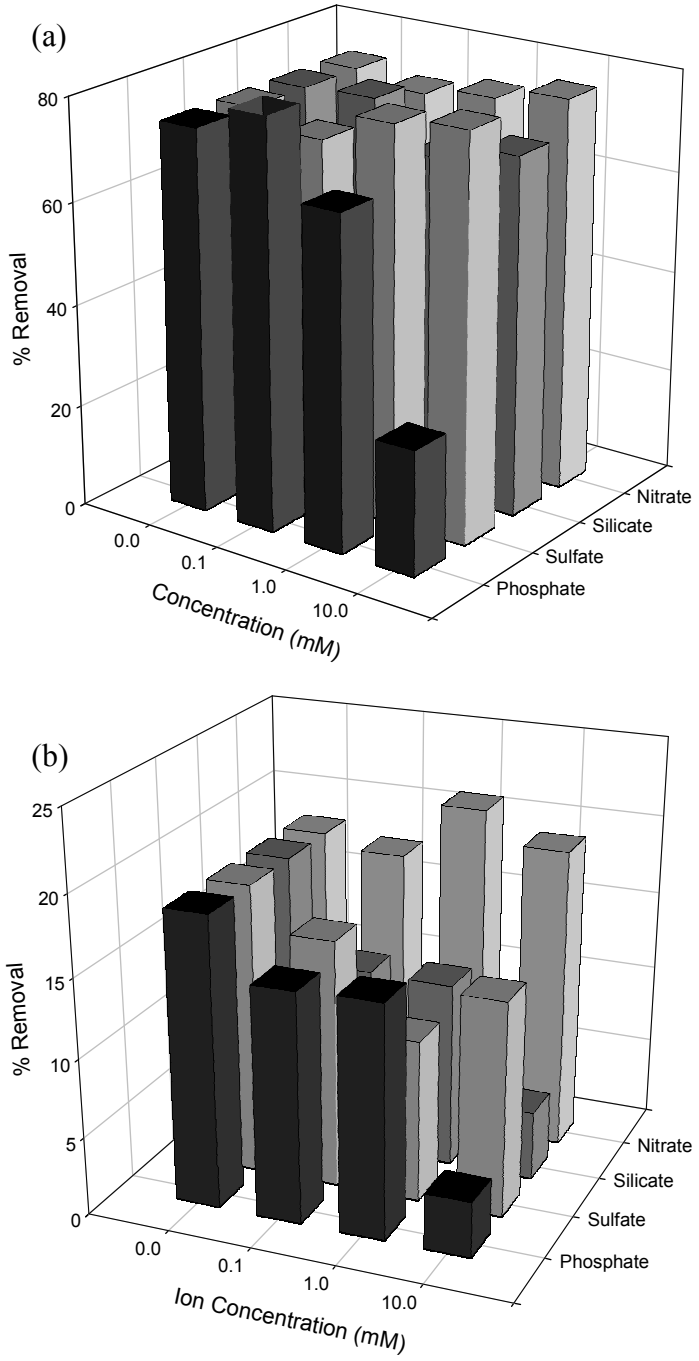

Figure 3.11 Arsenic removal in the presence of competing anions. (a) As(III), (b) As(V). 50 µmol/L of arsenic was reacted with 1 g/L of pyrite at pH 4.

3.3.2.4 Stability of Arsenic on Pyrite

Release experiments were performed by adding phosphate and by increasing pH in order to evaluate the stability of arsenic retained on pyrite. Pyrite with As(III) was prepared by reacting 100 μM of As(III) with 0.35 g/L of pyrite at pH 4 for 26 days. Pyrite with As(V) was prepared by reacting 100 μM of As(V) with 1 g/L of pyrite at pH 4 for 14 days. The suspensions of pyrite with arsenic were divided into two solutions. In one solution, phosphate was added to achieve a final phosphate concentration of 5 mM, and in the other solution, pH was increased to pH 12.

After adding phosphate, the concentration of As(III) continued to increase for about 48 hours resulting in about 37% of the amount of arsenic previously removed being released to the solution. However, after 48 hours, the concentration of arsenic started to decrease (Figure 3.12a). The addition of phosphate to the suspension of pyrite containing As(V) also caused an increase in arsenic concentration in solution that continued for about 20 hours resulting in about 20% of the previously removed arsenic being released to solution (Figure 3.13a). After 20 hours, the concentration in solution began to decrease, as was observed in experiments with As(III). About 90% of the arsenic released to solution was As(III), indicating that, after removal, As(V) was reduced to As(III) by reaction with pyrite.

The added phosphate seems to replace the weakly bound arsenic at the surface of pyrite, which increases arsenic concentration in the solution. Phosphate has been reported not to bind on pyrite significantly under anoxic conditions, since it mainly interacts with iron hydroxide or oxide regions on the pyrite surface (64). Investigation of

the pyrite surface have shown that a small portion of the surface contains iron (Fe(II)/Fe(III)) oxides and that iron hydroxide (≡Fe-OH) is the major functional group on the surface, depending on pH. Therefore, added phosphate might bind to iron hydroxide or oxide groups of the pyrite surface. It would not interact with thiol (≡S-H) groups, so they might be available to release sulfide into the solution. If this occurred, then the released arsenic might be removed from the solution later by forming arsenic sulfide precipitates on the pyrite surface.

Soon after pH was increased, the concentration of As(III) in solution increased to 65 μmol/L, i.e. about 70% of the arsenic removed by pyrite was released. Then, the arsenic concentration decreased and stabilized with an As(III) solution concentration of about 47 μmol/L (Figure 3.12b). For experiments with As(V), almost all of the arsenic removed by pyrite was released to the solution by the change of pH (Figure 3.13b) and it was released as As(III). After the initial rapid release, the concentrations of As(III) and total As decreased with time, while the concentration of As(V) increased for 48 hours. The concentrations of all arsenic species remained almost the same after 48 hours, with total arsenic concentration being around 60 μmol/L and about 70% of it being As(V). The suspensions of pyrite used for release experiments were prepared by reacting arsenic with pyrite at pH 4 for extended time period (26 days for As(III) and 14 days for As(V)). During reaction, partial dissolution of pyrite occurred resulting in a transfer of iron to the solution. When pH was increased in the release experiment, iron in the solution seemed to precipitate on the pyrite surface as Fe(II)/Fe(III) oxides or hydroxides. As(III) may be oxidized to As(V) by Fe(III)-OH on the surface of pyrite.

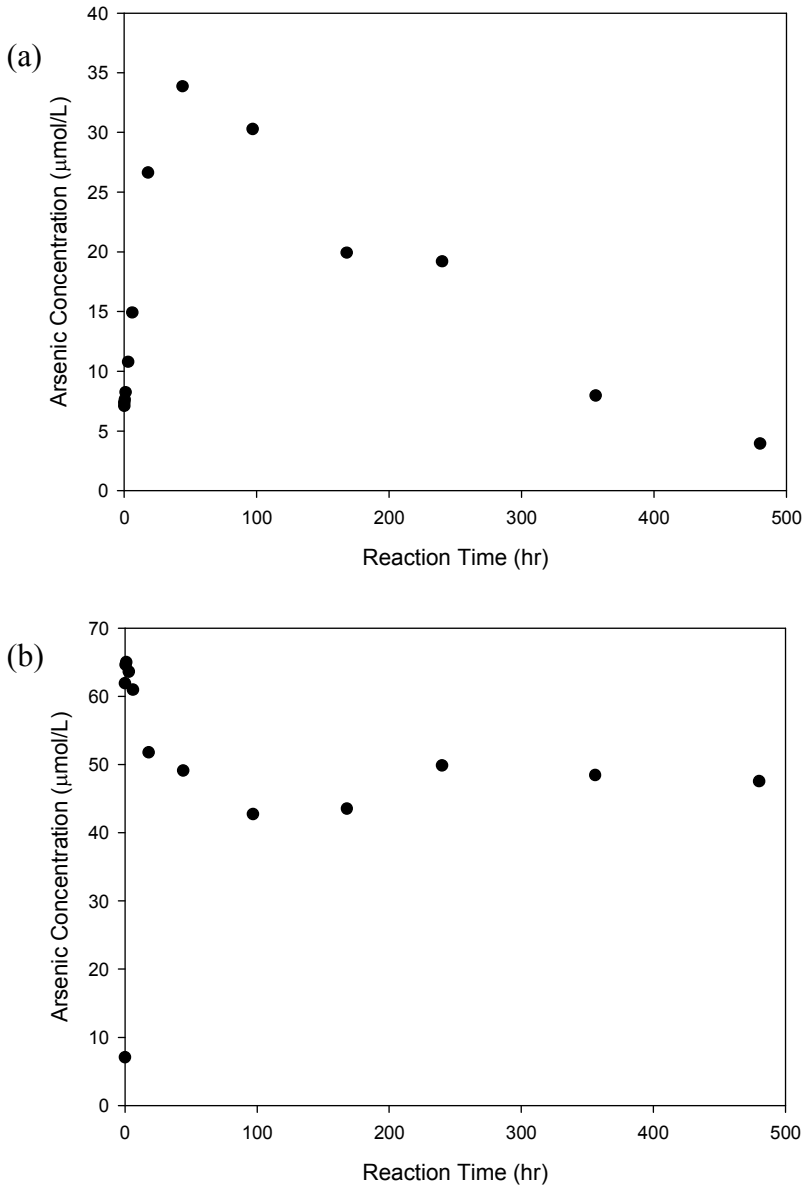

Figure 3.12 Release of As(III) from pyrite by (a) addition of phosphate and (b) increase of pH (pH 12).

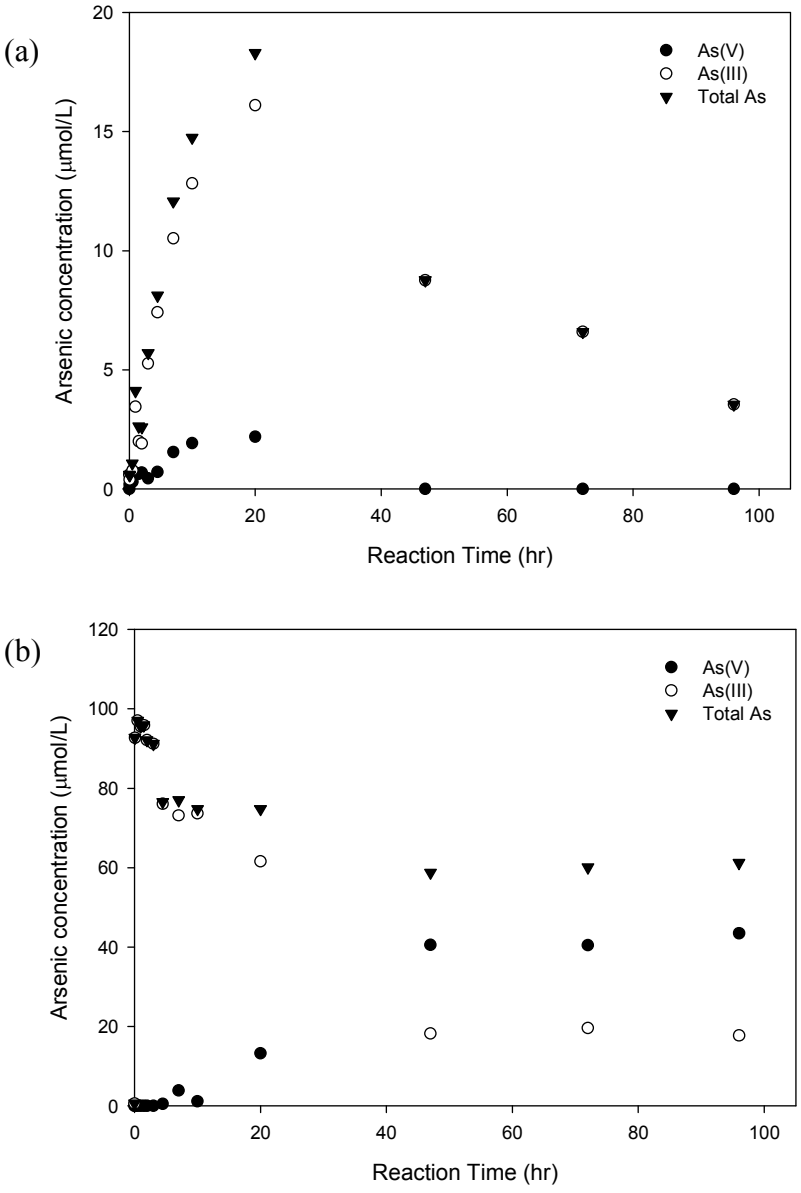

Figure 3.13 Release of As(V) from pyrite by (a) addition of phosphate and (b) increase of pH (pH 12).

The previous section (3.3.2.3) described how the presence of phosphate reduced arsenic removal by pyrite significantly. This section describes how the addition of phosphate resulted in the release of arsenic from pyrite followed by it being removed again. Thus, the presence of phosphate does not seem to affect the ultimate distribution of arsenic between the pyrite surface and the solution. However, changing pH affected stability of sorbed arsenic on the pyrite, which can be expected because arsenic removal by pyrite is highly affected by pH. Arsenic removal is lower at higher pH. One study reported that As(V) was released from pyrite at pH higher than pH 7. They reported that low pH ($pH < 4$) was required to maintain arsenic on pyrite (23). Arsenic may be present on the surface of pyrite as an arsenic sulfide solid phase such as orpiment. The solubility of orpiment increases with increasing pH (62), so the increase of pH might result in release of arsenic due to the dissolution of arsenic sulfide. At high pH, soluble iron may precipitate on the surface as iron oxides or hydroxides. It is likely that arsenic sorbed to surface iron oxides or hydroxides resulting in a decrease in the concentration of arsenic with time. Accordingly, maintaining pH would be important for stability of pyrite that has reacted with arsenic.

3.3.3 X-ray Photoelectron Spectroscopy Investigation

3.3.3.1 As(III) Reacted Pyrite

X-ray photoelectron spectroscopy study of the surface of arsenic reacted pyrite was performed. The surfaces of pyrite which was reacted with As(III) for 26 days at pH 4, 7, and 10 were investigated. XPS broadscans of reacted pyrites are shown in Figure 3.14. Table 3.5 shows the XPS surface atomic concentrations of the pyrite surface after reaction with As(III), which were calculated using Fe 2p, S 2p, O 1s, and As 3d peak areas from the broadscan spectra. As 3d atomic concentration was 13% on the surface of arsenic-reacted pyrite at pH 4, while As 3d concentrations were 1.5% and 1 % on the surfaces that reacted at pH 7 and pH 10, respectively. Oxygen was present less at pH 4 than at pH 7 and pH 10. The ratio of S to Fe (S/Fe) for pyrite should be typically around 2, but at pH 4 there is a Fe deficiency, as shown in the S/Fe ratio of 4.52.

Table 3.5 Atomic concentration of pyrite after reaction with As(III) for 26 days at pH 4, 7, and 10

	Atomic Concentration (%)		
	pH 4	pH 7	pH 10
Fe 2p	14.7	29.2	27.6
S 2p	66.5	57.1	59.8
O 1s	5.72	12.2	11.7
As 3d	13.1	1.48	0.92
S/Fe	4.52	1.95	2.16

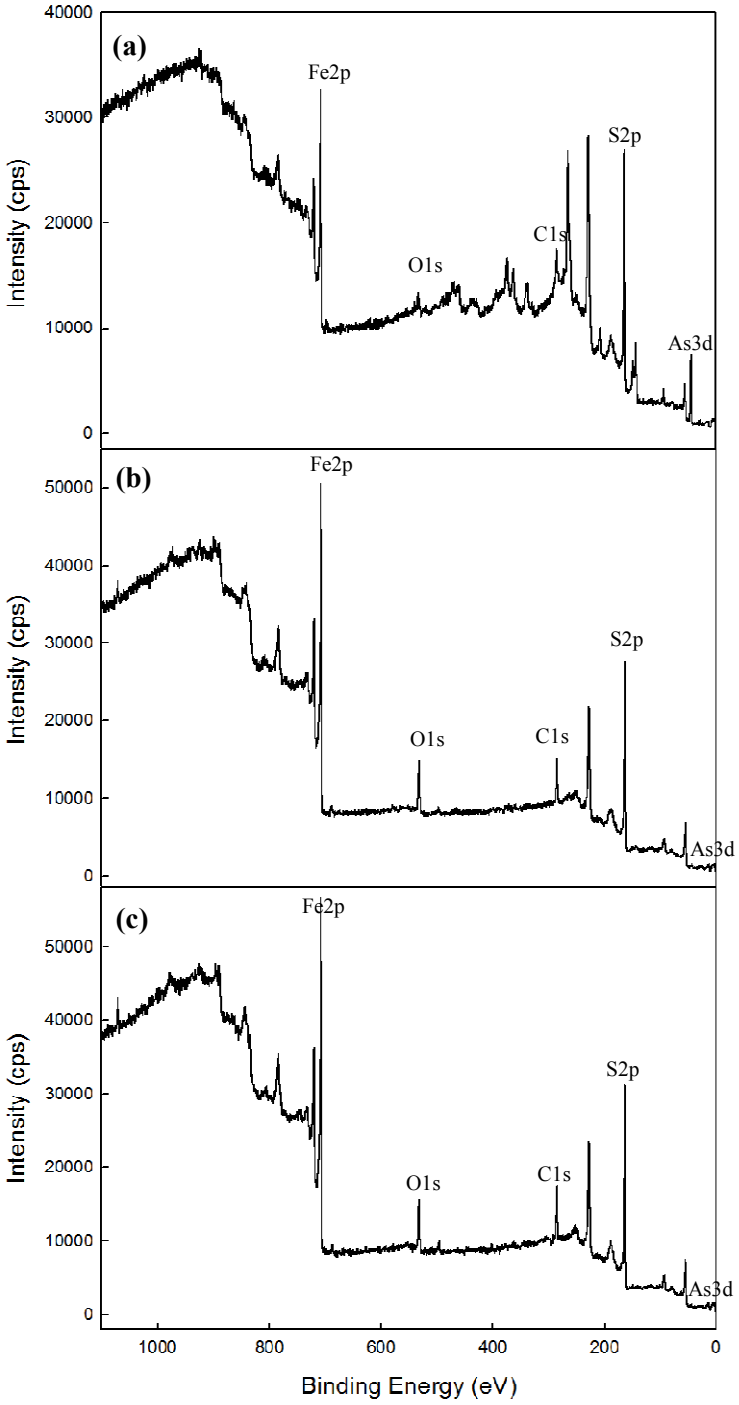

Figure 3.14 XPS broadscans of As(III) reacted pyrite for 26 day at (a) pH 4, (b) pH 7, (c) pH 10.

The XPS spectra of the S 2p, Fe $2p_{3/2}$, and As 3d, are reported in Figures 3.15, 3.16, and 3.17. The S 2p spectra were modeled as doublets of $2p_{1/2}$ and $2p_{3/2}$ separated by 1.18 eV and the area of the S $2p_{1/2}$ peak was 1/2 of the area of S $2p_{3/2}$ peak. The As 3d spectra were modeled as doublets of $3d_{3/2}$ and $3d_{5/2}$ separated by 0.69 eV. The area of the As $3d_{3/2}$ peak was 2/3 of the area of As $3d_{5/2}$ peak. The surface compositions are shown in Table 3.6.

Table 3.6 XPS peak parameters of pyrite after reaction with As(III) for 26 days at pH 4, 7, and 10

B.E. (eV)		Species	pH 4	pH 7	pH 10
S $2p_{3/2}$	161.9	S^{2-}	5.23	5.74	0.00
	162.9	S_2^{2-} (FeS_2)	94.1	92.7	95.5
	164.1	Polysulfide	0.00	0.00	2.25
	168.4	SO_4^{2-}	0.62	1.60	2.20
Fe $2p_{3/2}$	707.1	Fe(II)-S	75.3	69.5	72.0
	708.4	Fe(II)-S	13.6	13.4	13.4
	709.8	Fe(III)-S	6.84	9.02	7.96
	711.1	Fe(III)-O	3.17	5.56	4.68
	712.7	Fe(III)-O	1.11	2.53	2.02
As $3d_{5/2}$	41.9	As(0)	0.00	11.7	11.3
	43.1	As_4S_4	50.1	28.3	22.0
	43.4	As_2S_3	49.9	20.3	16.4
	44.5	As(III)-O	0.00	15.7	19.9
	45.2	As(V)-O	0.00	24.0	30.4

The major peak of S 2p spectrum of pyrite at all pH values is located at 162.9 eV, which is assigned to disulfide (S_2^{2-}) in bulk FeS_2 (38,39,41). The S 2p spectrum also contains smaller peaks at 161.9 eV at pH 4 and pH 7, which is interpreted to be monosulfide (S^{2-}) (38,39,41). The presence of monosulfide at the pyrite surface was suggested to have been formed by S-S bonds that were broken and the sulfur remaining bonded to Fe (41,42). The pyrite used here was synthesized with Fe^{3+} and HS^- using microwave energy. The fast synthesis under microwave irradiation may result in the rupture of S-S bonds and could produce monosulfide on the pyrite surface. The S 2p spectra also indicate the presence of oxidized sulfur on the surface as indicated by peaks located at 164.1 eV and 168.4 eV. The size of these peaks increases at higher pH, indicating that surfaces are more oxidized at higher pH.

The major peak in the Fe $2p_{3/2}$ spectrum of pyrite at all pH values is at 707.1 eV, which is consistent with the reported characteristic peak of pyrite. The peak at 708.4 eV is close to the peak reported as an FeS-like compound or as a surface defect (39). The Fe $2p_{3/2}$ spectrum also contains a tail at high bonding energies that was fitted with peaks associated with species containing Fe(III)-S, Fe(III)-OH, and Fe(III)-SO_4^{2-}bonds. These peaks are bigger in the spectra obtained at pH 7 and pH 10 than at pH 4. Oxidation of the pyrite surface is strongly dependent on the solution pH (39). Presence of more sulfate and Fe(III) on the surface at higher pH is evidence that the surface of arsenic-reacted pyrite was more oxidized at higher pH.

The major peaks of As $3d_{5/2}$ at pH 4 were attributed to species similar to As_4S_4 and As_2S_3 and were located at 43.1 eV and 43.4 eV. The As $3d_{5/2}$ spectrum indicates that neither As(III)-oxide arsenic, which was initially added, nor As(V)-oxide arsenic was detected at pH 4. The XPS data suggests that arsenic was removed from solution mainly by reduction and subsequent surface precipitation of phases similar to As_4S_4 and As_2S_3 during reaction with pyrite at pH 4. Meanwhile, the combined relative concentrations of As_4S_4 and As_2S_3 surface solid phases decreased to 48.6% and 38.4% at pH 7 and pH 10, respectively. The contribution of As(III)-oxide and As(V)-oxide arsenic to the total surface arsenic identified by XPS increased as pH increased. At higher pH, arsenic removal by surface precipitation of solid phases such as As_4S_4 and As_2S_3 seems to be less important than at lower pH where arsenic removal by sorption is also occurring. Also, elemental arsenic was observed on the surface at pH 7 and 10, indicating that arsenic was also removed by precipitation of the FeAsS-like phase suggested by Bostick et al (21).

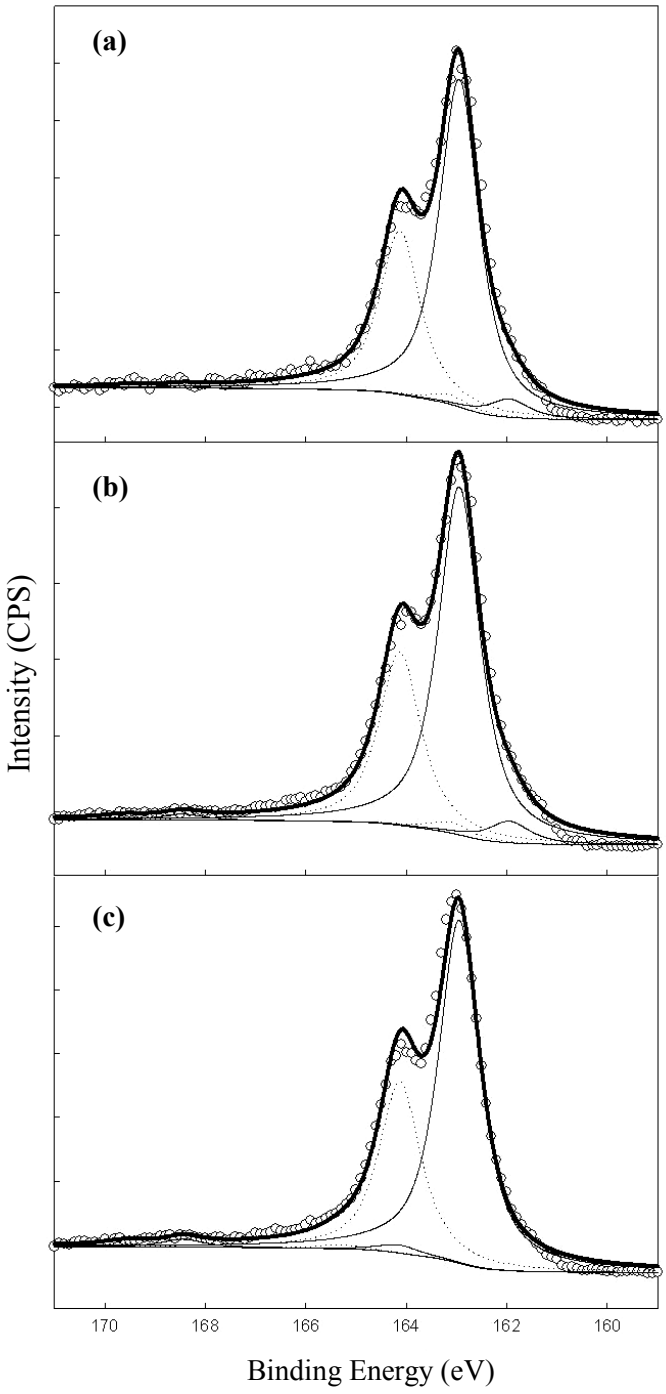

Figure 3.15 The S 2p XPS spectra of pyrite after reaction with As(III) for 26 days at (a) pH 4, (b) pH 7, (c) pH 10.

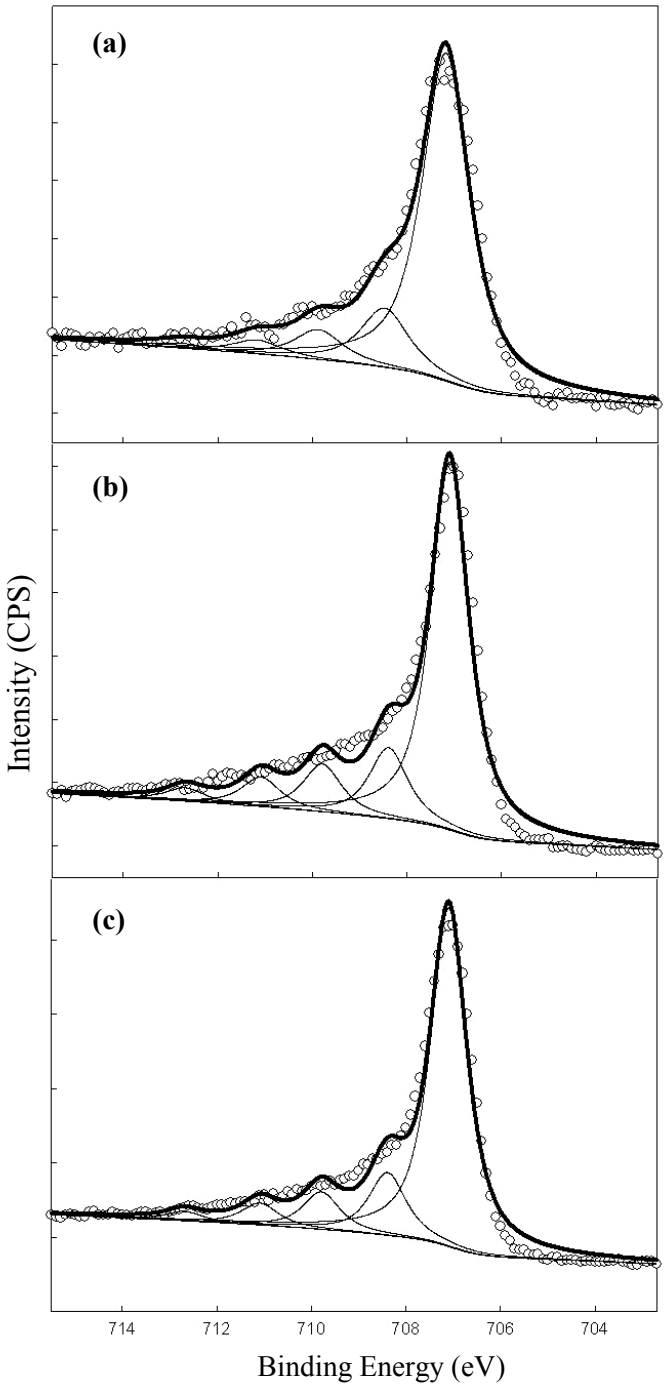

Figure 3.16 The Fe $2p_{3/2}$ XPS spectra of pyrite after reaction with As(III) for 26 days at (a) pH 4, (b) pH 7, (c) pH 10.

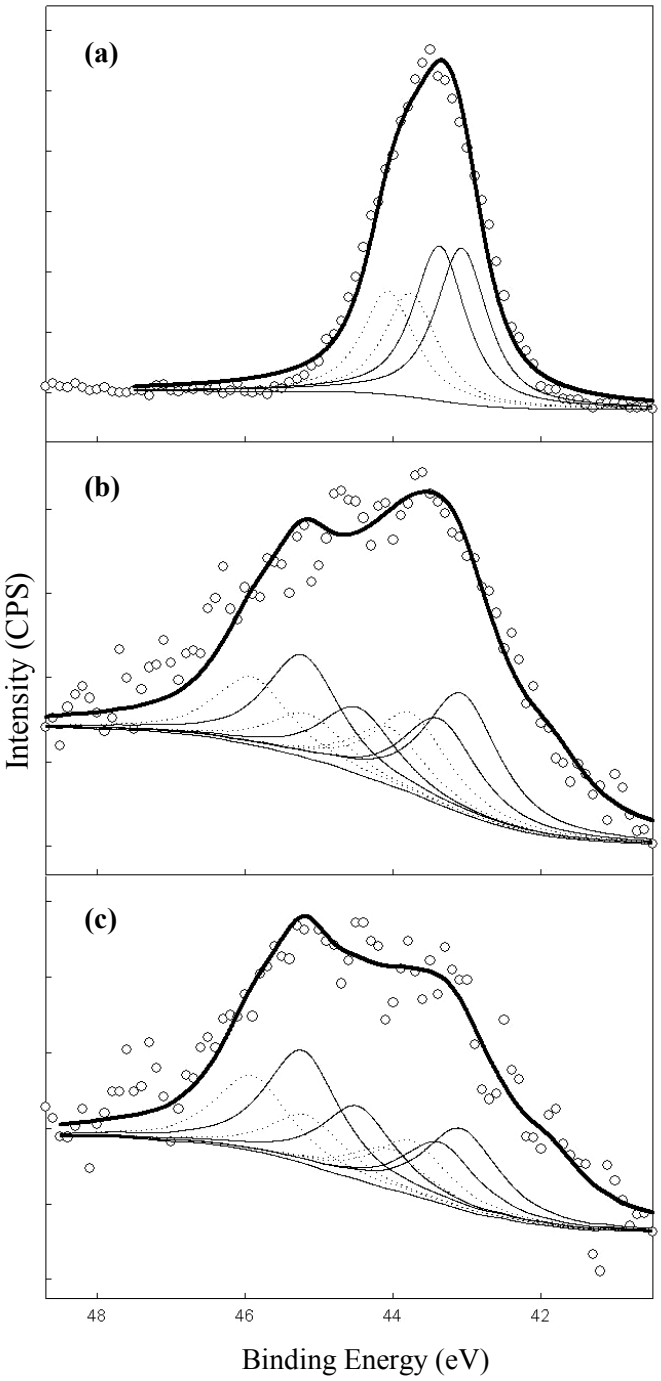

Figure 3.17 The As 3d XPS spectra of pyrite after reaction with As(III) for 26 days at (a) pH 4, (b) pH 7, (c) pH 10.

On the basis of XPS data, it is proposed that surface precipitation occurs when arsenic is removed by pyrite and forms solid phases similar to As_2S_3 and As_4S_4. However, under neutral to alkaline conditions, arsenic is removed and remains as As(III)-O and As(V)-O surface complexes as well as being converted to solids phases by surface precipitation. Also, precipitation of a FeAsS-like phase occurs under alkaline conditions. As pH increases, arsenic removal by surface precipitation of phases like As_2S_3 and As_4S_4 decreases, while removal by As(III)-O and As(V)-O surface complexes increases. The effect of pH was also observed during reaction of arsenic and mackinawite (65). It was reported that arsenic removal by precipitation of an As_4S_4-like precipitate dominated under acidic conditions and arsenite sorption dominated under alkaline conditions.

Under acidic conditions, arsenic removal continued for extended time periods without reaching equilibrium, but achieving high removals. The XPS results indicate that arsenic removal by precipitation of solid phases similar to As_2S_3 and As_4S_4 dominated under acidic conditions. In order for surface precipitation to occur, it must be preceded by mineral dissolution that contributes ions that participate in forming the surface precipitate (66). Surface precipitation of solid phases like As_2S_3 and As_4S_4 on pyrite can occur as suggested by Jia et al. (59). Initial surface complexation of arsenic would be followed by partial dissolution of pyrite. Then, solid phases like As_2S_3 and As_4S_4 would form on the surface by the reaction of the released sulfide ions and the sorbed arsenic. Pyrite solubility decreases at high pH (67), so the decreased dissolution of pyrite would

limit surface precipitation and result in lower removals at neutral and alkaline conditions.

3.3.3.2 Release Experiments

The surfaces of particles before and after the release experiments were investigated by XPS and the results compared. Relative surface concentrations of these pyrite surfaces were determined by XPS (Figure 3.18) and are shown in Table 3.7. These results show that contact with solutions of phosphate decreased the relative surface arsenic concentration from 13.1% to 8.93% and increased the relative surface concentration of iron. The increase in relative iron concentration might be caused by decrease of relative concentrations of arsenic and sulfur associated with arsenic after addition of phosphate. Phosphate was not observed on the surface, which is supported by the report that phosphate does not bind to pyrite significantly under anoxic conditions (64).

The XPS spectra of the Fe $2p_{3/2}$, S 2p, and As 3d, are reported in Figures 3.19, 3.20, and 3.21. The surface compositions are summarized in Table 3.8. The major peak of the As 3d spectrum after phosphate addition is specie similar to As_4S_4 (. This peak increased, while the peak associated with As_2S_3 peak decreased after phosphate addition. The arsenic released immediately after phosphate addition might later be removed by surface precipitation of As_4S_4.

As pH increased in the release experiment, the relative concentration of arsenic on the surface was reduced to 0.62%, while the relative concentrations of iron and

oxygen increased. The Fe $2p_{3/2}$ spectra indicate an increase in oxidized species of iron (Fe^{3+}). The suspensions of pyrite used for release experiments were prepared by reacting arsenic with pyrite at pH 4 for extended time period (26 days for As(III) and 14 days for As(V)). During reaction, partial dissolution of pyrite occurred resulting in a transfer of iron to the solution. When pH was increased in the release experiment, iron in the solution seemed to precipitate on the pyrite surface as iron oxides, which also increased oxygen concentration on the surface. Soon after pH was increased, about 70% of the arsenic on the surface of pyrite was released to solution, and then arsenic concentration decreased. The As 3d spectrum of pyrite after contact with the high pH solution shows an increase in oxidized arsenic, i.e. As(V) and As(III) oxides. The major peaks of the As 3d spectrum are associated with As(V)-oxide and As_2S_3. The released arsenic might be subsequently removed by formation of As(III)-O and As(V)-O surface complexes as well as solid phases similar to As_2S_3 and FeAsS as was observed for pyrite contacted with arsenic under alkaline conditions (3.3.3.1).

Table 3.7 Atomic concentration of pyrite before and after contact with two solutions (5 mM phosphate, pH 12) for 20 days

	Atomic Concentration (%)		
	26 day reacted	Phosphate addition	pH increase
Fe 2p	14.7	22.2	25.7
S 2p	66.5	60.9	47.0
O 1s	5.72	7.95	26.7
As 3d	13.1	8.93	0.62
S/Fe	4.52	2.75	1.83

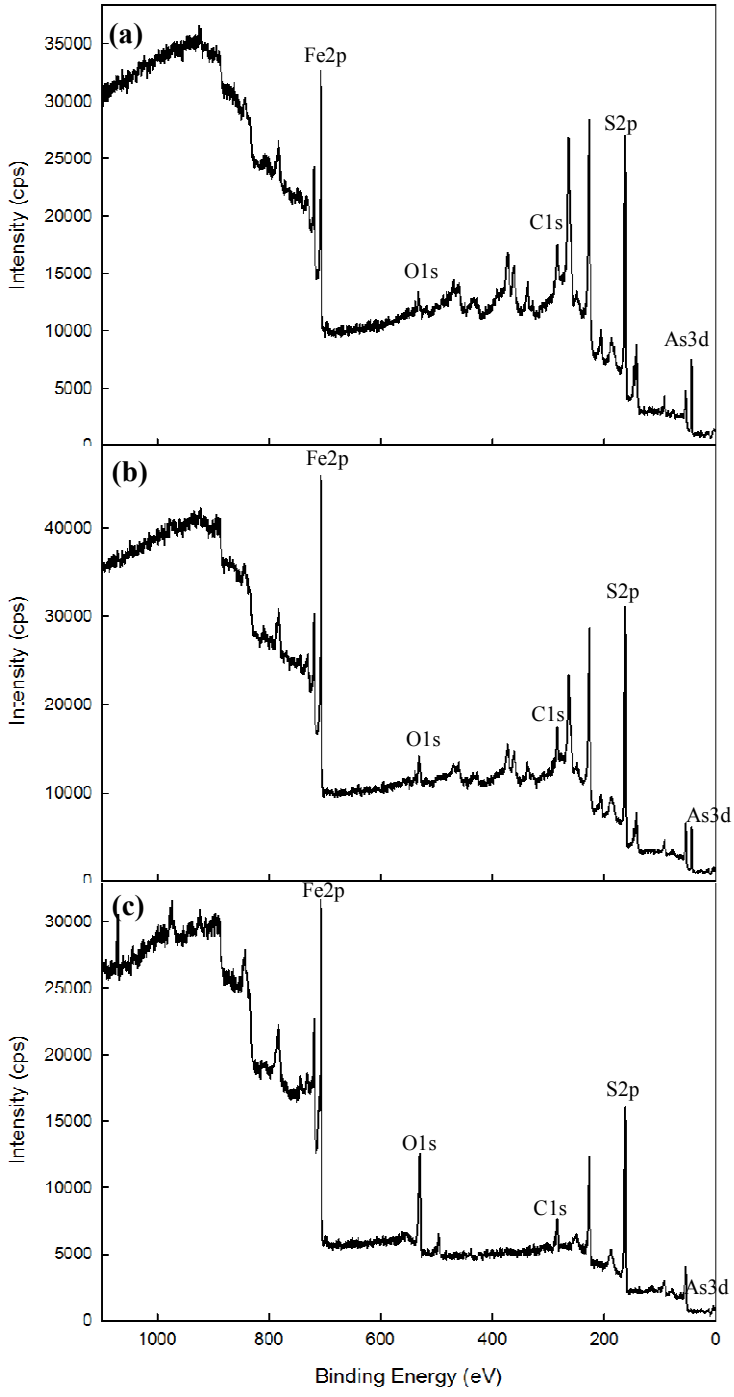

Figure 3.18 X-ray photoelectron broadscans of pyrite after reaction with As(III) for 26 days at pH 4 and (a) no further treatment, (b) contact with 5 mM phosphate solution for 20 days, (c) contact with a pH 12 solution for 20 days.

Table 3.8 XPS peak parameters of pyrite before and after contact with two solutions (5 mM phosphate, pH 12) for 20 days

B.E. (eV)		Species	26 day	P	pH
S $2p_{3/2}$	161.9	S^{2-}	5.23	1.03	0.00
	162.9	S_2^{2-} (FeS_2)	94.1	99.0	97.7
	164.1	Polysulfide	0.00	0.00	1.81
	168.4	SO_4^{2-}	0.62	0.00	0.47
Fe $2p_{3/2}$	707.1	Fe(II)-S	68.4	74.8	63.7
	708.4	Fe(II)-S	16.2	12.6	9.26
	709.8	Fe(III)-S	7.65	7.63	11.6
	711.1	Fe(III)-O	4.52	3.31	10.4
	712.7	Fe(III)-O	3.23	1.70	5.04
As $3d_{5/2}$	41.9	As(0)	0.00	0.00	13.5
	43.1	As_4S_4	50.1	69.7	0.04
	43.4	As_2S_3	49.9	29.8	30.5
	44.5	As(III)-O	0.00	0.52	11.7
	45.2	As(V)-O	0.00	0.00	44.3

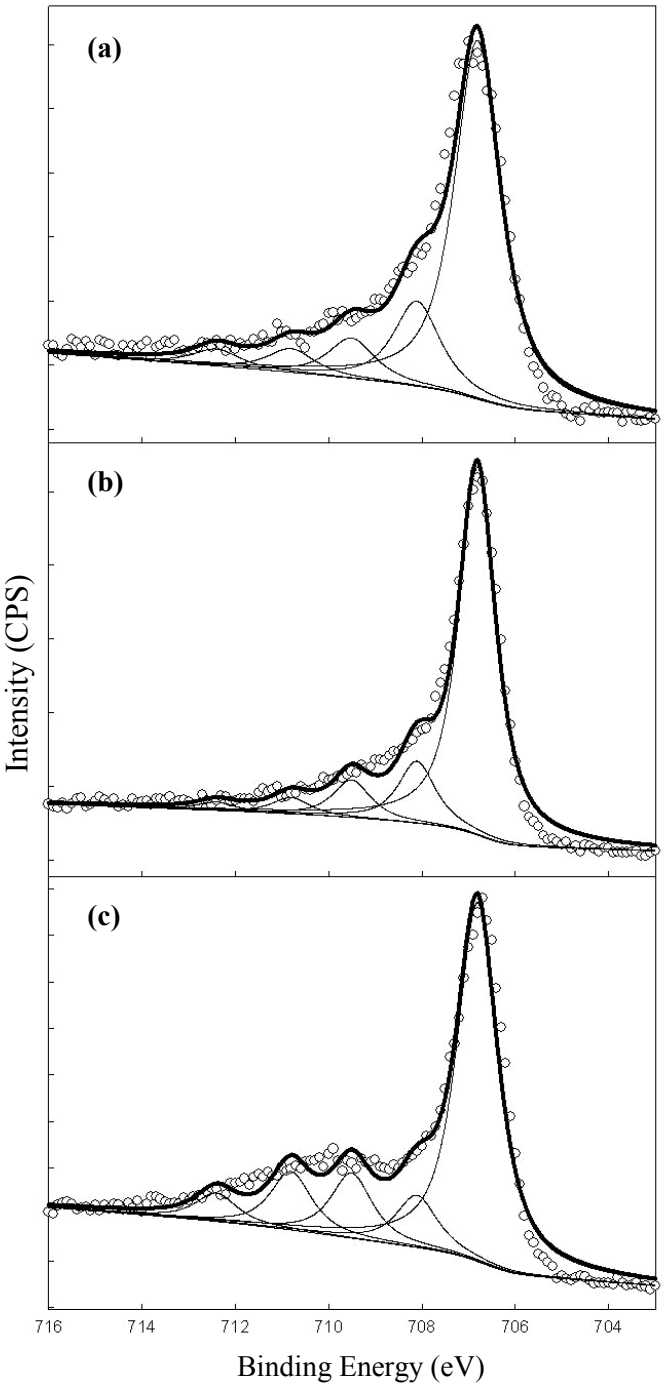

Figure 3.19 The Fe $2p_{3/2}$ XPS spectra of pyrite after reaction with As(III) for 26 days at pH 4 and (a) no further treatment, (b) contact with 5 mM phosphate solution for 20 days, (c) contact with a pH 12 solution for 20 days.

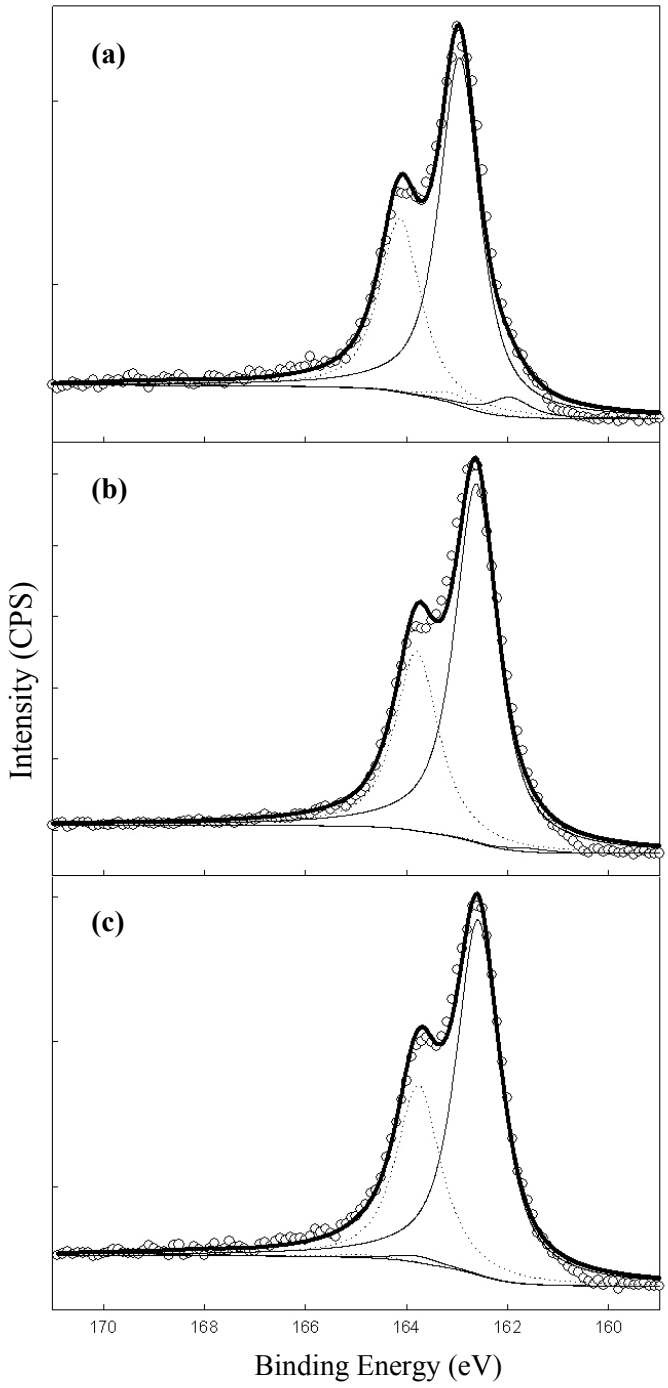

Figure 3.20 The S 2p XPS spectra of pyrite after reaction with As(III) for 26 days at pH 4 and (a) no further treatment, (b) contact with 5 mM phosphate solution for 20 days, (c) contact with a pH 12 solution for 20 days.

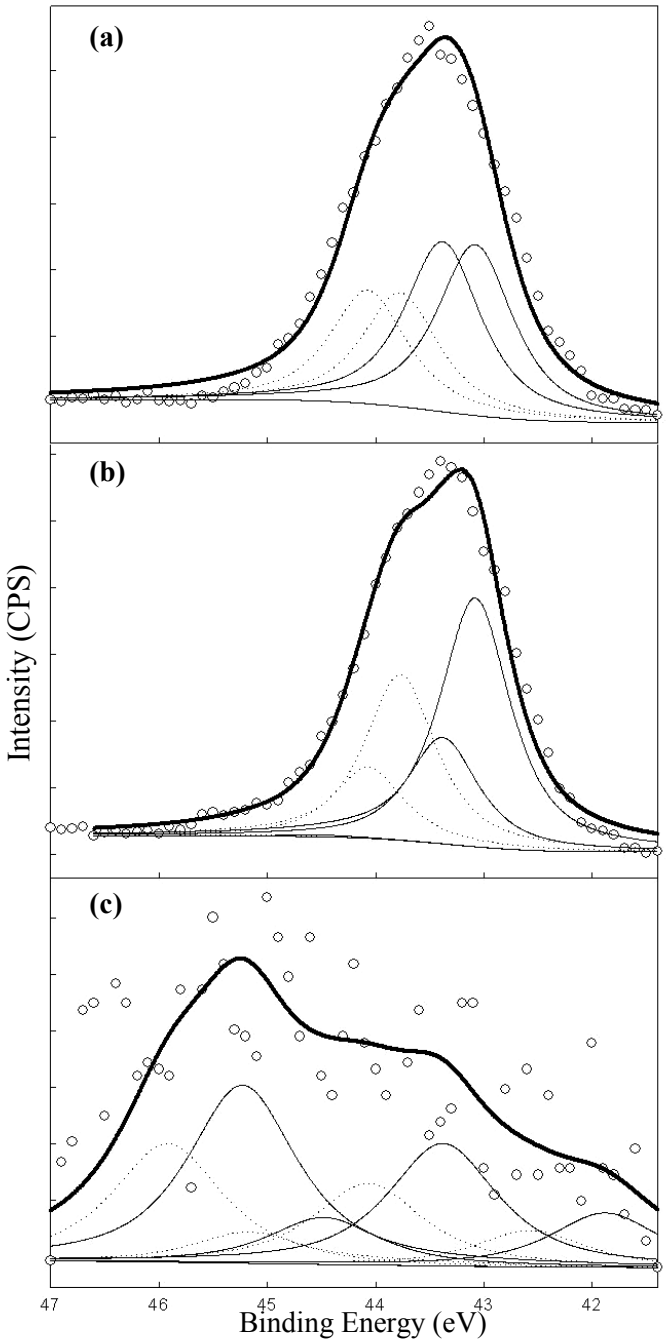

Figure 3.21 The As 3d XPS spectra of As 3d of pyrite after reaction with As(III) for 26 days at pH 4 and (a) no further treatment, (b) contact with 5 mM phosphate solution for 20 days, (c) contact with a pH 12 solution for 20 days.

CHAPTER IV

X-RAY PHOTOELECTRON SPECTROSCOPIC INVESTIGATION OF PYRITE AFTER REACTION WITH ARSENIC AS A FUNCTION OF pH

4.1 Introduction

Arsenic contaminated drinking water has been a big problem in many parts of the world including Bangladesh, China, India, Taiwan, Mexico, and the USA (1,3). Exposure of humans to elevated concentrations of arsenic in drinking water posses significant health risks, such as Blackfoot disease, skin, lung and bladder cancers, and disorders of the immune, nervous and reproductive systems (3). Arsenic is a trace element that occurs naturally in the atmosphere, water, soils, and rocks. Arsenic is present as a major constituent of many minerals including sulfides and oxides such as realgar (As_4S_4), orpiment (As_2S_3), arsenopyrite (FeAsS), arsenolite (As_2O_3), and scorodite ($FeAsO_4 \cdot 2H_2O$). Arsenic can be released to the surface and subsurface water by natural processes such as weathering and sedimentation and by human activities such as mining, smelting, burning of fossil fuels, and applying agricultural chemicals (1).

Mineral-water interactions play important roles in controlling the fate and transport of arsenic in natural water (1,5,6). Oxides of iron, aluminum, and manganese are known to be the major minerals controlling arsenic concentration in aquifers, because of their chemistry and abundance (1,5,6). However, under reduced conditions, sulfide minerals have been suggested to play an important role in regulating dissolved metal concentrations (11-13,47,48). The examination of sediments in Milltown

Reservoir (13) showed that vertical transition of redox states resulted in the shift in partitioning of arsenic from oxides into sulfides. Pyrite (FeS_2) is the most common sulfide mineral, which plays an important role as an electron source in geochemical processes in the environment (15). Natural pyrite contains various amounts of trace elements such as arsenic (As), lead (Pb), cobalt (Co), nickel (Ni), and selenium (Se) at concentrations that range from a few ppm to tens of thousands ppm. For example, arsenic contents in pyrite can vary between 2 and 96,000 ppm (16). Thus, interactions of trace elements with pyrite have received great attention.

X-ray absorption spectroscopy studies and electronic structure calculations suggest that arsenic can substitute for sulfur in pyrite by forming As-S dianion groups (17,18). Farquhar et al. (19) suggested that arsenic forms outer-sphere complexes with pyrite based on results of X-ray absorption spectroscopy. On the other hand, Bostick et al. (20,21) suggested that arsenic forms strong inner-sphere complexes or surface precipitates on pyrite. They suggested that initial reactions between As(III) and pyrite might form a FeAsS-like precipitate that could be converted to As_2S_3. Several other studies on interactions of arsenic with pyrite have been published (22,23). These studies have shown the affinity of pyrite for arsenic, but arsenic retention mechanisms are not fully understood yet.

The objective of this study is to investigate interactions of arsenic with pyrite in an anoxic environment and how these interactions are affected by pH. The surface of pyrite has been reported to change drastically depending on the pH (39) and arsenic occurs as different protonated oxyanionic forms depending on pH (1). In this study,

arsenic was reacted with pyrite at different pH values in an anoxic environment and the surface of pyrite was studied using x-ray photoelectron spectroscopy (XPS) to characterize surface species.

4.2 Experimental Section

4.2.1 Materials

All solutions were prepared using deaerated and deionized water. This water was prepared by bubbling purified nitrogen gas through deionized water for at least 2 hours. Deionized water was obtained from a Millipore Milli-Q system (18 MΩ). Then the water was purged overnight in an anaerobic chamber containing a mixture of 5% hydrogen and 95% nitrogen gases. Arsenite (As(III)) and arsenate (As(V)) solutions were prepared by dissolving $NaAsO_2$ and $Na_2HAsO_4 \cdot 7H_2O$, respectively (Sigma-Aldrich).

Pyrite was synthesized in a glove box containing nitrogen gas. Iron and sulfide solutions were prepared by dissolving ferric chloride ($FeCl_3 \cdot 6H_2O$) and sodium hydrosulfide ($NaHS \cdot xH_2O$) in deaerated deionized water. The 0.1 M iron solution and the 0.2 M sulfide solution were mixed in a polypropylene bottle and the pH of the mixture was adjusted to pH 4.0 by adding 5 M NaOH or 5 M HCl. Then, the mixed solutions were placed in a conventional microwave oven (1150 W, 2.45 GHz) and allowed to react for 10 minutes at a setting of 20% (microwave power applied for 20% of the time). The reacted samples were rapidly cooled to room temperature by placing them in cold water. The solids were washed with HCl, acetone, and carbon disulfide. The solid products were identified as pyrite by XRD. The surface area for the particles

was determined to be 15.9 m^2/g by a multipoint BET isotherm using N_2 as the adsorbate. Pyrite was dried and stored in the anaerobic chamber before use.

4.2.2 Removal Experiments

Removal kinetics were investigated with pyrite suspensions at pH 4, pH 7, and pH 10. Variation in pH was minimized by using 0.02 M acetate (pH 4), MOPS (4-morpholinepropanesulfunic acid, pH 7), or CAPS (3-cyclohexylamion-1-propanesulfonic acid, pH 10) buffers. Pyrite suspensions (1 g/L) were prepared in 0.02 M buffer solutions (acetate, MOPS, CAPS) and stabilized for three hours before reactions. Reactions were initiated by adding arsenic (As(III)) standard solution to a pyrite suspension. The initial arsenic concentration was 100 μM. The suspension was agitated using a magnetic stirrer. A 10-mL aliquot was sampled from the suspension at each reaction time for up to 29 days. The samples were immediately filtered using 0.2-μm or 0.02-μm membrane filters, and the filtrates were stored at 2 °C until analysis.

All steps in the preparation of samples and their reaction were carried out at room temperature in an anaerobic atmosphere containing 5% hydrogen and 95% nitrogen. The concentrations of arsenic in filtrates were measured to determine extents of arsenic sorption and reaction. Arsenic was analyzed using an atomic absorption spectrometer coupled with continuous hydride generation system (HGAAS). Arsenic was reduced to arsine (AsH_3) gas by continuous flow of sodium borohydride (1.5% $NaBH_4$ in 0.5% NaOH). The arsine gas was transferred to the flame AA by argon carrier

gas and its concentration was measured by comparison with standards. The method detection limit (MDL) for As(III) was 0.18 µg/L and for As(V) was 0.85 µg/L.

4.2.3 X-ray Photoelectron Spectroscopy

The surface of arsenic-reacted pyrite was characterized by Kratos Axis Ultra Imaging X-ray photoelectron spectroscopy (XPS) with monochromatic Al K-α X-rays. The arsenic-reacted pyrite particles were prepared on 0.2-µm or 0.02-µm membrane filters at each reaction time and dried and stored in the anaerobic chamber before analysis. A broadscan was obtained using 80 eV pass energy, while narrow high resolution scans of As 3d, Fe 2p, and S 2p were obtained using 40 eV pass energy. The charge effect was corrected using C 1s from contamination at 284.5 ± 0.1 eV. The obtained spectra were fitted using a curve-fitting program (XPSPEAK41). The spectra were fitted using a least-squares procedure with peaks of 80% of Lorentzian-Gaussian peak shape after subtraction of a Shirley baseline. The component peaks were identified by comparison of their binding energies with literature values (Table 4.1).

Table 4.1 Fe2p, S2p and As 3d XPS binding energies reported in the literature

	Species	Binding energy (eV)	References
Fe ($2p_{3/2}$)	Fe(II)-S	707.2	Bostick and Fendorf (21)
		707.0 (FeS_2 bulk), 706.05, 707.95	Nesbitt and Muir (38)
		707.5 ± 0.2	Bonnissel-Gissinger et al. (39)
		706.5, 707.45, 708.4	Pratt et al. (40)
	Fe(III)-S	709.3	Bostick and Fendorf (21)
		708.75, 709.85, 710.85, 711.75	Nesbitt and Muir (38)
	Fe(III)-OH	711.3	Bostick and Fendorf (21)
		710.3, 711.3, 712.4, 713.45	Nesbitt and Muir (38)
S ($2p_{3/2}$)	FeS_2 (bulk)	162.6	Bostick and Fendorf (21)
	FeS	160.8	NIST XPS database
	S_2^{2-}	162.4	Nesbitt and Muir (38)
		162.4 - 162.5, 162.7	Bonnissel-Gissinger et al. (39)
	S^{2-}	161.2	Bostick and Fendorf (21)
		161.65	Nesbitt and Muir (38)
		161.1, 161.3	Bonnissel-Gissinger et al. (39)
	Polysulfide	163.8, 163.2	Bostick and Fendorf (21)
		163.6	Nesbitt and Muir (38)
		165.3, 164.2, 163.8	Bonnissel-Gissinger et al. (39)
	$S_2O_3^{2-}$	166.8, 166.9	Bostick and Fendorf (21)
		166.45	Nesbitt and Muir (38)
	SO_4^{2-}	169.1, 169.0	Bostick and Fendorf (21)
		168.25	Nesbitt and Muir (38)
		169.1, 168.5	Bonnissel-Gissinger et al. (39)
As ($3d_{5/2}$)	As(-I)-S	41.2	Nesbitt et al (50)
	As(0)	41.8	Nesbitt et al (50)
	As_4S_4	43.1	Bullen et al (51), NIST XPS database (52)
	As_2S_3	43.4, 43.5	Bullen et al (51), NIST XPS database (52)
	As_2S_5	44.4	NIST XPS database (52)
	As(I)-O	43.47	Nesbitt et al (50)
	As(III)- O	44.54, 44.4	Nesbitt et al (50,53)
	As(V)-O	45.28, 45.15	Nesbitt et al (50,53)

4.3 Results and Discussion

4.3.1 Surface Characterization of Unreacted Pyrite

Pyrite suspensions in buffer solutions at pH 4, pH 7, and pH 10 were mixed for 3 hours before reaction with arsenic in order to let pyrite particles stabilize at each pH. After 3 hours, pyrite particles were sampled to investigate surfaces of unreacted pyrite at different pH values. Interestingly, in the pyrite suspensions at pH 7 and pH 10 small particles were observed, which were passing through the 0.2-μm membrane filter. The proportions of small particles increased as time in contact with the buffer solution increased, but the exact proportions were not measured during experiments. Smaller particles were gathered with 0.02-μm membrane filter and investigated separately with particles gathered on the 0.2-μm filter. Figure 4.1 shows SEM images of pyrite particles collected on 0.2-μm and 0.02-μm membrane filters after reacting with arsenic at pH 10. The particle size of synthesized pyrite before contact with the buffer solution was around 0.5 to 1 μm, but the size of particles gathered on the 0.02-μm membrane filter was around 0.05 μm (Figure 4.1(a)).

(a)

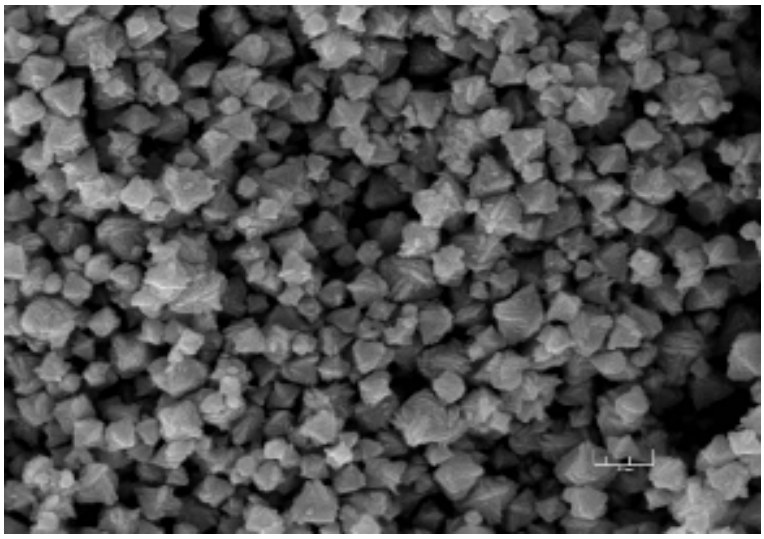

(b)

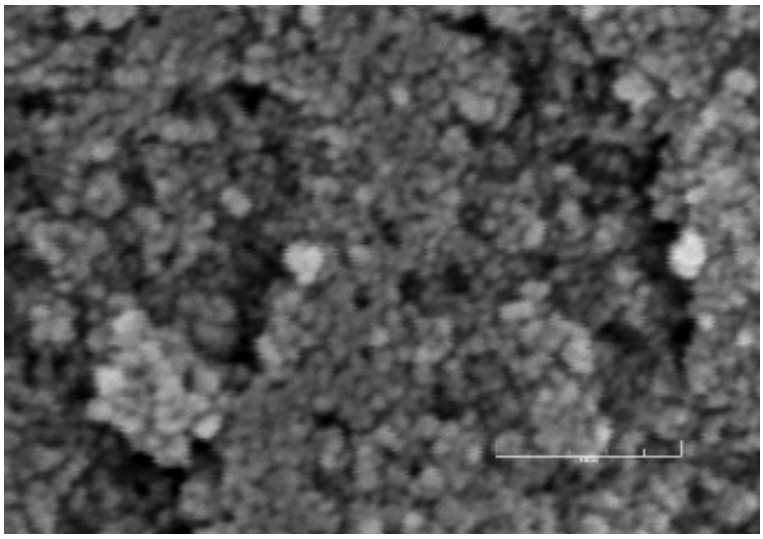

Figure 4.1 SEM images of (a) big particles and (b) small particles of pyrite after contact with buffer solution at pH 10.

The XPS broadscans for unreacted pyrite particles suspended at different pH values are given in Figure 4.2. Fe 2p, S 2p, and O 1s peak areas from the XPS broadscans were used to determine the surface atomic ratios shown in Table 4.2. At pH 4, the pyrite surface was composed of 31% Fe and 64% S with about 5% O. The S/Fe ratio is 2.08, which is consistent with the theoretical ratio of FeS_2. At pH 7, the surface composition of big particles is similar to that of pyrite at pH 4, except that the O content increases to about 10%. However, the surface composition of the small particles shows 40% O and the S/Fe ratio is reduced to 1.69. At pH 10, the surface composition of the big particles is similar to pyrite at pH 7, but 92.7% of the surface of small particles is covered by O and the S/Fe ratio is 1.57.

Table 4.2 Surface atomic composition (%) of particles of pyrite contacted with buffer solutions at pH 4, pH 7, and pH 10

		Fe 2p	S 2p	O 1s	S/Fe
pH 4		30.9	64.2	4.84	2.08
pH 7	Big	29.9	59.0	11.1	1.97
	Small	22.3	37.7	40.0	1.69
pH 10	Big	27.4	62.3	10.3	2.27
	Small	2.83	4.44	92.7	1.57

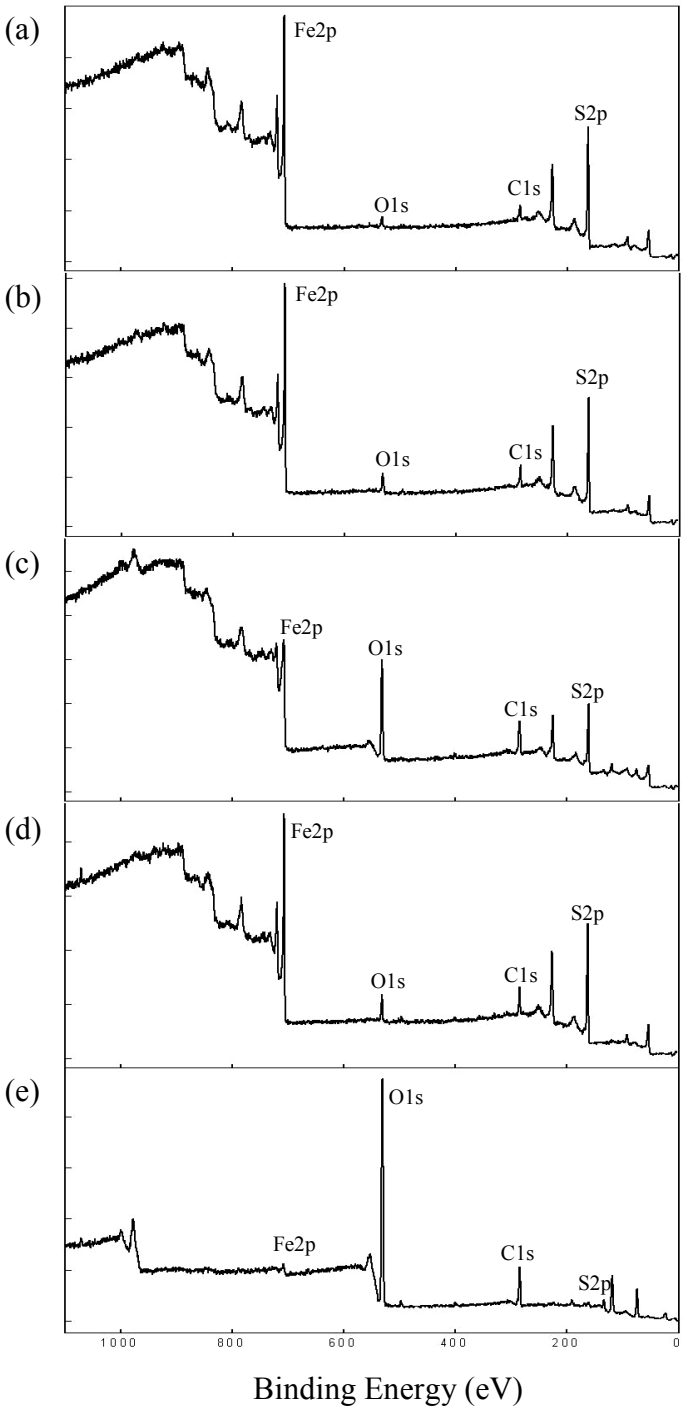

Figure 4.2 X-ray photoelectron broadscans of particles of pyrite of different sizes after contact with buffer solutions at different pH. (a) at pH 4, (b) big particles at pH 7, (c) small particles at pH 7, (d) big particles at pH 10, and (e) small particles at pH 10.

Figure 4.3 and Figure 4.4 present the narrow scan S 2p and Fe $2p_{3/2}$ spectra of pyrite suspended in buffer solutions at pH 4, pH 7, and pH 10. The S 2p spectra were modeled as doublets of $2p_{1/2}$ and $2p_{3/2}$ separated by 1.18 eV and the area of the S $2p_{1/2}$ peak was 1/2 of the area of S $2p_{3/2}$ peak. The surface compositions are shown in Table 4.3.

At pH 4, the major peak of the S 2p spectrum of pyrite is at 162.4 eV, which is assigned to disulfide (S_2^{2-}) of bulk FeS_2 (38,39,41). The S 2p spectra also contain smaller peaks at 161.4 eV and 163.6 eV, which are interpreted to be monosulfide (S^{2-}) and polysulfide (S_n^{2-}), respectively (38,39,41). The presence of monosulfide at the pyrite surface was suggested to be formed by sulfur released from broken S-S bonds that remains bonded to Fe (41,42). The pyrite used here was synthesized with Fe^{3+} and HS^- using microwave energy. The fast synthesis by high energy may result the rupture of S-S bonds and could produce monosulfide on the pyrite surface. The S 2p spectrum at pH 4 indicates the absence of highly oxidized sulfur, i.e. sulfate, on the surface.

At high pH, minor changes are observed in the S 2p spectra for the big particles compared to pyrite at pH 4. The major peak in S 2p spectra of big particles of pyrite at pH 7 and pH 10 is disulfide. However, the relative abundance of monosulfide decreases as pH increases (14.7% at pH 4, 11.3% at pH 7, 7.68% at pH 10). Meanwhile, the S 2p spectra of small particles at pH 7 and pH 10 show big differences when compared to spectra at pH 4 or to spectra of big particles at pH 7 and pH 10. The major peak is shifted to lower energy at 160.8 eV, which is assigned to the monosulfide of bulk FeS. The S 2p spectra show that the disulfide peak represents only 8.3% of the sulfur at pH 7

and 4.3% at pH 10. The second biggest peak in the S 2p spectra at pH 10 is located at 168.6 eV, which is assigned to SO_4^{2-}. More oxidized sulfur species are observed at higher pH.

At pH 4, the major peak of Fe $2p_{3/2}$ spectrum is at 706.9 eV, which is consistent with the reported characteristic peak iron in pyrite. The peak at 708.2 eV is close to the peak reported to be an FeS-like specie or to be surface defects (39). Considering the presence of monosulfide, the peak at 708.2 eV is believed to be the Fe(II)-S peak of FeS. The Fe $2p_{3/2}$ spectrum also contains a tail at high binding energies that was fitted with peaks of Fe(III)-S, Fe(III)-OH, and Fe(III)-SO_4^{2-}. The detection of monosulfide in the S 2p spectra suggests the presence of Fe(III) peaks on the surface of pyrite (41). The monosulfide has been suggested to be formed by rupture of S-S bonds and reduction of S^- to S^{2-} along with oxidation of Fe^{2+} to Fe^{3+} (41).

$$Fe^{2+}_{surface} + S^-_{surface} \rightarrow Fe^{3+}_{surface} + S^{2-}_{surface} \quad (4.1)$$

At high pH, the Fe $2p_{3/2}$ spectra of big particles are similar to the spectra at pH 4 as was observed for the S 2p spectra. However, the Fe $2p_{3/2}$ spectra of small particles contain more oxidized Fe peaks compared to big particles.

Table 4.3 XPS peak parameters for pyrite particles of different sizes after contact with buffer solutions at different pH

Binding Energy (eV)		Species	pH 4	pH 7		pH 10	
				big	small	Big	small
S $2p_{3/2}$	160.8	S^{2-} (FeS)	-	-	58.9	-	41.4
	161.4	S^{2-}	14.7	11.3	21.4	7.68	12.8
	162.4	S_2^{2-} (FeS_2)	83.4	88.5	8.27	91.6	4.30
	163.6	Polysulfide	1.96	0.128	5.83	0.724	3.91
	167.9	SO_4^{2-}	-	-	5.61	-	-
	168.6	SO_4^{2-}	-	-	-	-	37.6
Fe $2p_{3/2}$	706.9	Fe(II)-S	64.8	66.6	41.5	66.3	33.6
	708.2	Fe(II)-S	17.4	14.9	21.1	15.9	27.8
	709.6	Fe(III)-S	10.1	9.99	18.5	9.71	24.1
	710.9	Fe(III)-OH	5.10	5.73	11.8	5.59	8.01
	712.5	Fe(III)-SO4	2.58	2.74	6.99	2.45	6.49

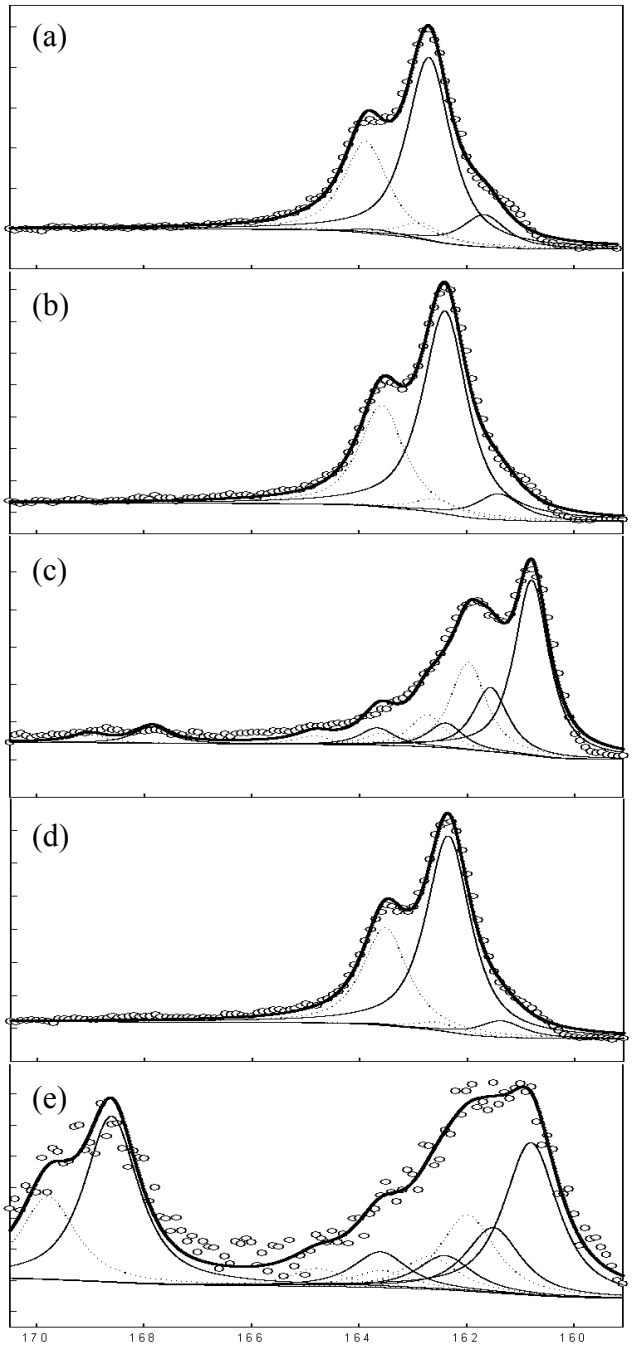

Figure 4.3 S 2p XPS spectra of particles of pyrite of different sizes after contact with buffer solutions at different pH. (a) at pH 4, (b) big particles at pH 7, (c) small particles at pH 7, (d) big particles at pH 10, and (e) small particles at pH 10.

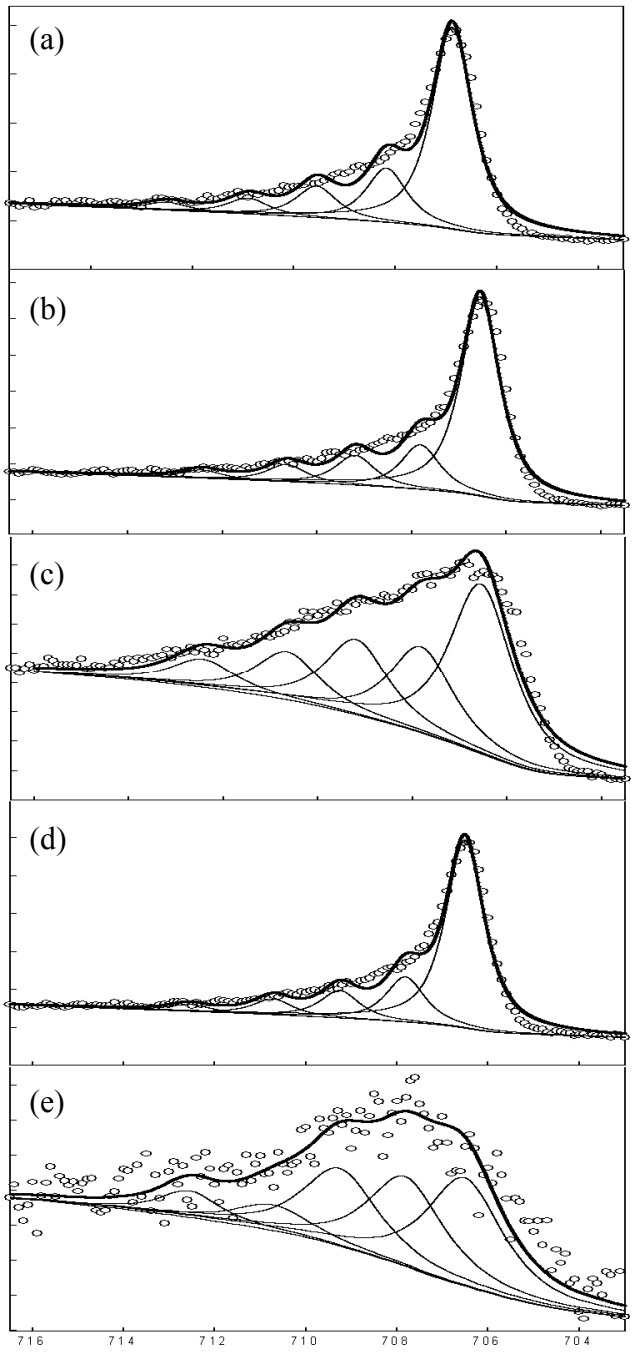

Figure 4.4 Fe $2p_{3/2}$ XPS spectra of particles of pyrite of different sizes after contact with buffer solutions at different pH. (a) at pH 4, (b) big particles at pH 7, (c) small particles at pH 7, (d) big particles at pH 10, and (e) small particles at pH 10.

In this study, small particles with size of around 0.05 μm were observed when pyrite was suspended in solutions with high pH values and the surface composition was observe to vary depending on pH. The surface of pyrite has been reported by others to change drastically with the pH (39). Bonnissel-Gissinger et al. (39) studied surface oxidation as a function of pH and reported that oxidation of the pyrite surface was faster as pH increased. Also, the surface of pyrite was reported to be covered by an oxidized overlayer at pH 10 (68). However, no studies have reported particle size change that is dependent on pH values. The pyrite used in this study could have a partially defective surface caused by microwave irradiation during synthesis. Pyrite was reported to be decomposed to pyrrhotite-like Fe-S phase and elemental sulfur when exposed to microwave energy (46).

$$(1\text{-}x)\ FeS_2 \rightarrow Fe_{1-x}S + (1 - 2x)\ S^0 \qquad (4.2)$$

The X-ray diffraction analysis of pyrite after microwave synthesis did not show the presence of pyrrhotite or other FeS compounds (Chapter II). This suggests that microwave energy applied during pyrite synthesis did not cause significant decomposition of pyrite; however, it could cause partial surface defects. Evidence of surface defects can be found in the S 2p and Fe $2p_{3/2}$ spectra at pH 4, which contains peaks associated with monosulfide S and FeS-like Fe. More explicitly, formation of the smaller particles observed at pH 7 and pH 10 seems to be caused by the defective surface, in a way that is similar to formation of oxidized FeS compounds. This is based on interpretation of the S 2p and Fe $2p_{3/2}$ spectra. The S 2p spectra of highly defective $FeS_2(100)$ prepared by exposure to an ion beam showed a major peak at a position

associated with monosulfide (69). The reduction in relative abundance of surface monosulfide on the big particles at high pH suggests that the monosulfide can be transformed to other forms. Also, the S/Fe peak area ratio (S/Fe = 1.69 and 1.57 at pH 7 and pH 10, respectively) is lower than the expected stoichiometry of pyrite (S/Fe = 2.0).

In this study, all experiments were conducted under anaerobic conditions in a chamber containing 5% hydrogen and 95% nitrogen. The oxygen level was controlled to concentrations below 1 ppm under all conditions by circulating the gas through a reactor with a Pt catalyst that removed traces of oxygen.

As pH increases, increased OH^- may cover the surface of pyrite especially at reactive sites. The monosulfide formed by broken S-S bonds was considered to be a chemically reactive defect state and strongly affected by oxidation reactions on the pyrite surface (70). Therefore, OH^- could selectively affect surface defective sites, e.g. pyrrhotite like Fe-S phase formed during microwave synthesis of pyrite. Furthermore, the Fe-S phase covered with hydroxide seemed to be dissociated from the bulk pyrite phase by repulsive forces and produced small particles covered by hydroxide and oxidized Fe and S compounds. Also, the selective oxidation of monosulfide at high pH can explain the fact that the surface compositions of big particles are almost the same regardless of pH. At higher pH (pH 10), the surfaces of small particles are covered by more oxygen (92.7%) and more oxidized S or Fe are observed.

4.3.2 Surface of Pyrite after Reaction with Arsenic at pH 4

Pyrite was reacted with As(III) for 29 days at pH 4. The arsenic concentrations in solution with time are shown in Figure 4.4. Arsenic removal continued to occur until complete removal was achieved in about 5 days. The surface of pyrite that had reacted with arsenic at pH 4 for different times was investigated with X-ray photoelectron spectroscopy. Fe 2p, S 2p, O 1s, and As 3d peak areas from the XPS broadscans were used to determine the surface atomic compositions shown in Table 4.4.

After 1 hr reaction, about 30% of arsenic initially in solution was removed by pyrite (Figure 4.5), and about 1% of the surface was covered by arsenic. The composition of oxygen slightly increased from 4.84% to 7.3%, which seems to be due to the introduction of oxygen associated with arsenic. The arsenic content on the surface is increasing as arsenic removal increases. Arsenic composition on the surface continued to increase to 5.28% after 3 days, and then slightly decreased to 4.4 % after 29 days, even though arsenic concentration in solution phase did not change after complete removal was observed after 5 days. Loss of Fe from the surface was observed over time. The S/Fe ratio increased with time. Fe deficiency was shown after 29 days by a S/Fe ratio of 2.67. Arsenic seems to substitute for Fe during reaction. The new form of arsenian pyrite was proposed by Deditius et al (71), in which arsenite (As^{3+}) substitutes for Fe [$(Fe,As)S_2$], in contrast to the common form of arsenian pyrite, in which arsenic (As^{1-}) substitutes for S in S_2^{2-} [$Fe(As,S)_2$].

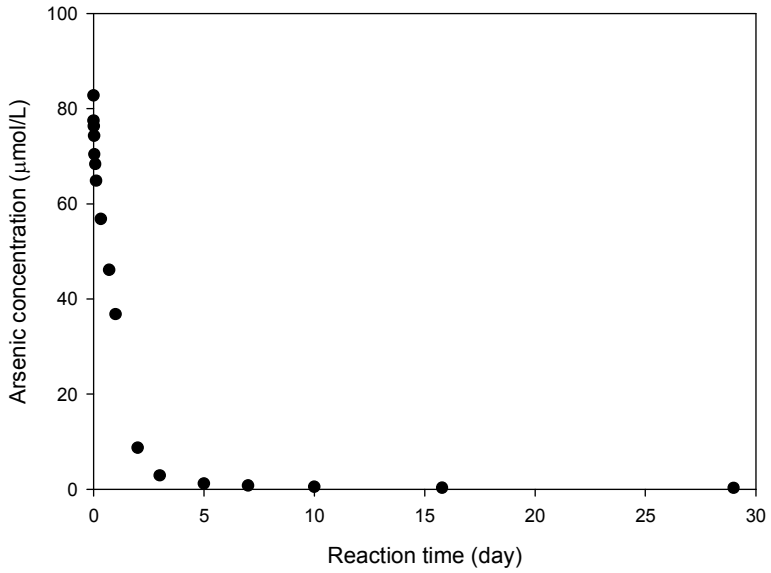

Figure 4.5 Arsenic concentrations over time in presence of pyrite at pH 4. Initial concentration of arsenic =100 μM, dose of pyrite = 1 g/L.

Table 4.4 Atomic composition (%) of the surface of pyrite after reaction with As(III) at pH 4 for various times

	Fe 2p	S 2p	O 1s	As 3d	S/Fe
Unreacted	30.9	64.2	4.84	-	2.08
1 hr	28.6	63.0	7.30	1.09	2.20
3 hr	29.1	64.5	4.87	1.47	2.22
8 hr	30.0	63.4	4.86	1.70	2.11
3 day	25.5	64.3	4.95	5.28	2.52
5 day	26.9	63.3	5.13	4.71	2.35
10 day	26.3	63.5	5.80	4.43	2.41
29 day	24.9	66.4	4.34	4.41	2.67

Figure 4.6, Figure 4.7, and Figure 4.8 present the narrow scan As 3d, S 2p, and Fe $2p_{3/2}$ spectra of pyrite reacted for 1 hr to 29 days with 100 μM As(III) at pH 4, respectively. The As 3d spectra were modeled as doublets of $3d_{3/2}$ and $3d_{5/2}$ separated by 0.69 eV. The area of As $3d_{3/2}$ peak was 2/3 of the area of As $3d_{5/2}$ peak. The S 2p spectra were modeled as doublets of $2p_{1/2}$ and $2p_{3/2}$ separated by 1.18 eV and the area of S $2p_{1/2}$ peak was 1/2 of the area of S $2p_{3/2}$ peak. The surface compositions are shown in Table 4.5.

After 1 hr reaction, the most intense peak of the As 3d spectrum is that of a specie that is similar to As_4S_4 ("As_4S_4-like As") and is located at a binding energy of 43 eV and representing 57.4% of surface arsenic (51,52). The second most intense peak is at 45.15 eV, which is assigned to As(V)-oxide (50,53). The As 3d spectra also contain smaller peaks at 43.3 eV, 44.4 eV, and 41.8 eV, which are interpreted to be specie similar to As_2S_3, As(III)-oxide, and elemental As, respectively (50-53). After 3 hr reaction, the intensity of the peak associated with As(V)-oxide decreases and the major peak becomes the one associated with the specie similar to As_4S_4 that represents 86.5 % of surface arsenic. After 29 days, the most intense peak is the one associated with As_4S_4-like As.

During reaction with arsenic, the major peak of the S 2p spectrum of pyrite is at 162.4 eV, which is assigned to disulfide (S_2^{2-}) of bulk FeS_2 (38,39,41). The S 2p spectra also contain smaller peaks at 161.4 eV and 163.6 eV, which are interpreted to be monosulfide (S^{2-}) and polysulfide (S_n^{2-}), respectively (38,39,41). The content of

monosulfide increases with time, while that of disulfide decreases. Increased amounts of oxidized sulfur species including polysulfide are not observed during reaction.

The major peak of Fe $2p_{3/2}$ spectrum of pyrite after reaction with arsenic is at 706.9 eV, which is consistent with the reported characteristic peak of pyrite. The peak at 708.2 eV is close to the peak reported as an FeS-like compound or as surface defects (39). The Fe $2p_{3/2}$ spectrum also contains a tail at high bonding energies that was fitted with peaks of Fe(III)-S, Fe(III)-OH, and Fe(III)-SO_4^{2-}. During reaction, there is no noticeable change in the pyrite-Fe(II)-S peak at 706.9 eV. The FeS-like peak at 708.2 eV slightly decreases as reaction continues, which is contrary to the observation that the peak associated with monosulfide increases in the S 2p spectra.

Pyrite was reacted with a solution that initially contained H_3AsO_3, i.e. As(III)-oxide. However, the major peak of the As 3d spectra of pyrite that had reacted with arsenic for 1 hr to 29 days was associated with As_4S_4-like As. The XPS data suggests that arsenic was removed from solution mainly by reduction and subsequent precipitation of an As_4S_4-like phase during reaction with pyrite. Arsenic removal with iron sulfide minerals has been investigated and formation of various solids including orpiment, arsenopyrite, and realgar has been reported (19-21,65). The XPS data in this study agree with the research on arsenic and synthetic mackinawite, in which arsenic is removed and forms a precipitate that is similar to realgar (As_4S_4) under acidic conditions and high arsenic concentration (65).

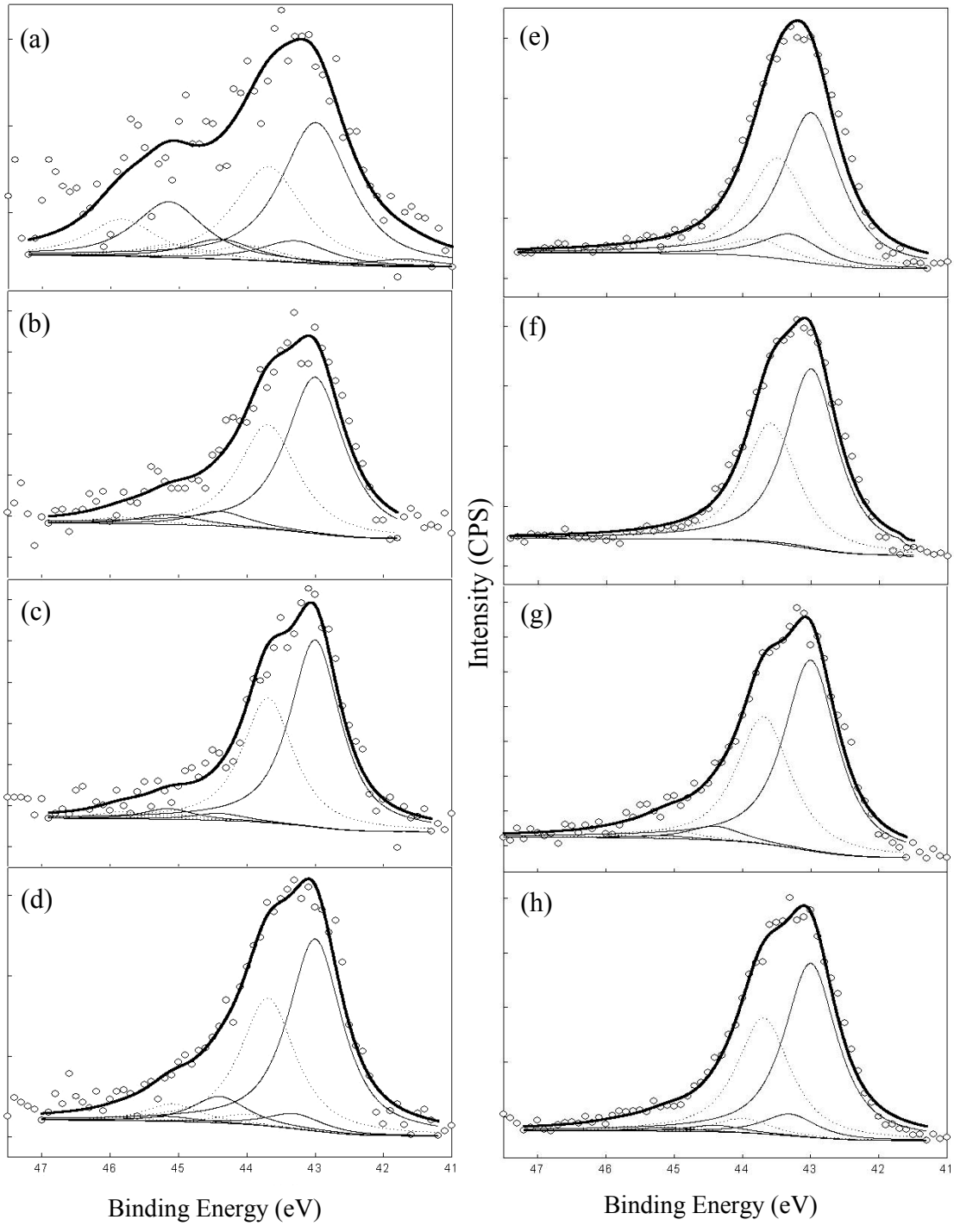

Figure 4.6 The XPS spectra of As 3d of pyrite after reaction with As(III) at pH 4. For (a) 1hr, (b) 3hr, (c) 8hr, (d) 1 day, (e) 3 day, (f) 5 day, (g) 10 day, and (h) 29 day.

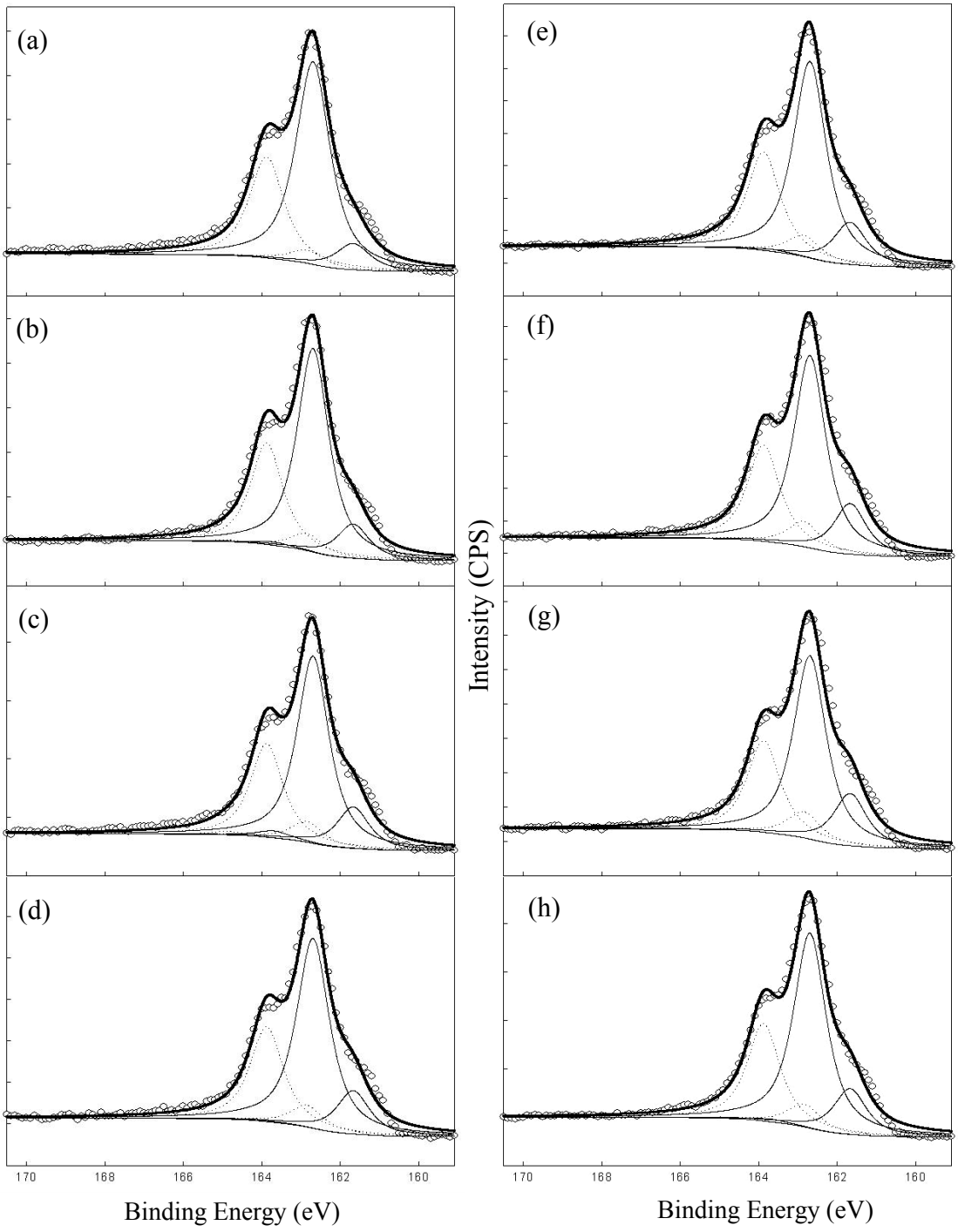

Figure 4.7 The XPS spectra of S 2p of pyrite after reaction with As(III) at pH 4. For (a) 1hr, (b) 3hr, (c) 8hr, (d) 1 day, (e) 3 day, (f) 5 day, (g) 10 day, and (h) 29 day.

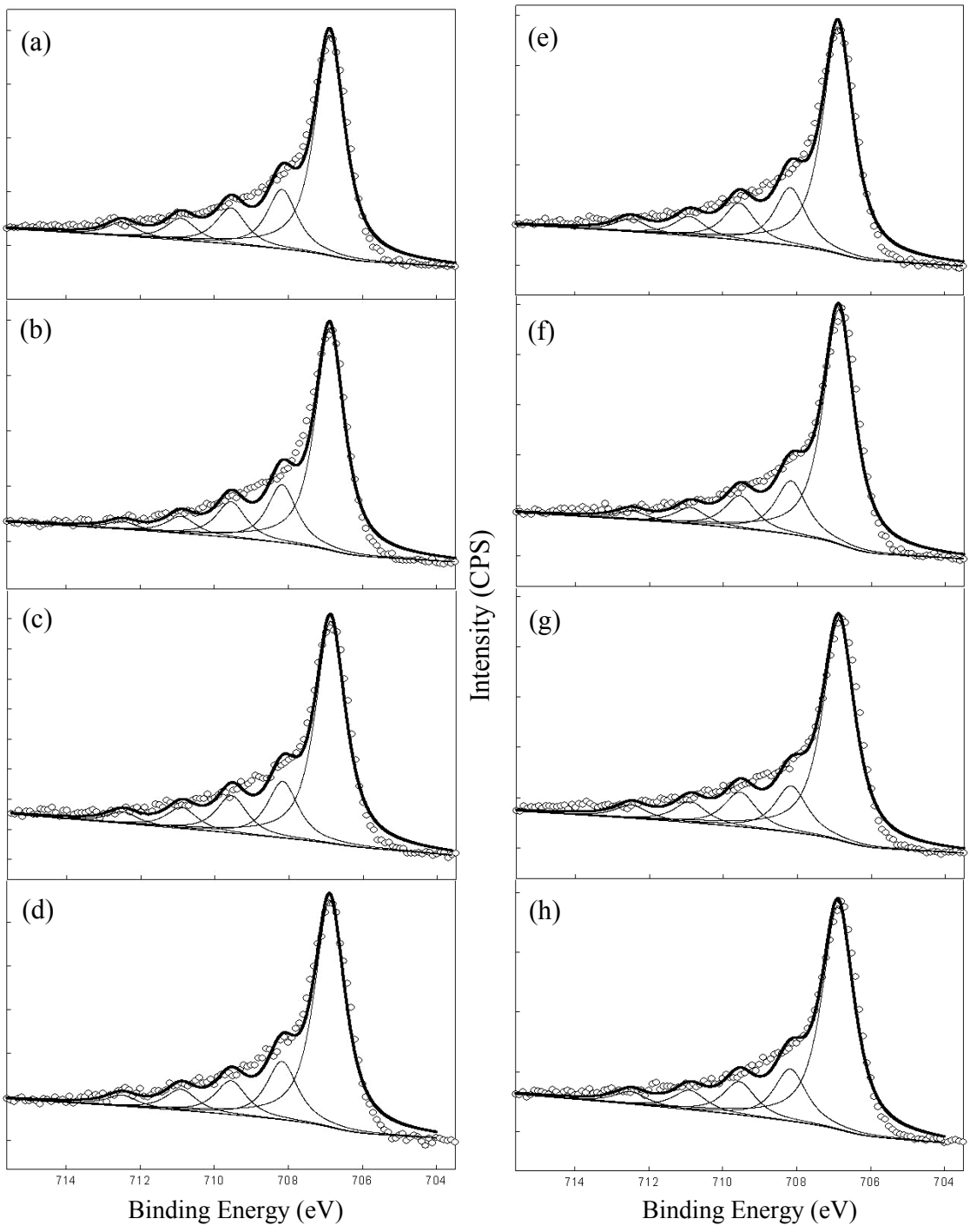

Figure 4.8 The XPS spectra of Fe $2p_{3/2}$ of pyrite after reaction with As(III) at pH 4. For (a) 1hr, (b) 3hr, (c) 8hr, (d) 1 day, (e) 3 day, (f) 5 day, (g) 10 day, and (h) 29 day.

Table 4.5 XPS peak parameters of pyrite after reaction with As(III) at pH 4 for various times

B.E. (eV)		Species	Relative Composition (%)								
			unreacted	1 hr	3 hr	8 hr	1 day	3 day	5 day	10 day	29 day
S $2p_{3/2}$	161.4	S^{2-}	14.7	11.5	14.2	17.6	18.5	17.5	20.8	22.2	18.8
	162.4	S_2^{2-} (FeS_2)	83.4	88.5	84.5	79.5	81.1	81.6	79.2	77.8	80.1
	163.6	Polysulfide	1.96	0.00	1.34	2.98	0.38	0.86	0.00	0.00	1.12
Fe $2p_{3/2}$	706.9	Fe(II)-S	64.8	62.7	65.2	63.6	64.5	64.0	67.7	65.5	65.5
	708.2	Fe(II)-S	17.4	16.9	17.0	16.2	16.6	16.3	15.5	13.8	15.3
	709.6	Fe(III)-S	10.1	10.3	10.5	10.7	9.7	10.5	9.4	10.4	9.73
	710.9	Fe(III)-O	5.10	6.20	5.00	6.08	6.04	5.48	4.78	6.29	5.72
	712.5	Fe(III)-O	2.58	3.92	2.30	3.35	3.17	3.69	2.58	3.98	3.70
As $3d_{5/2}$	41.8	As(0)	-	3.07	0.02	0.02	0.01	0.00	0.00	0.01	0.02
	43	As_4S_4	-	57.4	86.5	91.3	80.4	85.2	98.9	91.9	84.3
	43.3	As_2S_3	-	8.87	0.02	0.02	6.40	14.7	1.04	0.01	10.5
	44.4	As(III)-O	-	8.08	8.01	3.46	11.1	0.00	0.00	6.68	3.29
	45.15	As(V)-O	-	22.6	5.50	5.18	2.11	0.00	0.00	1.39	1.80

4.3.3 Surface of Pyrite after Reaction with Arsenic at pH 7

At pH 7, arsenic was removed rapidly within 24 hrs, and then slowly up to 29 days. About 60% of the initial arsenic was removed after 29 days (Figure 4.9). At this pH, the surface of big particles gathered on 0.2 μm-filter and small particles gathered on 0.02 μm-filter were studied separately. Arsenic was not detected by XPS investigation on surfaces of big and small particles until after 29 days (Table 4.6). After 29 days, arsenic was present at a relative concentration of 2.27% on big particles and 1.17 % on small particles. On the surface of big particles, oxygen was present at a relative concentration of about 10 %, which was higher than pH 4, and there was no noticeable change of atomic composition during reaction. For small particles, oxygen content was 40% before reaction with arsenic and oxygen content decreased during reaction.

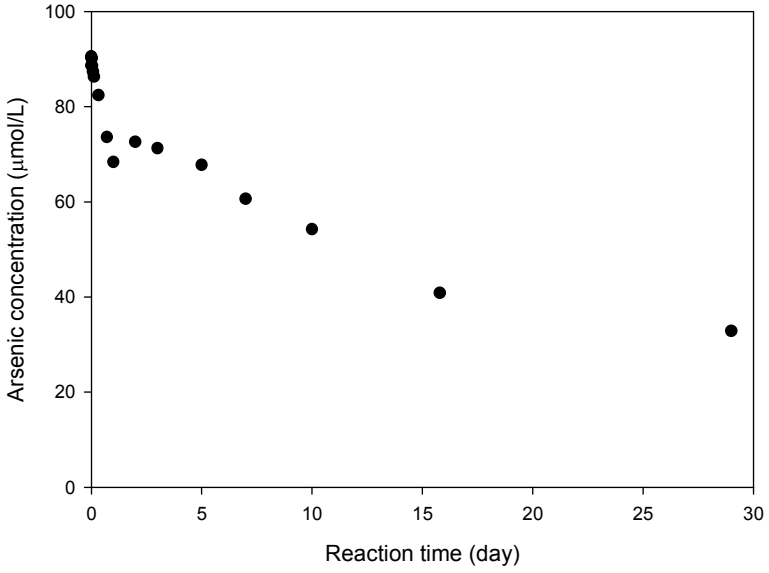

Figure 4.9 Arsenic concentrations over time in presence of pyrite at pH 7. Initial concentration of arsenic =100 μM, dose of pyrite = 1 g/L.

Table 4.6 Atomic composition (%) of the surface of pyrite after reaction with As(III) at pH 7 for various times

	Fe 2p	S 2p	O 1s	As 3d	S/Fe
Big particles					
unreacted	29.9	59.0	11.1	-	1.97
1 hr	28.0	59.3	12.7	-	2.12
1 day	28.9	59.2	11.8	-	2.05
5 day	28.8	61.9	9.32	-	2.15
29 day	27.0	59.6	11.2	2.27	2.21
Small particles					
unreacted	22.3	37.4	40.0	-	1.68
1 hr	24.1	37.5	38.4	-	1.56
1 day	30.7	54.1	15.2	-	1.76
5 day	27.1	48.4	24.6	-	1.78
29 day	26.9	47.4	24.1	1.70	1.76

Figure 4.10, Figure 4.11, and Figure 4.12 present the narrow scan As 3d, S 2p, and Fe $2p_{3/2}$ spectra of pyrite reacted for 1 hr, 5 day, and 29 day with 100 μM As(III) at pH 7, respectively. The surface compositions are shown in Table 4.7.

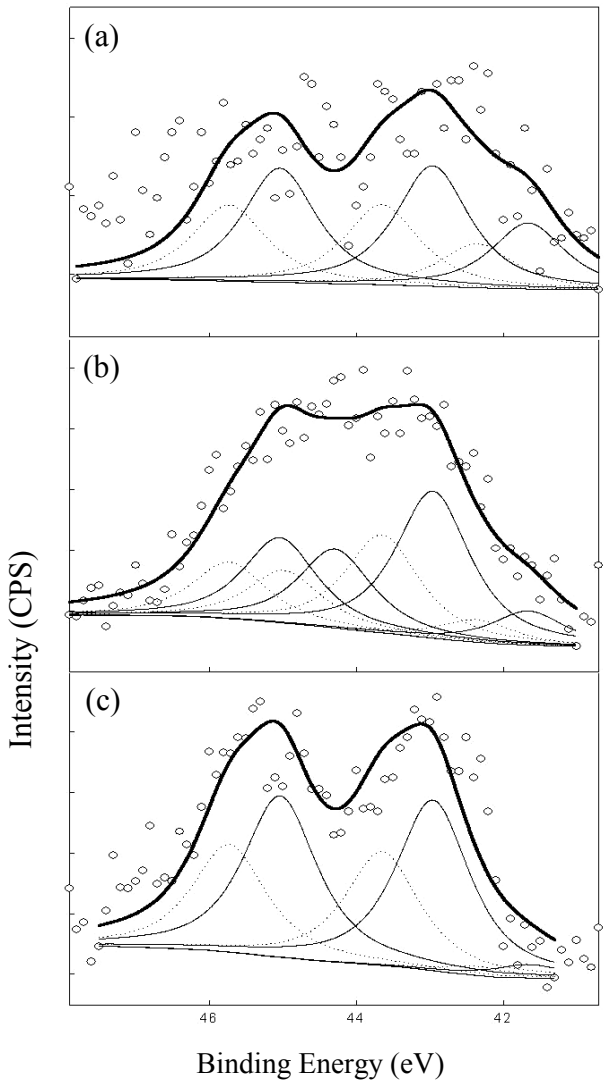

Figure 4.10 The XPS spectra of As 3d of pyrite after reaction with As(III) at pH 7. For (a) 5 day and (b) 29 day of big particles, and for (c) 29 day of small particles.

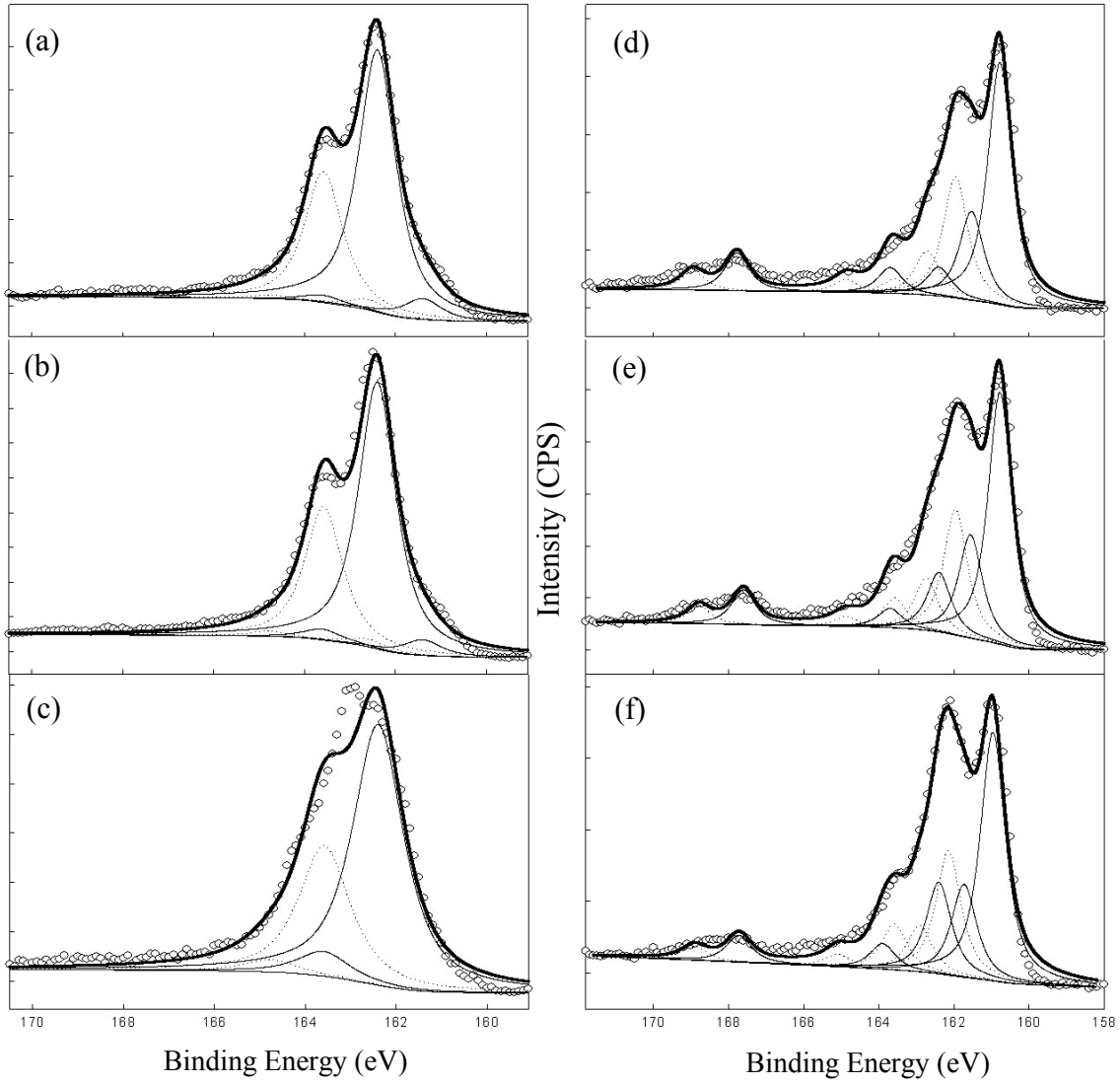

Figure 4.11 The XPS spectra of S 2p of pyrite after reaction with As(III) at pH 7. For (a) 1h, (b) 5d, and (c) 29d of big particles, and for (d) 1h, (e) 5d, and (f) 29d of small particles.

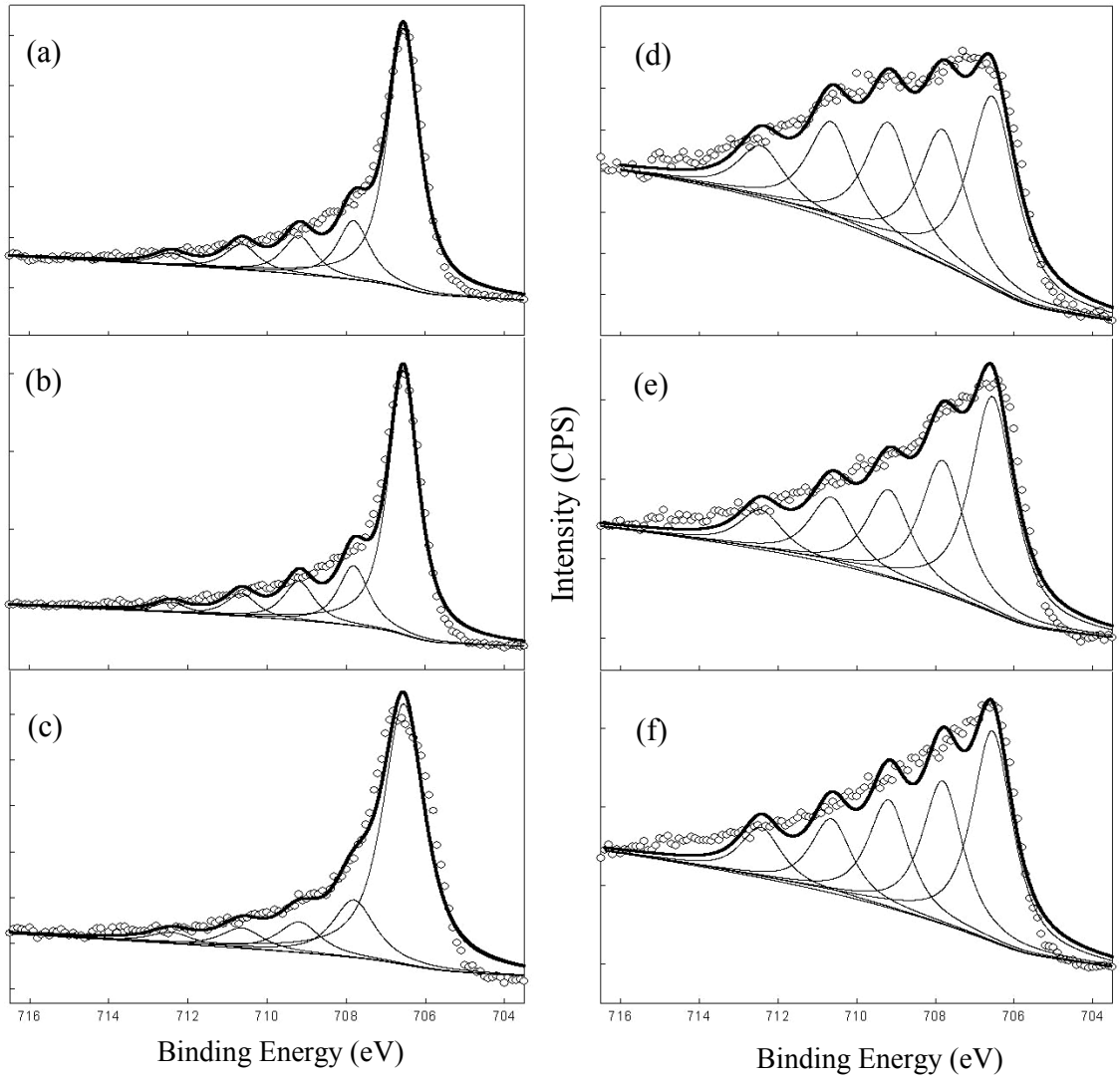

Figure 4.12 The XPS spectra of Fe $2p_{3/2}$ of pyrite after reaction with As(III) at pH 7. For (a) 1h, (b) 5d, and (c) 29d of big particles, and for (d) 1h, (e) 5d, and (f) 29d of small particles.

Table 4.7 . XPS peak parameters of pyrite after reaction with As(III) at pH 7 for various times

B.E. (eV)		Species	Relative composition of big particles (%)				Relative composition of small particles (%)			
			unreacted	1 hr	5 day	29 day	unreacted	1 hr	5 day	29 day
S $2p_{3/2}$	160.8	S^{2-} (FeS)	-	-	-	-	58.9	57.1	53.7	51.2
	161.4	S^{2-}	11.3	7.24	5.4	0.0	21.4	21.0	22.1	19.1
	162.4	S_2^{2-} (FeS_2)	88.5	90.2	91.0	91.3	8.3	6.80	12.7	18.8
	163.6	Polysulfide	0.128	2.54	3.69	8.65	5.83	6.09	4.12	5.26
	167.9	SO_4^{2-}	-	-	-	-	5.61	8.98	7.42	5.59
Fe $2p_{3/2}$	706.9	Fe(II)-S	66.6	65.7	66.7	68.5	41.5	32.4	39.8	35.9
	708.2	Fe(II)-S	14.9	15.0	15.1	15.1	21.1	22.6	24.6	24.4
	709.6	Fe(III)-S	9.99	9.8	9.9	8.1	18.5	19.9	16.2	18.4
	710.9	Fe(III)-O	5.73	6.49	5.73	5.34	11.83	16.34	12.19	12.64
	712.5	Fe(III)-O	2.74	3.07	2.57	2.97	6.99	8.83	7.31	8.63
As $3d_{5/2}$	41.8	As(0)	-	-	21.92	9.84	-	-	-	3.89
	43	As_4S_4	-	-	40.0	42.6	-	-	-	49.4
	43.3	As_2S_3	-	-	0.03	0.05	-	-	-	0.05
	44.4	As(III)-O	-	-	0.03	22.9	-	-	-	0.05
	45.2	As(V)-O	-	-	38.0	24.6	-	-	-	46.7

At pH 7, arsenic was not observed on the surfaces of both big and small particles until after 5 days. After 5 days, arsenic was detected on the big particles with a low intensity in the As 3d narrow scan. The low intensity could cause some error in interpretation. The major peaks of the As 3d spectra are an As_4S_4-like As specie and As(V)-O As with relative concentrations of 40% and 38%, respectively. The As 3d spectra also contain a peak at 41.8 eV, which is interpreted to be elemental As (50-53). After 29 days, the most intense peak of the As 3d spectra for big particles is an As_4S_4-like As with relative concentration of 42.6%. As(III)-O and As(V)-O peaks with similar intensity are observed with relative concentrations of 22.9% and 24.6%, respectively. The As 3d spectra also contain a small peak associated with elemental As. The As 3d spectra of small particles after reaction for 29 days contains two major peaks, one for As_4S_4-like As and one for As(V)-O. The As 3d spectra also contains a small elemental As peak.

The S 2p spectra of big particles reacted at pH 7 are almost identical to those for reaction at pH 4. They both have a major peak at 162.4 eV and small peaks at 161.4 eV and 163.6 eV. There is no noticeable change in the pyrite disulfide peak at 162.4 eV during reaction. The S 2p data for big particles show a decrease in monosulfide at 161.4 eV and an increase in polysulfide at 163.6 eV with time. The decrease in monosulfide suggests that monosulfide could be converted into oxidized S, i.e. polysulfide, or the chemically reactive surface monosulfide could be dissociated from bulk pyrite and produce small FeS-like particles. The amount of small particles was not quantitatively measured during the reaction, but it noticeably increased with time. The major peak in S

2p spectra of small particles reacted at pH 7 is associated with monosulfide of bulk FeS and is located at 160.8 eV. The second intense peak in the S 2p spectra is for monosulfide at 161.4 eV. It has a relative concentration of about 20%, which does not change during reaction. The S 2p spectra also contain small peaks for disulfide, polysulfide, and sulfate. During reaction, the monosulfide of bulk FeS decreases, while disulfide increases with time, suggesting that the monosulfide is consumed and converted into disulfide.

The Fe $2p_{3/2}$ spectra of big particles reacted at pH 7 are also almost identical with those obtained after reaction at pH 4. They both have a major peak at 706.9 eV and small peaks at higher binding energies that are associated with of Fe(III)-S, Fe(III)-OH, and Fe(III)-SO_4^{2-}. The Fe $2p_{3/2}$ spectra of small particles contain more oxidized Fe peaks at the high binding energy area above 709 eV compared to big particles. During reaction, there is no noticeable change in Fe $2p_{3/2}$ spectra of big and small particles reacted at pH 7.

The major peak of the As 3d spectra of both big and small particles reacted with arsenic at pH 7 was an As_4S_4-like As, which is the same as observed after reaction at pH 4. This suggests that solution arsenic was removed and reacted with pyrite to form a precipitate of an As_4S_4-like phase. However, As(III)-O and As(V)-O arsenic were also observed and only As(V)-O was observed on the surface of small particles. At this pH,

arsenic seemed to form As(III)-O and As(V)-O complexes with pyrite. Furthermore, As(III) seemed to be oxidized to As(V) by Fe^{3+} present on the surface, therefore, more As(V)-O was observed on the surfaces of small particles, which are more highly oxidized.

4.3.4 Surface of Pyrite after Reaction with Arsenic at pH 10

Arsenic was removed rapidly within 48 hrs, and then slowly for up to 29 days. About 60% of arsenic was removed after 29 days (Figure 4.13). As at pH 7, the surfaces of big and small particles were studied separately. Arsenic was not detected by XPS on pyrite particles until 29 day reaction, regardless of size (Table 4.8). After 29 days, arsenic was detected on big particles at a relative concentration of 1.3%, but arsenic was not detected on the surface of small particles during the survey scan. There was no noticeable change of atomic composition on the surface of big particles during reaction. For small particles at pH 10, before reaction most of the surface was covered by oxygen (92.7%), but during reaction oxygen content decreased with time. Also, S/Fe ratio increased with time.

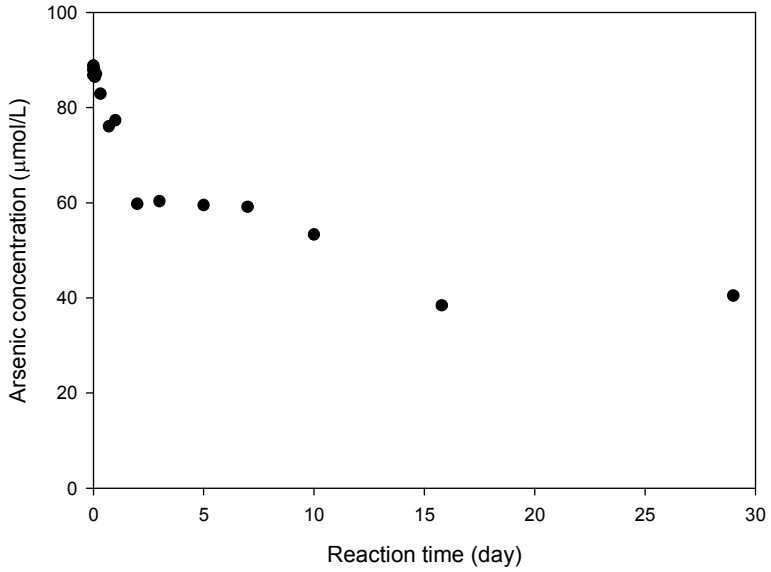

Figure 4.13 Arsenic concentrations over time in presence of pyrite at pH 10. Initial concentration of arsenic =100 µM, dose of pyrite = 1 g/L.

Table 4.8 Atomic composition (%) arsenic after reaction with arsenic at pH 10 for various times

	Fe 2p	S 2p	O 1s	As 3d	S/Fe
Big particles					
unreacted	27.4	62.3	10.3	-	2.27
3 hr	25.3	62.3	12.4	-	2.47
8 hr	27.0	61.6	11.4	-	2.29
1 day	28.2	61.9	9.88	-	2.20
29 day	26.1	60.7	11.9	1.30	2.33
Small particles					
unreacted	2.83	4.44	92.7	-	1.57
3 hr	30.7	49.1	20.2	-	1.60
8 hr	22.2	46.3	31.3	-	2.09
1 day	25.5	48.3	26.2	-	1.89
29 day	24.9	45.9	29.2	-	1.85

Figure 4.14, Figure 4.15, and Figure 4.16 present the narrow scan As 3d, S 2p, and Fe $2p_{3/2}$ spectra of pyrite reacted for 3 hr, 8 hr, 1 day, and 29 day with 100 μM As(III) at pH 10, respectively. The surface compositions are shown in Table 4.9.

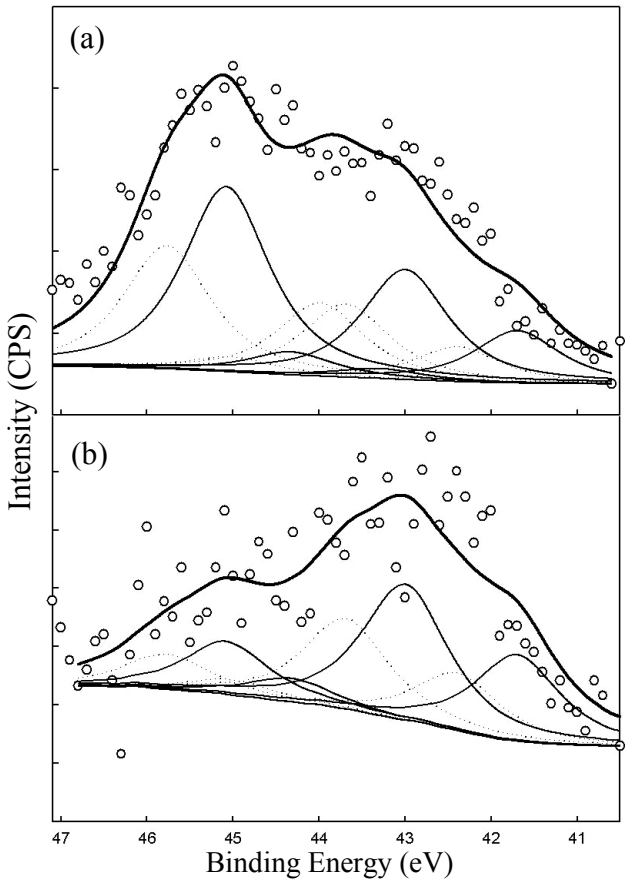

Figure 4.14 The XPS spectra of As 3d of pyrite after reaction with As(III) at pH 10. For 29 day (a) big particles and (b) small particles.

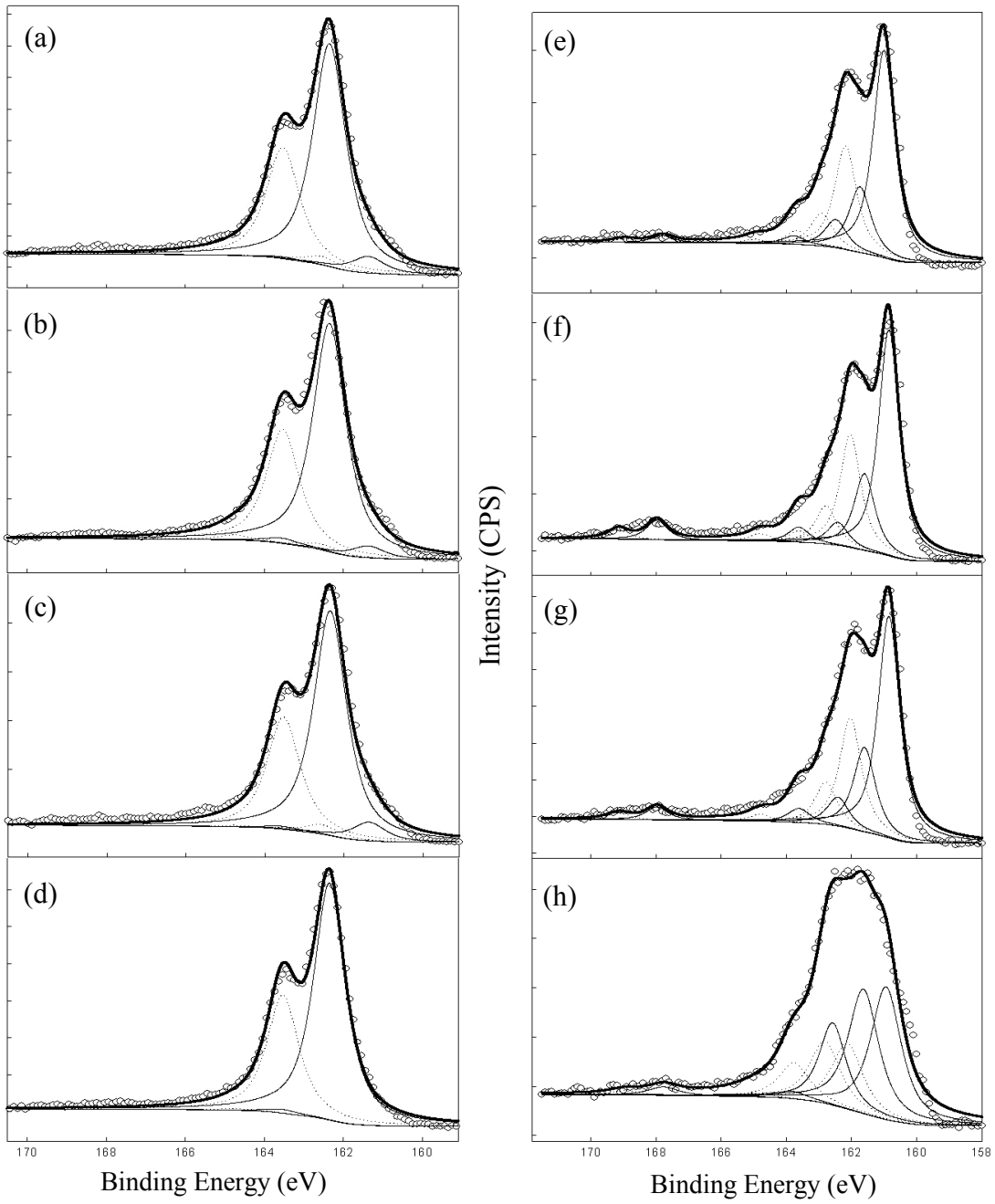

Figure 4.15 The XPS spectra of S 2p of pyrite after reaction with As(III) at pH 10. For (a) 3 hr, (b) 8 hr, (c) 1 day, and (d) 29d of big particles, and for (e) 3 hr, (f) 8 hr, (g) 1 day, and (h) 29 day of small particles.

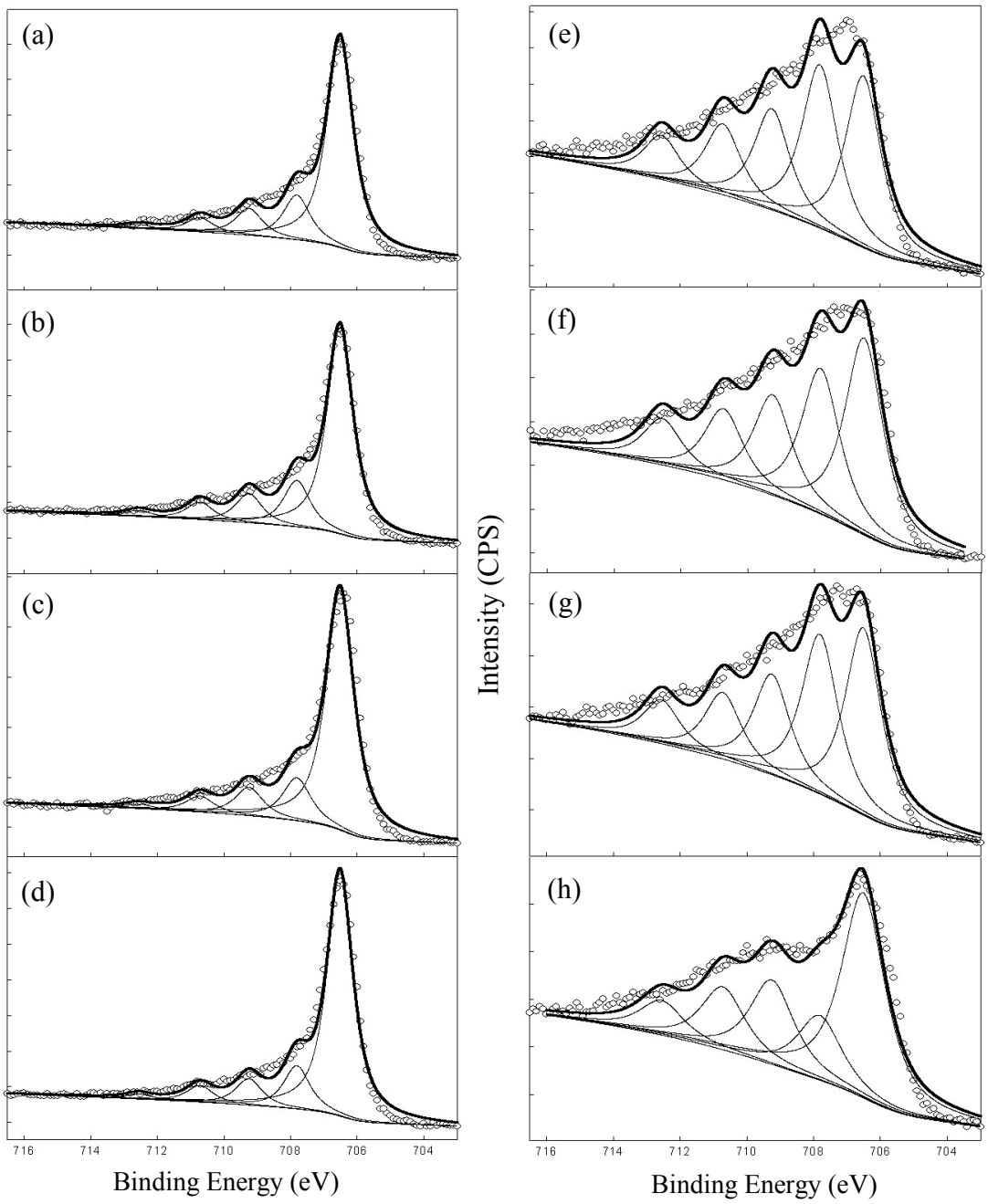

Figure 4.16 The XPS spectra of Fe $2p_{3/2}$ of pyrite after reaction with As(III) at pH 10. For (a) 3 hr, (b) 8 hr, (c) 1 day, and (d) 29d of big particles, and for (e) 3 hr, (f) 8 hr, (g) 1 day, and (h) 29 day of small particles.

Table 4.9 XPS peak parameters of pyrite after reaction with As(III) at pH 10 for various times

B.E. (eV)		Species	Relative composition of big particles (%)					Relative composition of small particles (%)				
			unreacted	3 hr	8 hr	1 day	29 day	unreacted	3 hr	8 hr	1 day	29 day
S $2p_{3/2}$	160.8	S^{2-} (FeS)	-	-	-	-	-	41.4	65.4	62.7	61.2	38.5
	161.4	S^{2-}	7.68	6.88	4.80	7.60	0.0	12.8	20.7	21.3	23.4	36.1
	162.4	S_2^{2-} (FeS_2)	91.6	92.4	92.4	91.2	98.4	4.3	8.93	6.37	8.0	20.8
	163.6	Polysulfide	0.72	0.74	2.82	1.18	1.56	3.91	2.70	4.16	3.87	2.13
	167.9	SO_4^{2-}	-	-	-	-	-	37.6	2.25	5.51	3.61	2.48
Fe $2p_{3/2}$	706.9	Fe(II)-S	66.3	69.9	67.5	72.3	72.7	33.6	31.2	35.1	33.6	45.4
	708.2	Fe(II)-S	15.9	15.0	15.2	13.0	12.9	27.8	29.6	26.0	28.6	14.3
	709.6	Fe(III)-S	9.71	9.01	9.60	8.56	7.90	24.1	18.4	17.9	18.0	18.7
	710.9	Fe(III)-O	5.59	4.74	5.75	4.79	4.98	8.01	12.8	12.7	11.9	13.9
	712.5	Fe(III)-O	2.45	1.31	2.00	1.40	1.54	6.49	8.02	8.30	7.85	7.68
As $3d_{5/2}$	41.8	As(0)	-	-	-	-	12.4	-	-	-	-	28.9
	43	As_4S_4	-	-	-	-	26.2	-	-	-	-	45.5
	43.3	As_2S_3	-	-	-	-	11.9	-	-	-	-	0.055
	44.4	As(III)-O	-	-	-	-	5.45	-	-	-	-	7.85
	45.2	As(V)-O	-	-	-	-	44.0	-	-	-	-	17.7

At pH 10, arsenic was not observed until 29 days of reaction for both big and small particles. After 29 days, the most intense peak of the As 3d spectra for big particles is As(V)-O with a relative concentration of 44%. The As 3d spectra also contain peaks associated with As_4S_4-like As and elemental As with relative concentrations of 26.2% and 12.4%, respectively. Arsenic was detected on small particles reacted for 29 days with low intensity on narrow scan of As 3d. The major peak of the As 3d spectra of small particles is an As_4S_4-like As with relative concentration of 45.5%. The As 3d spectra contains peaks showing 28.9% elemental As, 17.7% As(V)-O, and 7.8% As(III)-O.

The S 2p spectra of big particles reacted at pH 10 are almost identical with those for particles reacted at pH 4 or pH 7. They have a major peak at 162.4 eV and small peaks at 161.4 eV and 163.6 eV. As at pH 7, the monosulfide peak at 161.4 eV decreases with time and no peak at 161.4 eV was observed after reaction for 29 days. The major peak in the S 2p spectra of small particles reacted at pH 10 is monosulfide of bulk FeS, which is located at 160.8 eV. The S 2p spectra also contain peaks for monosulfide, disulfide, polysulfide, and sulfate. Before reaction, the S 2p spectra of small particles contain an important sulfate peak at 167.9 eV with relative concentration of 37.6%, but after reaction, the sulfate peak decreases to relative concentrations of only a few percent (2 to 5%). This is related to oxygen content on the surface. Before reaction, most of surface of small particles at pH 10 was covered by oxygen (92.7%), but the oxygen content decreased with time. After reaction for 29 days, the peak for

monosulfide of bulk FeS decreases, while the peaks for monosulfide at 161.4 eV and disulfide increase.

The Fe $2p_{3/2}$ spectra of big particles reacted at pH 10 are also almost identical with those for pyrite reacted at pH 4. They have a major peak at 706.9 eV and small tail at high binding energies that is fitted with peaks of Fe(III)-S, Fe(III)-OH, and Fe(III)-SO_4^{2-}. During reaction, there is no noticeable change in Fe $2p_{3/2}$ spectra of big particles reacted at pH 10. The Fe $2p_{3/2}$ spectra of small particles contain more oxidized Fe peaks at the high binding energy area above 709 eV compared to big particles. During reaction, surface Fe(II)-S is enhanced and oxidized Fe species are diminished.

The major peak of the As 3d spectra on the surface of big particles reacted with arsenic at pH 10 was associated with As(V)-O arsenic and a peak associated with As_4S_4-like As was present at a relative concentration of 26.2%. At pH 10, arsenic removal by precipitation of an As_4S_4-like phase seems to be less important than at lower pH and arsenic removal by sorption is dominant. Also, elemental arsenic was observed on the surfaces of particles, indicating that arsenic was also being removed by precipitation of a FeAsS-like phase. Fast formation of a FeAsS-like precipitate was suggested by Bostick et al (21).

4.3.5 Summary

In this study, arsenic removal by pyrite was strongly affected by pH. Under acidic conditions, arsenic removal continued until complete removal was achieved. However, in neutral to alkaline conditions, fast removal of arsenic was followed by slow removal that resulted in a maximum of about 60% of total arsenic being removed. In the neutral to alkaline conditions, a defective pyrrhotite-like Fe-S phase that resulted from microwave irradiation during synthesis of pyrite dissociated from bulk pyrite to form small particles with more oxidized surface, while surfaces of big particles (bulk pyrite) were almost identical with those of pyrite reacted under acidic conditions.

Arsenic was removed by precipitation of an As_4S_4-like phase during reaction with pyrite under acidic conditions. However, under neutral to alkaline conditions, arsenic was found on the surface as As(III)-O and As(V)-O surface complexes as well as an As_4S_4-like precipitate. As pH increases, arsenic removal and formation of an As_4S_4-like precipitate decreased, while removal and formation of As(III)-O and As(V)-O surface complexes increased. Under alkaline conditions, a FeAsS-like phase was also detected. The effect of pH has also been observed during reaction of arsenic with mackinawite (65). Arsenic removal by was associated with precipitation of a As_4S_4-like precipitate under acidic conditions and with adsorbed arsenite species under alkaline conditions.

The role of sulfide minerals in regulating dissolved arsenic concentrations have been emphasized in anoxic environments, but arsenic retention mechanisms are not fully understood yet (11-13,47,48). This study showed that pyrite was effective in removing

arsenic in anoxic environmental. However, arsenic removal by pyrite was complex depending on pH. Further study is required to fully understand arsenic fate and transport in anoxic environment.

CHAPTER V

SUMMARY AND CONCLUSION

In this study, a procedure using microwaves was studied to develop a fast and reliable method for synthesizing pyrite. Interactions of arsenic with pyrite was investigated in an anoxic environment in order to better understand geochemical cycling of arsenic and to better predict arsenic fate and transport in the environment. Arsenic-pyrite interactions were investigated using macroscopic (solution phase experiments) and microscopic (X-ray photoelectron spectroscopic investigation) approaches.

Pyrite was successfully synthesized within few minutes via reaction of ferric iron and hydrogen sulfide using a conventional microwave oven. The SEM study revealed that the nucleation and growth of pyrite occurred on the surface of elemental sulfur, where polysulfides are available. Pyrite formation by reaction of ferric iron and hydrogen sulfide using microwave energy can be summarized by the following reactions.

$$2Fe^{3+} + HS^- = 2Fe^{2+} + S^0 + H^+ \qquad (5.1)$$

$$(n\text{-}1)S^0 + HS^- = S_n^{2-} + H^+ \qquad (5.2)$$

$$Fe^{2+} + S_n^{2-} + HS^- = FeS_2 + S_{n-1}^{2-} + H^+ \qquad (5.3)$$

Compared to conventional heating, using microwave energy results in formation of smaller particulates of pyrite and does so within a minute. Higher levels of microwave power can form pyrite faster, but faster reaction can lead to the formation of pyrite with defects.

Arsenic removal by pyrite was strongly dependent on pH and arsenic species. Both arsenite (As(III)) and arsenate (As(V)) had a strong affinity for the pyrite surface under acidic conditions, but As(III) was more effectively removed than As(V). Under acidic conditions, arsenic removal continued to occur almost linearly with time until complete removal was achieved. However, under neutral to alkaline conditions, fast removal was followed by slow removal and complete removal was not achieved in our experimental conditions. A BET isotherm equation provided the best fit to arsenic removal data, suggesting that surface precipitation occurred at high arsenic/pyrite ratio. The addition of competing ions did not substantially affect the ultimate distribution of arsenic between the pyrite surface and the solution, but changing pH affected arsenic stability on pyrite.

X-ray photoelectron spectroscopy (XPS) revealed that arsenic was removed by precipitation of solids phases similar to As_2S_3 and As_4S_4 during reaction with pyrite under acidic condition. However, under neutral to alkaline conditions, arsenic was removed and formed As(III)-O and As(V)-O surface complexes, as well as As_2S_3/As_4S_4-like precipitates. As pH increases, arsenic removal followed by As_2S_3/As_4S_4-like precipitates decreased, while removal followed by formation of As(III)-O and As(V)-O surface complexes increased. Under alkaline conditions, an FeAsS-like phase was also detected.

The role of sulfide minerals in regulating dissolved arsenic concentrations has been emphasized in anoxic environments. Current studies show that arsenic retention in anoxic environments is controlled by sulfide minerals like pyrite. Arsenic is removed

from solution and retained on the surface of iron sulfide minerals after reaction to form As_2S_3/As_4S_4-like precipitates or FeAsS-like precipitates. Sulfide minerals are effective in removing arsenic in anoxic environments. However, arsenic retention on sulfide minerals can be affected by characteristics of the surrounding environment, such as pH and redox potential. When pH is increased, release of arsenic retained on the sulfide minerals can occur due to the high solubility of As_2S_3/As_4S_4-like precipitates at high pH conditions. Sulfide minerals can be oxidized in aerobic conditions, which can lead to a change in redox states of arsenic and release of arsenic retained on the sulfide minerals. This is believed to be the cause of arsenic contamination observed in acid mine drainage areas and some arsenic contaminated areas. Therefore, further study on the effect of pH and redox processes is required in order to understand long term stability of arsenic retention on sulfide minerals as well as the fate and transport of arsenic in the environment.

LITERATURE CITED

(1) Smedley, P. L.; Kinniburgh, D. G. A review of the source, behavior and distribution of arsenic in natural waters. *Appl. Geochem.* **2002**, *17*, 517-568.

(2) Safiuddin, M.; Karim, M. M. Water resources management in the remediation of groundwater arsenic contamination in Bangladesh. In *Aquatic Arsenic Toxicity and Treatment*; Backhuys Publishers: Leiden, Netherlanda, 2003.

(3) WHO, Arsenic and Arsenic Compounds, Environmental Health Criteria 224, 2001.

(4) EPA, National Primary Drinking Water Regulations; Arsenic and Clarifications to Compliance and New Source Contaminants Monitoring, 40 CFR Parts 9, 141 and 142, 2001.

(5) Stollenwerk, K. G. Geochemical Processes Controlling Transport of Arsenic in Groundwater: A Review of Adsorption, In *Arsenic in Ground Water: Geochemistry and Occurrence*; Kluwer Academic Publishers: Boston, 2003.

(6) Inskeep, W. P.; McDermott, T. R.; Fendorf, S. Arsenic(V)/(III) Cycling in Soils and Natural Waters: Chemical and Microbiological Processes. In *Environmental Chemistry of Arsenic*; Marcel Dekker, Inc: New York, 2002.

(7) Dixit, S.; Hering, J. G. Comparison of arsenic(V) and arsenic(III) sorption onto iron oxide minerals: Implication for arsenic mobility. *Environ. Sci. Technol.* **2003**, *37*, 4182-4189.

(8) Raven, K. P.; Jain, A.; Loeppert, R. H. Arsenite and arsenate adsorption on ferrihydrite: Kinetics, equilibrium, and adsorption envelopes. *Environ. Sci. Technol.* **1998**, *32*, 344-349.

(9) Manning, B. A.; Fendorf, S.; Goldberg, S. Surface structures and stability of arsenic(III) on goethite: Spectroscopic evidence for inner-sphere complexes. *Environ. Sci. Technol.* **1998**, *32*, 2383-2388.

(10) Nickson, R. T.; McArthur, J. M.; Ravenscroft, P.; Burgess, W. G.; Ahmed, K. M. Mechanism of arsenic release to groundwater, Bangladesh and West Bengal. *Appl. Geochem.* **2000**, *15*, 403-413.

(11) Belzile, N.; Lebel, J. Capture of arsenic by pyrite in near-shore marine sediments. *Chem. Geol.* **1986**, *54*, 279-281.

(12) Hyland, M. M.; Jean, G. E.; Bancroft, G. M. XPS and AES studies of Hg(II) sorption and desorption reactions on sulphide minerals. *Geochim. Cosmochim. Acta* **1990**, *54*, 1957-1967.

(13) Moor, J. N. Partitioning of arsenic and metals in reducing sulfidic sediments. *Environ. Sci. Technol.* **1988**, *22*, 432-437.

(14) Berner, R. A. Sedimentary pyrite formation: An update. *Geochim. Cosmochim. Acta* **1984**, *48*, 605-615.

(15) Berner, R. A. Sedimentary pyrite formation. *Am. J. Sci.* **1970**, *268*, 1-23.

(16) Abraitis, P. K.; Pattrick, R. A. D.; Vaughan, D. J. Variations in the compositional, textural and electrical properties of natural pyrite: Review. *Int. J. Miner. Process.* **2004**, *74*, 41-59.

(17) Savage, K. S.; Tingle, T. N.; O'Day, P. A.; Waychunas, G. A.; Bird, D. K. Arsenic speciation in pyrite and secondary weathering phases, Mother Lode Gold District, Tuolumne County, California. *Appl. Geochem.* **2000**, *15*, 1219-1244.

(18) Blanchard, M.; Alfredsson, M.; Brodholt, J.; Wright, K.; Catlow C.; Richard A. Arsenic incorporation into FeS_2 pyrite and its influence on dissolution: A DFT study. *Geochim. Cosmochim. Acta* **2007**, *71*, 624-630.

(19) Farquhar, M. L.; Charnock, J. M.; Livens, F. R.; Vaughan, D. J. Mechanisms of arsenic uptake from aqueous solution by interaction with goethite, lepidocrocite, mackinawite, and pyrite: An X-ray absorption spectroscopy study. *Environ. Sci. Technol.* **2002**, *36*, 1757-1762.

(20) Bostick, B. C.; Chen, C.; Fedorf, S. Arsenite retention mechanisms within estuarine sediments of Pescadero, CA. *Environ. Sci. Technol.* **2004**, *38*, 3299-3304.

(21) Bostick, B. C.; Fendorf, S. Arsenite sorption on troilite (FeS) and pyrite (FeS_2). *Geochim. Cosmochim. Acta* **2003**, *67*, 909-921.

(22) Zouboulis, A. I.; Kydros, K. A.; Matis, K. A. Arsenic(III) and arsenic(V) removal from solutions by pyrite fines. *Sep. Sci. Technol.* **1993**, *28*, 2449-2463.

(23) Jingtai, H.; Fyfe, W. S. Arsenic removal from water by iron-sulphide minerals. *Chin. Sci. Bull.* **2000**, *45*, 1430-1434.

(24) Yang, H.; Huang, C.; Lib, X.; Shi, R.; Zhang, K. Luminescent and photocatalytic properties of cadmium sulfide nanoparticles synthesized via microwave irradiation. *Mater. Chem. Phys.* **2005**, *90*, 155–158.

(25) Liao, X.-H.; Zhu, J.-J.; Chen, H.-Y. Microwave synthesis of nanocrystalline metal sulfides in formaldehyde solution. *Mater. Sci. Eng. B* **2001**, *85*, 85–89.

(26) Roberts, W. M. B.; Walker, A. L.; Buchanan, A. S. The chemistry of pyrite formation in aqueous solution and its relation to the depositional environment. *Mineral. Deposita* **1969**, *4*, 18-29.

(27) Rickard, D. T. Kinetics and mechanism of pyrite formation at low temperature. *Am. J. Sci.* **1975**, *275*, 632-652.

(28) Luther III, G. W. Pyrite synthesis via polysulfide compounds. *Geochim. Cosmochim. Acta* **1991**, *55*, 2839-2849.

(29) Schoonen, M. A. A.; Barnes, H. L. Reaction forming pyrite and marcasite from solution: I. Nucleation of FeS_2 below 100 ºC. *Geochim. Cosmochim. Acta* **1991**, *55*, 1495-1504.

(30) Schoonen, M. A. A.; Barnes, H. L. Reaction forming pyrite and marcasite from solution: II. Via FeS precursors below 100 ºC. *Geochim. Cosmochim. Acta* **1991**, *55*, 1505 -1514.

(31) Schoonen, M. A. A.; Barnes, H. L. Mechanisms of pyrite and marcasite formation from solution: III. Hydrothermal processes. *Geochim. Cosmochim. Acta* **1991**, *55*, 3491-3504.

(32) Wilkin, R. T.; Barnes, H. L. Pyrite formation by reactions of iron monosulfides with dissolved inorganic and organic sulfur species. *Geochim. Cosmochim. Acta* **1996**, *60*, 4167-4179.

(33) Howarth, R. W. Pyrite: Its rapid formation in a salt marsh and its importance in ecosystem metabolism. *Science* **1979**, *203*, 49-51.

(34) Ohfuji, H.; Rickard, D. Experimental syntheses of framboids - a review. *Earth-Sci. Reviews* **2005**, *71*, 147-170.

(35) Hayes, B. L. Recent advances in microwave-assisted synthesis. *Aldrichimica Acta* **2004**, *37*, 66-77.

(36) Wei, D.; Osseo-Asare, K. Particulate pyrite formation by the Fe^{3+}/HS^- reaction in aqueous solutions: Effects of solution composition. *Coll. Surf. A: Physicochem. Eng. Aspects* **1996**, *118*, 51-61

(37) Lord III, C. J. A Selective and precise method for pyrite determination in sedimentary materials. *J. Sed. Pet.* **1982**, *52*, 664-666.

(38) Nesbitt, H. W.; Muir, I. J. X-ray photoelectron spectroscopic study of a pristine pyrite surface reacted with water vapor and air. *Geochim. Cosmochim. Acta* **1994**, *58*, 4467-4679.

(39) Bonneissel-Gissinger, P.; Alnot, M.; Ehrhardt, J. J.; Behra, P. Surface oxidation of pyrite as a function of pH. *Environ. Sci. Technol.* **1998**, *32*, 2839-2845.

(40) Pratt, A. R.; Muir, I. J.; Nesbitt, H. W. X-ray photoelectron and Auger electron spectroscopic studies of pyrrhotite and mechanism of air oxidation. *Geochim. Cosmochim. Acta* **1994**, *58*, 827-841.

(41) Nesbit, H. W.; Banchroft, G. M.; Pratt, A. R.; Scaini, M. J. Sulfur and iron surface states on fractured pyrite surfaces. *Am. Mineral.* **1998**, *83*, 1067-1076.

(42) Uhlig, I.; Szargan, R.; Nesbitt, H. W.; Laajalehto, K. Surface states and reactivity of pyrite and marcasite. *Appl. Surf. Sci.* **2001**, *179*, 222-229.

(43) Graham, U. M.; Ohmoto, H. Experimental study of formation mechanisms of hydrothermal pyrite. *Geochim. Cosmochim. Acta* **1994**, *58*, 2187-2202,.

(44) Perreus, L.; Loupy, A. A tentative rationalization of microwave effects in organic synthesis according to the reaction medium, and mechanistic considerations *Tetrahedron* **2001**, *57*, 9199-9223.

(45) Ni, Y.; Liu, H.; Wang, F.; Liang, Y.; Hong, J.; Ma, X.; Xu, Z. Shape controllable preparation of PbS crystals by a simple aqueous phase route. *Crystal Growth & Design* **2004**, *4*, 759-764.

(46) Huang, J. H.; Rowson, N. A. Heating characteristics and decomposition of pyrite and marcasite in a microwave field. *Miner. Eng.* **2001**, *14*, 1113-1117.

(47) Kornicker, W. A.; Morse, J. W. Interactions of divalent cations with the surface of pyrite. *Geochim. Cosmochim. Acta* **1991**, *55*, 2159-2171.

(48) Jean, G. E.; Banchroft, G. M. Heavy metal adsorption by sulphide mineral surfaces. *Geochim. Cosmochim. Acta* **1986**, *50*, 1455-1463.

(49) Foster, A. L. Spectroscopic investigations of arsenic species in solid phases. In *Arsenic in Ground Water*; Kluwer Academic Publishers: Boston, 2003.

(50) Nesbit, H. W.; Muir, J.; Prawn, A. R. Oxidation of arsenopyrite by air and air-saturated, distilled water, and implications for mechanism of oxidation. *Geochim. Cosmochim. Acta* **1995**, *59*, 1773-1786.

(51) Bullen, H. A.; Dorko, M. J.; Oman, J. K.; Garret, S. J. Valence and core-lovel binding energy shifts in realgar (As_4S_4) and pararealgar (As_4S_4) arsenic sulfides. *Surf. Sci.* **2003**, *531*, 319-328.

(52) NIST X-ray Photoelectron Spectroscopy Database. http://srdata.nist.gov/xps/

(53) Nesbitt, H. W.; Canning, G. W.; Bancroft, G. M. XPS study of reductive dissolution of 7Å-birnessite by H_3AsO_3 with constraints on reaction mechanism. *Geochim. Cosmochim. Acta* **1998**, *62*, 2097-2110.

(54) McLintock, I. S. The Elovich equation in chemisorption kinetics. *Nature* **1967**, *216*, 1204-1205.

(55) Chien, S. H.; Clayton, W. R. Application of Elovich equation to the kinetics of phosphate release and sorption in soils. *Soil Sci. Soc. Am. J.* **1980**, *44*, 265-268.

(56) Sposito, G.A. Geochemical Processes at Mineral Surfaces. In *American Chemistry Society Symposium*; Am. Chem. Soc.: Washington DC, 1986.

(57) Axe, L.; Anderson, P. R. Adsorption onto Oxides: The Role of Diffusion. In *Surface of Nanoparticles and Porous Materials*; Marcel Dekker Inc.: New York, 1999.

(58) Sparks, D. L. *Kinetics of Soil Chemical Processes*; Academic Press, Inc., 1989.

(59) Jia, Y.; Xu, L.; Fang, Z.; Demopoulos, G. P. Observation of surface precipitation of arsenate on ferrihydrite. *Environ. Sci. Technol.* **2006**, *40*, 3248-3253.

(60) Wei, D. *Materials Science and Engineering*; Ph.D. Dissertation, The Pennsylvania State University, University Park, PA, 1995.

(61) Fornasiero, D.; Eijt, V.; Ralston, J. An electrokinetic study of pyrite oxidation. *Coll. Surf.* **1992**, *62*, 63-73.

(62) Webster, J. G. The solubility of As2S3 and speciation of As in dilute and sulphide-bearing fluids at 25 and 90°C. *Geochim. Cosmochim. Acta* **1990**, *54*, 1009-1017.

(63) Benjamin, M. M. *Water Chemistry*; McGraw-Hill: Boston, 2002.

(64) Elsetinow, A. R.; Schoonen, M. A. A.; Strongin, D. R. Aqueous geochemical and surface science investigation of the effect of phosphate on pyrite oxidation. *Environ. Sci. Technol.* **2001**, *35*, 2252-2257.

(65) Gallegos, T. J.; Hyun, S. P.; Hayes, K. F. Spectroscopic investigation of the uptake of arsenite from solution by synthetic mackinawite. *Environ. Sci. Technol.* **2007**, *41*, 7781-7786.

(66) Li, L.; Stanforth, R. Distinguishing adsorption and surface precipitation of phosphate on goethite. *J. Colloids Interface Sci.* **2000**, *230*, 12-21.

(67) Demoisson, F.; Mullet, M.; Humbert, B. Pyrite oxidation by hexavalent chromium: Investigation of the chemical processes by monitoring of aqueous metal species. *Environ. Sci. Technol.* **2005**, *39*, 8747-8752.

(68) Hacquard, E.; Bessiere, J.; Alnot, M.; Ehrhardt, J. J. Surface spectroscopic study of the adsorption of Ni(II) on pyrite and arsenopyrite at pH 10. *Surf. Interface Anal* **1999**, *27*, 849-860.

(69) Guevremont, J. M.; Bebie, J.; Elsetinow, A. R.; Strongin, D. R.; Schoonen, M. A. A. Reactivity of the (100) plane of pyrite in oxidizing gaseous and aqueous environments: Effects of surface imperfections. *Environ. Sci. Technol.* **1998**, *32*, 3743-3748.

(70) Kendelewicz, T.; Doyle, C. S.; Bostick, B. C.; Brown Jr. G.E. Initial oxidation of fractured surfaces of FeS_2(100) by molecular oxygen, water vapor, and air. *Surf. Sci.* **2004**, *558*, 80-88.

(71) Dedititius, A. P.; Utsunomiya, S.; Renock, D.; Ewing, R. C.; Ramana, C. V.; Becker, U.; Kesler, S. E. A proposed new type of arsenian pyrite: Composition, nanostructure and geological significance. *Geochim. Cosmochim. Acta* **2008**, *72*, 2919-2933.

VITA

Name:	Eun Jung Kim
Address:	Department of Civil Engineering, Texas A&M University, 3136 TAMU, College Station, TX 77843-3136
Email Address:	ejbird@tamu.edu
Education:	B.S., Environmental Engineering, University of Seoul, 2000 M.S., Environmental Engineering and Science, Pohang University of Science and Technology, 2002 Ph.D., Civil Engineering, Texas A&M University, 2008